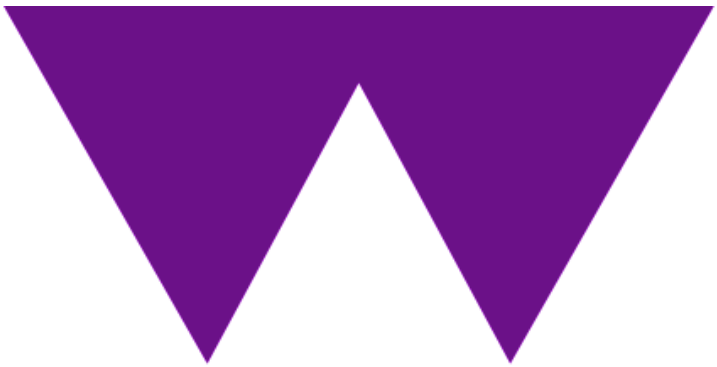

WARWICK

THE UNIVERSITY OF WARWICK

Sub-MHz Ultrasound for Thick Section and High Attenuation Materials

By

Mohd Noorul Ikhsan bin Mohamed

A thesis submitted to the School of Engineering,

University of Warwick

for the degree of Doctor of Philosophy (Ph.D.)

July 2016

Declaration

The work described in this thesis was conducted by the author, except where stated otherwise, in the School of Engineering, University of Warwick between the dates of March 2013 and July 2016. No part of this work has been previously submitted by the author to the University of Warwick, or to any other academic institution for admission to a higher degree.

M.N.I.B Mohamed, 11 July 2016

Abstract

This thesis described research on materials that exhibit a high degree of attenuation over the sound energy, especially those that are thick and bulky, where penetration of ultrasonic signals becomes difficult. Materials such as viscoelastic polymers, composites (especially multi-layered structures) and also concrete are among the so-called high ultrasonic attenuation materials. Hence, there is a huge need to develop advanced tools, devices and post-processing algorithm that can help to evaluate their integrity. This research thus focused on designing an ultrasonic system which is capable of examining the internal integrity of highly attenuating materials. To reach this aim, an innovative combination of Sub-MHz frequencies (below 1 MHz) excitations in the form of coded waveforms such as chirps and binary coded, together with specifically realized piezo-composite transducers was used for the research activity. The system was then used in combination with advanced signal processing techniques, i.e. pulse compression and other algorithms to enhance the acquired signal quality. Industrial samples of polyurethane structure used in deep-sea oil and gas industries, ceramic bricks used in furnaces, multi-layered structures used in the aerospace industries were tested using the developed system. All the tested samples had different properties that require different approaches during the experiment as well as the data analysis. As a consequence, the research activity focused not only on the use of the innovative sub-MHz inspection system above-described, but also on developing novel algorithms for the data processing tailored for each particular inspected material. It was shown that the system, is capable of revealing anomalies (i.e. cracks, manufacturing and artificial defects) within the tested samples. Furthermore, the advanced signal processing and image reconstruction techniques exploited helped in retrieving the correct shape and dimensions of those defect with respect to the standard imaging procedure. This research work can hopefully be a meaningful contribution towards solving the NDT problems within these industries.

Contents

List of Tables

List of Figures

Publications

The following papers have been published or submitted from this thesis:

Conference:

i. Sub-MHz Ultrasound for Thick Sections and Attenuating Materials, **School of Engineering, Postgraduate Symposium** (19 May 2014)

ii. Pulse Compression Ultrasonic Non Destructive Evaluation of Thick Polymer Samples, **European Convention of NDT (ECNDT), Prague Czech Republic** (6-10 Oct 2014)

iii. Concrete Structure Integrity Testing using Sub-MHz Ultrasound, **School of Engineering, Postgraduate Symposium** (12 May 2015)

iv. Low Frequency Coded Waveform for the Inspection of Concrete Structures, **IEEE International Ultrasonic Symposium (IUS), Taipei, Taiwan** (21-24 Oct 2015)

v. Multi-layered composite testing using low frequency ultrasonic pulse-compression techniques, **World Conference of NDT (WCNDT), Munich, Germany** (13-17 June 2016)

Journal:

i. Ikhsan Mohamed, Stefano Laureti, David Hutchins, Lee Davis, Marco Ricci, Ultrasonic NDE of thick attenuating polymer samples using pulse compression, submitted to **Journal NDT & E International** on 12 May 2016

Acknowledgements

I would like to express my deepest gratitude to my supervisor, Professor David Hutchins for his excellent supervision and encouragement during the course of my research. His experiences and calmness in guiding me to finish this PhD journey had played a very big part. My sincere thanks to Dr Lee Davis for the hours that he spent in the labs demonstrating the equipment, and the ideas that he shared with me throughout this works.

I would like to thank to the team of technicians of the School of Engineering, especially to Mr Colin Bank for his continuous support in concrete samples preparation. A big thank you to my colleagues, Dr Stefano Laureti and Dr Omololu Akanji for all the encouragement and endless help that was continuously offered to me throughout my time at Warwick University. Also, special thanks to Dr Marco Ricci from University of Perugia, Italy for his support.

Appreciations to my parents and parents-in-law for the non-stop encouragement and the prayers that really gave me strength in completing this study. Tons of love to hard-core supporter (my kids: Aliff, Aiman, Aqil and Amira) for giving me the support, time and space to complete this thesis. Finally, very special appreciation to the special person in my live, my beloved wife Dr Ismawati who always been there for me throughout this special journey.

List of Abbreviations

BP	British Petroleum
CCPF	Closed-cell Polyurethane Foam
CFRP	Carbon Fibre Reinforced Plastic
CUI	Corrosion Under Insulation
DC	Direct Current
DSP	Digital Signal Processing
DVI	Digital Visual Interface
EMAT	Electro Magnetic Acoustic Transducer
ET	Eddy Current Technique
FIT	Finite Integration Technique
FFT	Fast Fourier Transform
FM	Frequency Modulated
GCS	Golay Complementary Sequences
HDPE	High Density Polyethylene
LSAFT	Linear Systematic Aperture Focusing Technique
MFC	Macro Fibre Composite
MT	Magnetic Particle Technique
NDE	Non-destructive Evaluation
NDT	Non-destructive Technique
NPP	Nuclear Power Plant
OCPF	Open-cell Polyurethane Foam
PBX	Polymer Bonded Explosive
PHWR	Pressurised Hot Water Reactor
PIP	Pipe-in-pipe
PT	Dye Penetrant Testing
PuC	Pulse Compression
PXI	PCI Extension Instrumentation
PZT	Piezoelectric Transducer
ROI	Region of Interest
RT	Radiography Testing
SAFT	Synthetic Aperture Focusing Technique

SNR	Signal to Noise Ratio
TFM	Total Focusing Method
TOF	Time of Flight
TV	Total Variation
USB	Universal Series Bus
UT	Ultrasonic Testing

Chapter 1

Introduction to Ultrasonic Testing

1.1 Introduction

This thesis is concerned primarily with materials that have a high degree of attenuation, especially those that are thick and bulky, where penetration of ultrasonic signals becomes difficult. Materials such as viscoelastic polymers, composites (especially multi-layered) and concrete are high ultrasonic attenuation materials. This study has been focussed on designing an ultrasonic system which is capable of examining the internal integrity of these materials. This was done by using a combination of low frequencies (below 1 MHz), and signal processing involving coded waveforms such as chirps and binary coded signals. These were then used in combination with the pulse compression signal processing technique, plus other methods to enhance the signal. Several samples were tested using the developed system. These materials comprised of those used in deep-sea oil and gas industries, ceramic bricks used in furnaces, concrete used for construction, and multi-layered structures used in the aerospace industries.

This introductory chapter will begin with some discussion on the basic properties of sound, such as transmission mechanisms through a medium, absorption, attenuation, propagation across the interface, beam spread and mode conversion. There is also some discussion of ultrasonic transducer design and piezoelectric materials. The last section gives an overview of the remaining chapters of the thesis.

1.2 Properties of ultrasound

Sound waves are mechanical vibrations that travel through air or other mediums and can be detected when they reach a sound detector (e.g. human and animal ears). Sometimes sound refers to only those vibrations with frequencies that are within the audible range for humans or animals. Typically, humans are only capable of detecting sounds within the frequency range of 20 Hz - 20 kHz, but the absolute value for the limit of human hearing is uncertain and depends on the individual's capabilities and age [1-2]. Sound is produced by the movement of a body or sound generator, which transfers energy to the particles of the surrounding medium such as solid, liquid or gas. This energy propagates through the medium; thus the energy spreads away from the vibrating medium like ripples on the surface of a body of water. The frequency, *f*, of any mechanical vibration associated with a sound wave is related to the speed of the propagation in the medium, *c*, and the wavelength of the oscillation, λ, this relationship can be defined by the following equation:

$$f = \frac{c}{\lambda} \tag{1.1}$$

Ultrasound is a term that refers to sound at frequencies above the normal audible range, whereas sound at frequencies below the level of human hearing is called infrasound [3]. Ultrasonic is the application of ultrasound and Ultrasonic Testing (UT) is a testing technique that utilises ultrasound. UT has become an important inspection tool in various fields including medical, aerospace, nuclear industry, construction, oil and gas, petrochemical, food industry etc. [4]. Problems arise when performing Non-destructive Evaluation (NDE) on large industrial infrastructure, especially for construction materials composed of highly attenuating materials such as composites and concrete. These materials are difficult to test using ultrasound because they attenuate the ultrasonic signal during propagation through the sample.

In a bulk solid medium, sound waves can propagate via four main types of modes, as determined by the way the particles in the medium oscillate. Sound can propagate either in the form of longitudinal waves, shear waves, as plate waves in thin materials, and as a Rayleigh wave when it propagates on the surface of a medium [5]. Longitudinal and shear waves are the two modes of propagation most widely used in ultrasonic testing. The particle movement during the ultrasonic signal propagation of longitudinal and shear waves is illustrated in Figure 1.1.

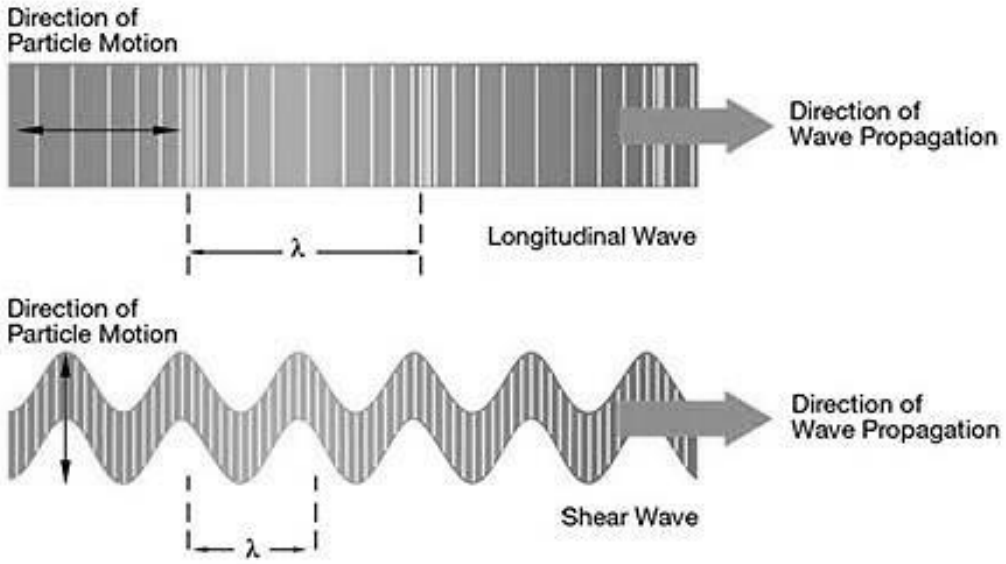

Figure 1.1: Typical ultrasound wave propagation, longitudinal wave (above) and shear wave (below)[6]

Longitudinal waves (Figure 1.1) have a particle motion in the medium parallel to the direction of the wave front. Longitudinal waves are the fastest ultrasound mode among all the modes that are commonly used in ultrasonic NDT, with a velocity *c* of approximately 5,000 m/s in steel. The wave might be converted into a shear wave through refraction and reflection processes when propagating in solid media. Shear waves (also known as transverse waves) are a wave mode where the particle motion is perpendicular to the wave direction. The velocity of shear waves is lower than that of longitudinal waves and the

wavelength is thus smaller compared to longitudinal waves at the same frequency. A typical shear wave velocity in steel is approximately 5,800 m/s. Shear waves can convert to longitudinal waves at a boundary through reflection and refraction processes. Meanwhile, surface waves, also known as Rayleigh waves, represent an oscillating motion that travels along the surface of a medium to a depth of one wavelength. Ocean waves are an example of surface waves. Lamb waves can occur in plates, where motion of the two surfaces is coupled together. There are two types of Lamb wave, asymmetric and symmetric, and they can occur in numerous modes depending on the plate thickness in relation to the wavelength [7]. Table 1.1 is a list of ultrasonic longitudinal velocity in a range of materials.

Material	**Longitudinal velocity *c* [m/s]**
Steel	5,800
Acrylic (Perspex)	2,730
Plexiglas	1,700
Polyurethane	1,900
Fiberglass	2,740
Aluminium	6,320
Concrete	3,200–3,600
Dry air	344
Water	1,480

Table 1.1: Velocity of ultrasonic longitudinal waves in different type of materials

1.3 Attenuation of ultrasound

When ultrasound waves are transmitted through a material, its amplitude tends to diminish with distance, due to a combination of diffraction/beam spreading and signal loss

due to absorption of energy and scattering from changes in impedance. Attenuation refers to the overall reduction in intensity of the wave front as it travels through a medium [8]. If I_0 is the initial intensity, in watts per square meter, of a progressive ultrasonic wave, the intensity I at distance x is

$$I = I_0 e^{-2x} \tag{1.2}$$

Ultrasonic attenuation is the sum of absorption and scattering which depends on the damping capacity and scattering of grain boundary in a particular material [5]. The most common method of finding the attenuation coefficient of a material is by using an ultrasonic source and detector transducer separated by a known distance. From equation 1.2, the attenuation coefficient can be calculated by taking the ultrasonic amplitude at different distances or thicknesses. However, the measurement using this technique is highly influenced by the coupling conditions of the tested material and the ultrasonic transducers. A detailed description of the method and measurement used to determine the attenuation coefficient will be described more detail in Chapter 4.

When ultrasound hits an interface with an irregular shape, and its dimensions are smaller than the diameter of the ultrasound beam, the incident beam will be reflected in many different directions. This phenomenon is known as scattering [9-10]. Scattering is often the main form of attenuation in heterogeneous materials [11]. The basic concept in ultrasonic testing is to utilise scattering phenomena that occurs from defects (flaws, cracks, inclusions etc.). Scattering from grains in a metal (backscattering noise) can cause a problem in ultrasonic testing as it decreases the signal to noise ratio (SNR) for each ultrasonic measurement. As will be seen later in this thesis, materials such as refractory bricks and concretes with coarse aggregate can significantly increase this problem.

In general, two important sources of noise can be considered in the case of ultrasonic signals. The first source is caused by scattering of ultrasonic waves from the coarse grains, this effect is known as backscattering noise. The larger the grain size or the greater the number of grains leads to a higher noise level and can masks the fault echo, thus decreasing the SNR. Another source of noise is caused by the electronic circuitry. The electronic noise doesn't have the same effect as the backscattering noise and the level is much lower than backscattering noise. In ultrasonic testing, both backscatter and electronic noise contributions are critical, and ways of reducing their effects are very important [12]. Signal loss also occurs because of absorption, where ultrasonic energy is converted to heat within the medium [13].

1.4 Effects at interfaces

When a wave encounters a boundary between two materials, most of the acoustic energy will be transmitted into the material. Some of the energy will be reflected, due to the different impedance of the materials [14]. Acoustic impedance, *Z*, may be defined as the product of a medium's density, ρ, and its acoustic velocity, *V*: as shown in the equation below:

$$Z = \rho V \tag{1.3}$$

This relationship determines the reflection properties at a boundary. There are many studies involving acoustic impedance conducted in this field to enhance the ability of ultrasonic system [7,15-17]. In addition, an understanding of the value of the acoustic impedance of the material to be tested are not only able to help in providing a good experimental set up, but also assist the analysis and data processing procedure [12,18].

The reflection coefficient (R) between two media with impedances Z_1 and Z_2 was derived in the nineteenth century by Poisson and the reflection coefficient is expressed mathematically as follows:

$$R = \frac{Z_2 - Z_1}{Z_2 + Z_1} \tag{1.4}$$

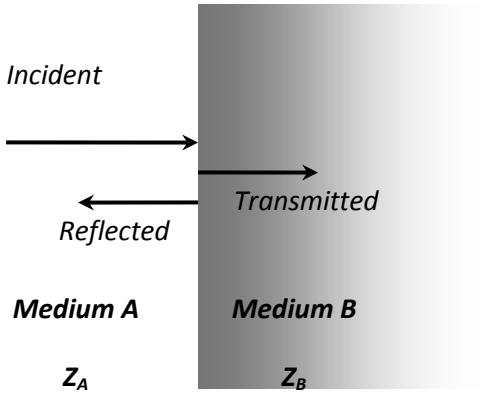

Figure 1.2: Reflection and refraction of an incident plane wave at an interface between two media

When a sound wave crosses a boundary between two dissimilar materials with different speeds, at any angle other than normal incidence, both its speed and wavelength will alter causing the incident wave to bend according to the speed in the medium [7,19]. This phenomenon is known as refraction and is shown schematically in Figure 1.3. The relationship between the angles of the wave before and after it crosses the boundary between the two materials is described by Snell's Law as:

$$\frac{\sin\theta_i}{\sin\theta_t} = \frac{V_A}{V_B} \tag{1.5}$$

Where θ_i – is the incidence angle, θ_t – the refraction angle, V_A – the velocity in medium *A* and V_B – is the velocity in medium *B*

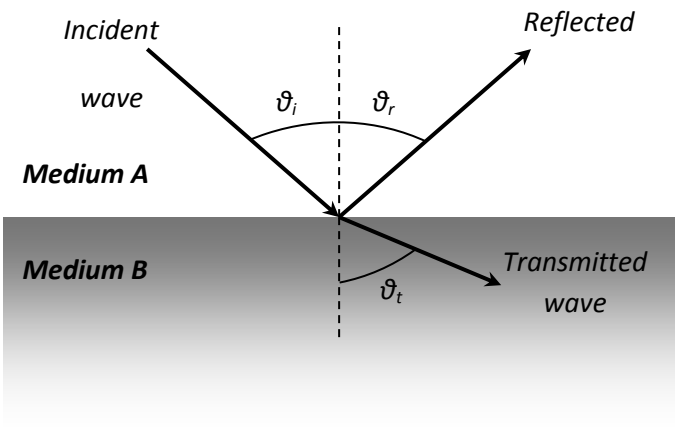

Figure 1.3: Reflection and refraction angle of an incident plane wave at an interface between two media.

From Figure 1.3 it can be seen that the angle of the reflected wave is equal to the angle of the incident wave, $\theta_i = \theta_r$, with this expression being valid for both incident longitudinal and shear waves. However, when $V_B > V_A$ it is possible to have an incidence angle with the refraction angle, $\theta_t = 90^o$, where the transmitted wave travels along the interface between the two media. In this situation, the incident angle is known as the critical angle. For incident angles greater than the critical angle, the wave is completely reflected and no energy is transmitted into the second medium [20].

Mode conversion [11] can occur when one of the media is a solid [23]. The incident angle and the critical angles of a material also play an important role in determining the occurrence of mode conversion [21]. Many ultrasonic applications have been designed to utilise the mode conversion phenomena [20,22-23]. One popular example of mode conversion is the conversion of longitudinal waves into shear waves and vice versa. Figure 1.4 shows a simple example of mode conversion.

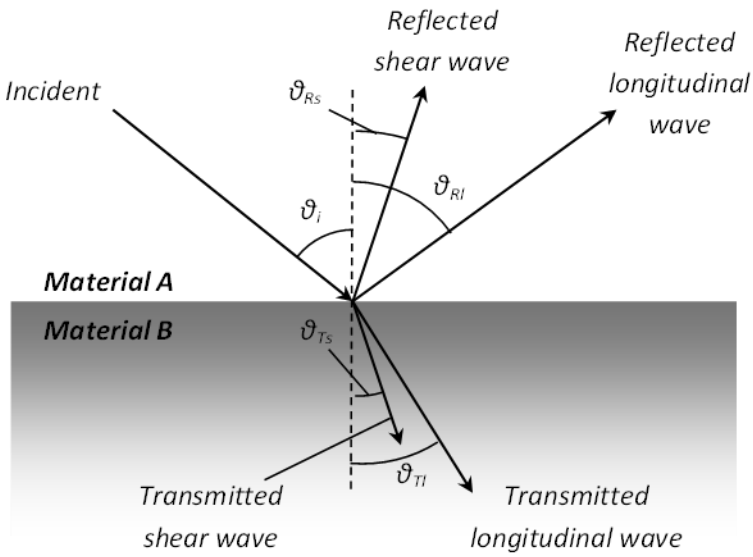

Figure 1.4: Showing mode conversion of a longitudinal wave incident upon a boundary between two materials.

Assuming that both the velocity and pressure in both mediums are constant at all points on the boundary, Snell's law gives:

$$\frac{\sin\theta_i}{V_{lA}} = \frac{\sin\theta_{Rs}}{V_{sA}} = \frac{\sin\theta_{Ts}}{V_{lB}} = \frac{\sin\theta_{Tl}}{V_{sB}} \quad , \tag{1.6}$$

where V_{lA} and V_{sA} are the velocities of the longitudinal and shear waves respectively in medium *A* and v_{lB} and v_{sB} are the velocities of the longitudinal and shear waves respectively in medium *B*. Due to mode conversion, there are two critical angles at which surface waves are produced. At the first critical angle, if a longitudinal wave is incident upon a surface, the generated surface wave will have a longitudinal component in the direction of propagation, and a transverse component perpendicular to the surface also known as Rayleigh wave. If the wave is incident upon a plate of finite thickness, then the transmitted wave will bounce between the two surfaces of the plate with mode conversion occurring as the waves are reflected. As a result, the longitudinal wave and shear wave inside the plate are coupled together; the resultant wave is then a Lamb wave.

1.5 Ultrasonic transducers

The transducer is one of the most important component of an ultrasonic system. The most essential part in the ultrasonic transducer is the piezoelectric element, which functions to convert electrical signals into mechanical vibrations and convert mechanical vibrations into electrical signals. There are several factors that influence the behavior of a transducer such as the type of material, mechanical and electrical construction and external mechanical loads. Mechanical construction comprises of parameters such as the radiation surface area, mechanical damping, housing, connector type and other variables of physical construction.

There are various types of transducers for specific purposes according to the applications needed. For example, a transducer which has a high center frequency is suitable for the detection of small defects in homogeneous materials because of its resolution power, but it is not suitable for testing composite materials or concrete. Resolution is the ability to locate defects near the surface or in close proximity in the material and a highly damped transducer usually produces better resolution.

Understanding the concept of frequency range or bandwidth of ultrasound is very important in order to choose an appropriate transducer for any application. Lower frequencies in general provide greater energy and penetration in a material (still depending on the type of material), while higher frequency transducers provide greater sensitivity to small discontinuities even though their penetration power isn't optimal. Meanwhile, highly damped transducers will respond to a broader frequency range and can give the transducer better resolving power.

The majority of transducers used for ultrasonic NDT contain piezoelectric materials [24]. The active element in ultrasonic transducer (Figure 1.6) is the core of the transducer as it converts the electrical energy to acoustic energy, and vice versa. As illustrated in Figure 1.5, when an electric field is applied across the material, the polarized molecules will align

themselves with the electric field, resulting in induced dipoles within the molecular or crystal structure of the material (Figure 1.5(b))[25]. This alignment of molecules will cause the material to change dimensions. This phenomenon is known as electrostriction. In addition, a permanently-polarized material will produce an electric field when the material changes dimensions as a result of an imposed mechanical force. This phenomenon is known as the piezoelectric effect. There are materials that naturally have the piezoelectric ability such as topaz and quartz but the most common piezoelectric material used in UT transducers is PZT (Lead Zirconate Titanate), although other materials are used for special applications, such as in environments where a high temperature exists.

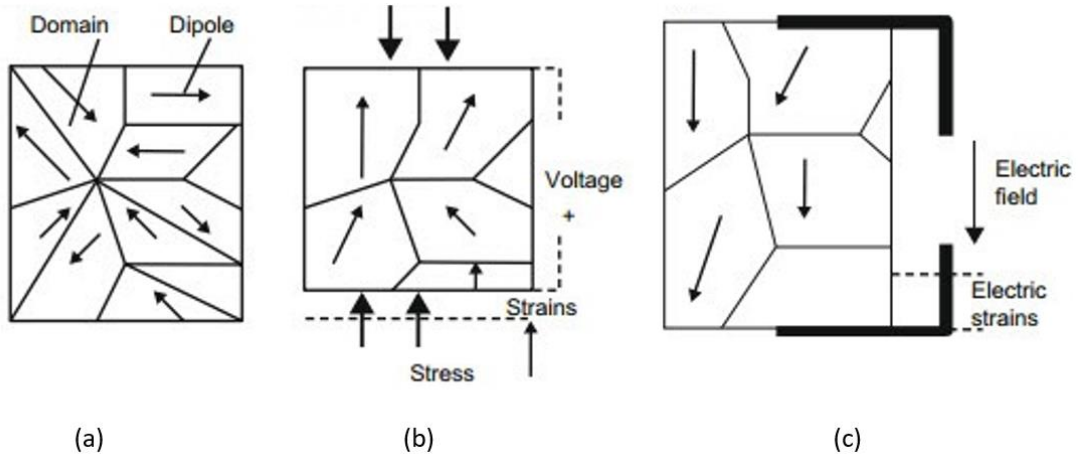

Figure 1.5: Behaviours of piezoelectric materials: (a) non polarized state when no electricity are applied, (b) polarized state when compression stressed are imposed, (c) polarized state when electric field is applied [25]

The typical construction of a conventional piezoelectric transducer is shown in Figure 1.6(a). Normally, materials are tested using a contact method, where the transducers are held against the sample, usually with some form of a coupling gel to remove any air layer that would hinder transmission. The most important component of an ultrasonic transducer is the active element which determines the central frequency and other properties of the transducer. In addition, other components include the backing material, wear plate, matching layer, and electrical circuits.

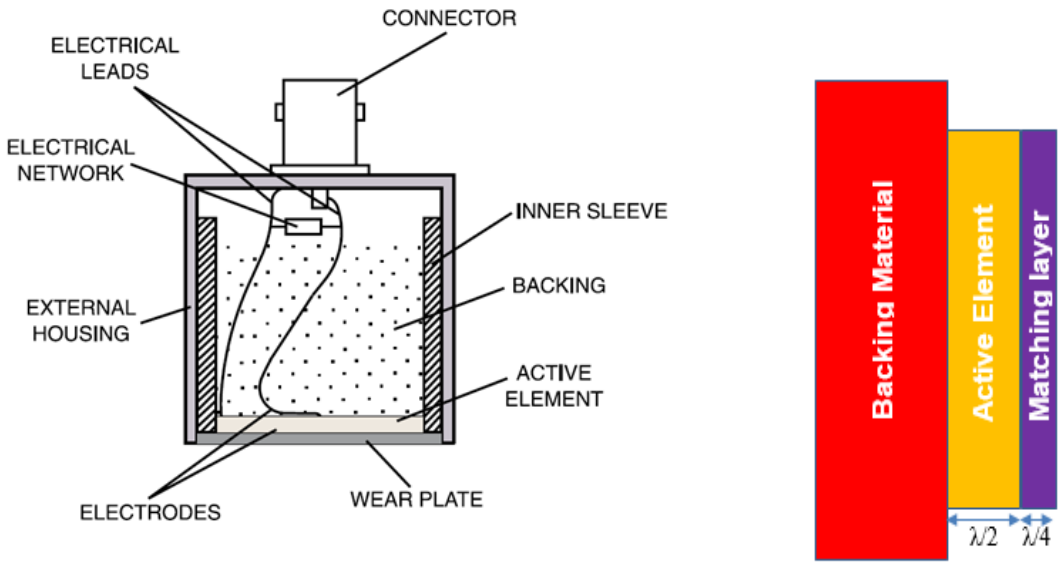

Figure 1.6: Schematic of typical construction of a piezoelectric transducer. (a) A typical contact transducer, and (b) use of a matching layer in water immersion [25].

In immersion, suitable liquid such as water and oil are used as the coupling medium. In order to get as much energy out of the transducer as possible, an impedance matching called matching layer is placed between the active element and the face of the transducer (Figure 1.6(b)). Optimal impedance matching can be achieved by having the matching layer with the thickness of 1/4 of the desired wavelength. This condition is for the maximum transmission amplitude into the medium.

Besides the active element, the backing material is also one of the most important component for an ultrasonic transducer. The backing material is a material that has a great influence on the damping characteristics of the transducer. The most effective backing material is the one with impedance similar to the active element. This kind of backing material can produce better sensitivity when used in the ultrasonic transducer. As the mismatch in impedance between the active element and the backing material increases, material penetration increases but transducer sensitivity is reduced.

1.6 Thesis overview

This thesis looks at novel applications of ultrasound at Sub-MHz frequencies in assessing materials with high degree of attenuation. Chapter 1 started by describing some basic background of ultrasonic wave propagation and discussion on the basic properties of sound, such as transmission mechanisms through a medium, absorption, attenuation, propagation across the interface, beam spread and mode conversion. There are also some explanations on ultrasonic transducer design and piezoelectric materials.

Chapter 2 is an overview of ultrasonic testing of highly attenuation materials. This includes a brief discussion on propagation of ultrasonic signals in high attenuation materials, as well as a review of attenuation and scattering mechanism that are a very important element in this study.

Chapter 3 gives details of experimental design, including a discussion about ultrasonic coded signal such as frequency modulated chirps and the binary sequences. An explanation of signal processing techniques is also included in this chapter.

Chapter 4 contains a description of the system that was specifically developed to deal with such attenuating materials. It covers both the hardware and the software that has been used within the system, as well as the way they have been integrated together.

Chapter 5 involves one of the industrial samples that has been used in this study, namely a polyurethane polymer structure. It was shown how the developed system that utilised sub-MHz frequency ultrasound can be used to detect some anomalies within the polyurethane structure.

Chapter 6 is the second chapter concerning experimental work, this time involving concrete samples. The chapter gives a review on structural problems in reinforced concrete and some brief discussions on the testing of on refractory brick anchors. There is also

discussion on several signal processing techniques that have been introduced to solve specific problems involving sample of concrete.

Chapter 7 focusses on composites from two different industries, namely insulating materials from oil and gas industry and the multi-layered composites that are widely used as an aircraft structure. It has been shown how the developed ultrasonic technique can detect some changes under the insulators. Besides, it has also shown the procedures have been used to test the multi-layered honeycomb structure.

Finally, the conclusions are presented in Chapter 8, together with suggestions for further work.

References

[1] C. S. Desilets, J. D. Fraser, and G. S. Kino, "The design of efficient broad-band piezoelectric transducers," *IEEE Trans. Sonics Ultrason.*, vol. 25, no. 3, pp. 115–125, 1978.

[2] G. Rus, S. C. Wooh, and R. Gallego, "Design of ultrasonic wedge transducer," *Ultrasonics*, vol. 43, no. 5, pp. 391–395, 2005.

[3] J. Shriki, "Ultrasound physics," *Critical Care Clinics*, vol. 30, no. 1. pp. 1–24, 2014.

[4] H. Choi and J. S. Popovics, "NDE application of ultrasonic tomography to a full-scale concrete structure.," *IEEE Trans. Ultrason. Ferroelectr. Freq. Control*, vol. 62, no. 6, pp. 1076–85, 2015.

[5] A. A. T. Grattan K T V, *Ultrasonic sensors*. IOP Publishing Ltd., 1997.

[6] "wave propagation." [Online]. Available: https://www.nde-ed.org/EducationResources/CommunityCollege/Ultrasonics/Physics/wavepropagation.htm.

[7] Y. Inoue, H. Kikura, H. Murakawa, M. Aritomi, and M. Mori, "A study of ultrasonic propagation for ultrasonic flow rate measurement," *Flow Meas. Instrum.*, vol. 19, no. 3–4, pp. 223–232, 2008.

[8] R. Lakes, H. S. Yoon, and J. Lawrence Katz, “Ultrasonic wave propagation and attenuation in wet bone,” *J. Biomed. Eng.*, vol. 8, no. 2, pp. 143–148, 1986.

[9] M. Hardt, N. V Ruiter, and H. Gemmeke, “Analysis of The Influence of Multiple Scattering on The Reconstruction of Ultrasound Tomography Signals using Synthetic Aperture Focussing Technique,” in *Systems, Signals and Image Processing (IWSSIP), 2012 19th International Conference on*, 2012, pp. 11–13.

[10] R. Bruce, “Ultrasonic Scattering from Imperfect Interfaces: A Quasi-Static Model,” vol. 4, 1985.

[11] K. K. Shung, “Ultrasonic Scattering in Biological Tissues,” *The Journal of the Acoustical Society of America*, vol. 94, no. 5. p. 3033, 1993.

[12] S. K. Verma, S. S. Bhadauria, and S. Akhtar, “Review of Nondestructive Testing Methods for Condition Monitoring of Concrete Structures,” vol. 2013, no. 2008, 2013.

[13] M. L. Mather, P. H. Charles, and C. Baldock, “Measurement of ultrasonic attenuation coefficient in polymer gel dosimeters.,” *Phys. Med. Biol.*, vol. 48, no. 20, pp. N269–75, 2003.

[14] S. Popovics, J. L. Rose, and J. S. Popovics, “The behaviour of ultrasonic pulses in concrete,” *Cem. Concr. Res.*, vol. 20, no. 2, pp. 259–270, 1990.

[15] M. J. W. Povey, “Ultrasonics in food engineering Part II: Applications,” *J. Food Eng.*, vol. 9, no. 1, pp. 1–20, 1989.

[16] I. D. Park G, Cudney H, “Impedance-based health monitoring of civil structure components,” *J. Infrastruct. Syst.*, vol. 6, no. 4, pp. 153–1670, 2000.

[17] G. M. L. Svilainis, “Power amplifier for ultrasonic transducer excitation,” *Issn 1392-2114 Ultragarsas*, vol. 1, no. 58, pp. 30–36, 2006.

[18] V. Bucur and I. Böhnke, “Factors affecting ultrasonic measurements in solid wood,” *Ultrasonics*, vol. 32, no. 5, pp. 385–390, 1994.

[19] J. A. Gallego-Juárez, *Ultrasonic Transducers*. 2012.

[20] G. Walter, “Mode Conversion of Ultrasonic Waves at Flat Boundaries,” *IEEE Trans. Sonics Ultrason.*, vol. 11, no. 1, pp. 1–3, 1964.

[21] Y. Cho, “Estimation of ultrasonic guided wave mode conversion in a plate with

thickness variation.," *IEEE Trans. Ultrason. Ferroelectr. Freq. Control*, vol. 47, no. 3, pp. 591–603, 2000.

[22] J. M. Castro, D. F. Geraghty, S. Honkanen, C. M. Greiner, D. Iazikov, and T. W. Mossberg, "Demonstration of mode conversion using anti-symmetric waveguide Bragg gratings," *Opt. Express*, vol. 13, no. 11, pp. 4180, 2005.

[23] K. J. Langenberg, M. Berger, T. Kreutter, K. Mayer, and V. Schmitz, "Synthetic aperture focusing technique signal processing," *NDT International*, vol. 19. pp. 177–189, 1986.

[24] K. Colquhoun, A. Alam, and D. Wilson, "(iv) Basic science: Ultrasound," in *Current Orthopaedics*, 2005, vol. 19, no. 1, pp. 27–33.

[25] M. Pasquale, "Mechanical sensors and actuators," in *Sensors and Actuators, A: Physical*, 2003, vol. 106, no. 1–3, pp. 142–148.

Chapter 2

Review of Ultrasonic Testing of Highly Attenuating Materials

2.1 Introduction

Non-destructive Evaluation (NDE) has been defined as a method or technique used to examine objects, materials, or systems without impairing their future usefulness [1]. NDE techniques are widely used in the world within various fields including construction, manufacturing, medicine, agriculture, defence and power generation (especially nuclear power) [2-4]. It has become a very important element in human life, widely used to examine the structural integrity of plant, building, structure or system. Ultrasonic testing (UT) is one of the important technique in NDE. This technique was introduced relatively late compared to other NDE techniques such as Magnetic Particle Technique (MT) [5], Radiography Technique (RT) [6], Dye Penetrant (PT) [7], and Eddy Current Technique (ET) [8]. Besides that, other techniques are including Laser Shearography, Electromagnetic Acoustic Transducer (EMAT) and Infra-Red Thermography [9-11].

Each NDE technique provides its own advantages and disadvantages and there are also limitations that make these NDE techniques complement each other. For example, the radiography technique has advantages over objects of high density and thickness because of its high penetrating power (depending on the type of radiation and the power used) but is limited in its ability on layered materials [12] even though it also can be used on these kind of materials with some additional arrangement. The fact that it uses ionic radiation often adds additional safety constraints to the user. Optical techniques such as laser shearography have a high resolution [13] but do not work well in thicker samples. In UT, various technologies are available, but some have limited use. For example, Electromagnetic

Acoustic Transducers (EMATs) can only be used on electrically conducting objects, and cannot be used on many polymer composites and concrete, even though they have been reported for use in carbon fibre composites (where there is some conductivity in the carbon fibre themselves) [14-15]. Although UT is an important technique in NDE, there are still limitations to the existing technique. This research will investigate one of these – the ways in which ultrasound can be used to inspect materials that have a high degree of attenuation where attenuation and scattering limit the effectiveness of NDE. The following will briefly review conventional ultrasonic NDE, before going on to describe some specific problems such as attenuation and scattering in difficult materials.

2.2 Ultrasonic testing (UT)

UT has become an important inspection tool in many industrial fields, and is used routinely in many industries for NDE and condition monitoring. Ultrasound can be used in many different modes, including longitudinal and shear waves in thick samples and guided modes in thinner plates. For example, ultrasonic guided waves have been used to inspect Carbon Fibre Reinforce Composite (CFRP) rods which are widely used in aerospace applications [3]. This ultrasonic technique has proven to be a good tool in defect detection of CRPF with multiple dimensions. Lillamand *et al.* [16] proposed to evaluate the mechanical stress state of a concrete body via ultrasonic waves by using the link between ultrasonic velocities and mechanical stresses provided by the acoustoelasticity theory.

In the nuclear industry, ultrasonic testing has been playing a big role where safety precautions are a serious matter, hence all parts and structures in nuclear power plants must be ensured to be in 100 percent safe conditions at all times, and most of these parts and structures have been tested using ultrasonic techniques for decades. For example, ultrasonic guided wave dispersion curves had been used to inspect feeder pipes in the pressurized hot

water reactor (PHWR) [17]. Hundreds of kilometres of pipeline, especially the elbows and welded joints in nuclear power plants (NPP) are vulnerable to aging and other types of damage. Therefore, the condition of a piping system requires regular inspection, so that the plant can be kept in a safe condition at all times. Failure to ensure that the component and structures are in good condition can harm not only the company but also jeopardise thousands of people in surrounding areas.

Ultrasonic testing has also been applied in the oil and gas and petrochemical for many years. This technique is becoming more popular, especially in structural health pipe monitoring by attaching a sensor to monitor pipe structural deterioration [18-19]. In addition, the fact that the guided wave technique has become more reliable, has opened a new dimension in ultrasonic testing in recent years. The technique can offer continuous monitoring which makes it relevant for structural health monitoring and it has often been used as a process to implement a damage identification strategy for varied infrastructures [2].

Ultrasound technology has also been used in food industry in many aspects from monitoring process, food processing to velocity measurement [20]. Ultrasonic non-contact method is becoming more popular in the food industry because of hygiene and also the fact that it can offer a fast and real time measurement. Gan *et al.* [21] have reported the use of non-contact ultrasonic in performing quality measurement of food product. Meanwhile, Pallav *et al.* [22] had also used Air-coupled ultrasonic in evaluating food products.

An example of an important industrial material is concrete. Popovic and Shickert [23] were among the earliest reserchers who had tried to utilise ultrasonic wave in assessing concrete behavior [24-25]. Later on, the ability of the ultrasonic system in performing in-situ assessment has been recognized, and this trend is increasing when compared to traditional random sampling of concrete for material analysis. Additionally, ultrasonic has

been used as testing tools in various sectors and for that reason, several methods of testing and analysis have been introduced to meet the growing needs of industry. Utrasonic characterization techniques have thus been used to study the physical properties of this material [26]. The strength of concrete is one of the main features that has been studied, using ultrasonic pulse velocity and ultrasonic signal behaviour [27]. The advancement in computer technology has also paved the way for researchers to use modelling techniques in combination with ultrasonic techniques [28].

2.3 Propagation of ultrasonic signals in high attenuation materials

Ultrasonic propagation depends on the geometry and the physical characteristics of the material [29]. The presence of a defect or imperfection causes scattering and reflection, and this is the basis for some ultrasonic testing, where the scattered and reflected signal is used to determine the location and nature of the defect. Time of flight diffraction (TOFD) for example, a method that utilized ultrasonic testing technique. TOFD is very effective in locating defects in welded samples where it provides a wide area of coverage with a single beam by exploiting ultrasonic beam spread [29]. But for materials that have inhomogeneous particles such as concretes, the situation becomes more complicated because of the presence of granular aggregate in concrete can be misinterpreted as a defect or inclusion. Thus, for example, the signal scattered from aggregate may mask the defect signal.

The amplitude of the reflected signal is usually affected by certain characteristic of the defect or inclusion, such as its conformation (geometry contour), orientation (90^0 reflectors visible, at 0^0 practically invisible), roughness (high roughness involves scattering), the size (area), While, the characteristics of the test sample that affects the amplitude of the signal reflection are related to its degree of surface roughness, which depends on the transmission of ultrasonic beam through the interface transducer and material [30-31]. In

practice, defects are of finite size, and reflected signals depend on the ratio between the wavelength (**λ**) produced by the transducer and the size of the discontinuity (anomaly, defect, inclusion or even the particle size of the material (q)). There are three main cases of interest:

$q \geq \lambda$: Size of discontinuity greater than the wavelength of the propagated ultrasonic signal. This situation is good because the ultrasonic wave is reflected back according to the rules of geometrical acoustic, creating a well - defined reflected beam from the obstacle (called geometric scattering).

$q = \lambda$: Size of discontinuity is the same as the wavelength of the propagated ultrasonic signal (known as Mie scattering). The reflection and scattering effects are very complicated.

$q \leq \lambda$: Size of discontinuity is much smaller than the wavelength of the propagated ultrasonic signal. The obstacle reflects the signal in all directions (called Rayleigh scattering). Signals returned to the transducer will be very small in amplitude.

The above phenomena will happen following interaction with both defects and any components within the material structure itself. Concrete is an excellent example, where aggregate is likely to cause scattering and reflection from different aggregate sizes. This will affect not only the ability to distinguish the wanted signal from background scattering, but also will cause the ultrasonic signal to lose amplitude as it travels through the material, hence decreasing the SNR of the measurement. In extreme cases, the following can occur:

i. Interaction of ultrasonic signal and the particles inside the material that lead to loss the most of signal or in the worst case the whole signal being attenuated or absorbed.

ii. If the particle size of the object being tested is large, such as aggregates in concrete material, they can cause ultrasonic signal lost due to scattering effect and which is often misinterpreted as a defect or inclusion.

Because of the complicated situations outlined above, various authors have investigated computer simulation methods to consider highly scattering and attenuating media. Liu *et al*.[32] reviewed modelling of ultrasonic wave propagation in polymer matrix particulate and fibrous composites. Meanwhile, Nakahata *et al.* [33] introduced three-dimensional numerical modelling to understand the characteristics of ultrasonic propagation in concrete material and for that they have proposed a time-domain simulation tool based on the finite integration technique (FIT) and an image-based modelling approach. In addition there are many other studies that have investigated the propagation of the ultrasonic signal in the range of anisotropic materials using novel approaches [34-35].

Although many methods and techniques have been introduced to enhance the ability of ultrasonic testing system in materials with high attenuation and scattering [36], there are still limitations with existing methods especially low in SNR. Additional problems arise in certain situations, such as the stability of transducers at high temperature [37-38].

2.4 Attenuation and scattering mechanisms

The general idea with ultrasonic techniques is that a higher spatial resolution is obtained by increasing the frequency. However, attenuation and scattering also increase considerably with frequency, to the extent that the effective range allowed for ultrasonic inspection is limited. Attenuation relates to two distinct physical phenomena: scattering and intrinsic absorption (leading to attenuation). Attenuation is a measure of dissipative energy, converted to heat, as the wave travels through the material. Absorption occurs in all

materials as the result of thermodynamic relaxation mechanism that converts energy from ultrasonic wave into some other form [39].

Lionetto *et al*. [38] reported their study of polymer characterization using ultrasonic wave propagation. They presumed that the absorption of ultrasonic waves was related to the energy dissipation in the material. They concluded that the extent of energy absorption was related to molecular rearrangements in the polymer structure, such as glass transition, melting, secondary transitions, and to chemical reactions such as those occurring during curing of thermosetting resins. Scattering is often the predominant form of attenuation in heterogeneous materials, causing the waves to scatter in a direction that is different from the incident wave. Scattering effects should be considered in ultrasonic systems since they can have a significant effect on the measured ultrasonic properties, making the velocity and attenuation dependent on particle size as well as concentration [40].

Researchers have been trying to enhance the capabilities in assessing the types of materials with low SNR, such as concrete and composites. Among these improvements, techniques using pulsed laser generation and detection have been introduced [41]. Scales and Malcolm [42] reported that laser can be used to excite and detect ultrasonic waves in a wide range of materials. In this study, they demonstrated that a hybrid laser ultrasonic technique is capable of visualising the complex dynamics of diffraction, multiple scattering, and mode conversion of the ultrasonic signal in the tested object. Alongside the hybrid techniques, researchers are also trying to improve the ability of ultrasonic testing using signal and image processing methods [43]. For example, Zhu *et al.* [44] implemented adaptive filtering and detection in order to enhance the capability of their ultrasonic experimental set up. Laboratory measurements have been compared with theoretical calculations to investigate the influence of the shape and dimension of the transducer on the sound field patterns [31,45]. King [27] developed a quasi-static model for the ultrasonic

transmission and reflection on the imperfect interfaces. Meanwhile, Li *et al.* [46] presented a result that focused on the relationship between thickness and ultrasonic signals. In all cases, the aim was to improve defect detectability.

2.5 Some typical materials of interest

This thesis looks at various different materials in which attenuation and scattering are important features. Many studies have been performed in order to improve the ultrasonic testing results for these materials [43-45]. Some of these are now described.

2.5.1 Polymer-based materials

There are two types of polymer-based materials which are of interest to this thesis, because of their properties in terms of signal loss. The first of these is viscoelastic polymers and rubbers, where loss is mainly due to attenuation within the material itself. In thick sections, even moderate levels of attenuation can cause signal loss and a decrease in SNR. The second class of materials is polymer matrix composites. These contain polymers and other additives, such as fibres and powders, to give them additional mechanical and other properties of interest. The macroscopic properties of this type of composite are sensitive to the shape, size, and distribution of inclusions. While substantial research efforts have been made to calculate the effective elastic moduli of a polymer composite matrix, the dynamic ultrasonic behaviour in this material differs greatly from the static material response, as the propagation of periodic and transient waves is complicated due to the combination of wave scattering from material interfaces and dissipation in the matrix [32].

Among the studies conducted on the propagation of ultrasonic waves in polymer is the work performed by Yang [47], where a nonlinear ultrasonic technique for detecting micro damage in polymer bonded explosive (PBX) was described. This technique has been used to study the relationship between the degree of damage PBX components with

nonlinear coefficient and signal distortion. In addition, there are other studies that have utilized ultrasonic testing techniques that visualize the propagation of ultrasonic waves in solids, including composite laminates [48]. It provides a moving diagram of traveling waves through the use of a pulsed laser source that scans a test piece. A non-contact scan by the pulsed laser for ultrasound generation with reception at a fixed point enables the inspection of an arbitrarily shaped object. The results of this study successfully visualised the wave scattering due to impact-induced delamination. Therefore, they also concluded that the reliable detection of damage and the advantages of the proposed technique are applicable to inspections of composite structures. Fibre reinforced polymers is a very important material especially for aircraft structure. Because of it properties and behaviours, ultrasonic became one of the most important testing technique used to inspect its structural integrity. There are several studies that have been done in this area [1,4,49-50].

2.5.2 Concrete Materials

Concrete has become one of the important materials in the building and construction industry for the past few centuries. However, its physical properties are really hard to be penetrated by ultrasonic signals and present many difficulties to NDE practitioners when performing their duties. Because of these reasons, researchers keep searching for better way to inspect this material, which usually comprises of cement, sand and aggregate (which can be up to a few centimeters in diameter) [16,18,31]. This means that there is a specific frequency range suitable for use in the testing of concrete as described latter in this chapter. Within this commonly used range, the wavelength (λ) is smaller than the size concrete sample to be tested (L) but larger than the particle size of a grain within a sample of concrete (d). The use of ultrasonic signal wavelength size larger than the size of the concrete is to reduce the interaction between heterogeneities and ultrasonic waves, also known as

scattering. Therefore, the range in which most conventional imaging procedure can be operated is determined by the expression:

$$d < \lambda < L$$

One of the most popular study of ultrasonic technique of concrete was performed by Krause *et al.* [51], in this study, they applied pulse-echo and simulation of wave propagation to test concrete specimens with metal ducts. In view of the fact that some materials cause high scattering of ultrasonic signals, researchers have been trying to enhance UT techniques to boost the capabilities of the existing methods. Kazys *et al.* [52] used air-coupled ultrasonic techniques to investigate the detection and visualization of defects in composite materials using the interaction of Lamb Waves with inhomogeneities. Air-coupled ultrasonic techniques have also been used to investigate the benefit of using time-frequency analysis for both waveform retrieval and imaging in the presence of low signal levels [53].

There are many other ultrasonic techniques that have been developed such as time reversal technique and broadband backscatter technique. Fink *et* al. [54] used broadband backscatter to improve the signal amplitude of ultrasonic measurements when performing non-destructive evaluation in acoustical inhomogeneous materials. Adaptive filtering and detection techniques were used in a study where a cell-averaging constant false alarm rate (CFAR) detector was used by them to detect signals automatically [44]. Normally, this technique is suitable for a sample that can cause grain boundary scattering when tested using ultrasonic techniques.

The Systematic Aperture Focusing Technique (SAFT) is a promising approach in UT which has been used for the past two decades [55-57]. Li *et al*. [58] used this technique to validate the potential of this technique and they established an experimental system to perform a cross-surface scan of the test specimen. A SAFT processing program was applied in their study to produce a 2-D display of the inner structure of the specimen based on the

measured backscattered ultrasonic signals. One of the most important features in SAFT is that this technique can be used to improve SNR of the measurement [60]. Blouin et al. [61] were the earliest researchers that proved this technique was capable of improving SNR of ultrasonic measurement.

2.5.3 Multi-layered composite structures

Composite materials are increasingly used in the production of aerospace and marine structures, because of their high strength to weight ratio. A multi-layered composite structure is a structure that consists of several layers of certain materials such as aluminum or composite bonded together using adhesive material. This structure typically has strong physical properties but is light making it an important material in a wide range of industries, particularly the aerospace industry. Neither commercial aerospace industry nor military application have widely employed a variety of bonded aluminium and composite structures as the main parts of their body. In fact, almost all the aircraft that are available today use multi-layered structure containing adhesive materials in both the manufacturing process and maintenance of important parts of the structure.

Although the process of research and development to produce a stronger and durable adhesive are continuously conducted, each multi-layered structure still requires a reliable NDT technique. In this regards, the technique has been used to ensure the integrity of the structures especially at the bond line area either in manufacturing or maintenance. However, up to now there is no technique that can be claimed as totally reliable and trustworthy especially for testing involving so called kissing bonding structure which has good mechanical bonding but poor adhesion. Failure to detect this condition can be dangerous, especially considering critical components in an aerospace structure. Composite materials such as carbon fiber reinforced plastics (CFRP), glass fiber laminated metal and also multi-

layered honeycomb structure are major components of modern aircraft construction. Due to the requirements of safety and reliability, the materials must be tested during the manufacturing process as well as periodic maintenance.

There are a wide range of inspection approaches for composite materials such as ultrasonic, radiography, laser shearography, and mechanical impedance analysis. [1,10,62]**.** Among these inspection strategies, ultrasonic methods have been widely applied to composite structures in the aerospace sector, for inspection both during manufacture and in service. An ultrasonic technique that is extensively used to test these materials is the immersion ultrasonic technique. Air-coupled techniques can attract more attention even though its capability is not as good as immersion techniques. This is due to some components made of honeycomb structures are not suitable for immersion technique because they are required to be tested in a water tank which can cause water ingress to the structure.

Since phased arrays were introduced some years ago, they were become increasingly popular, and they are progressively used to replace single element transducers that are normally used in the immersion technique. Li *et al* [46] introduced procedures that improved detectability of ultrasonic array system based on modifications to the Total Focusing Method (TFM) of processing ultrasonic array data to form an image. They have shown that the TFM has been modified to include the directional dependence of ultrasonic velocity in an anisotropic composite laminate, and practical procedures for measuring the direction-dependent velocity profile. To date, the use of arrays for composite inspection has been primarily motivated by the desire to increase inspection speed of normal incidence inspection. In general NDT inspection, the use of arrays can provide advantages because it can accelerate the testing time for several different measurements. Inspections carried out using a single-element can be run simultaneously using the array.

2.6 Rationale of the research

Despite the fact that many techniques and methods have been introduced to enhance the capability of ultrasonic techniques and improve its weaknesses, especially when dealing with inhomogeneous materials such as concrete and composites, there is still a loophole that should be explored in the field of UT. Among the elements that can be studied is ultrasonic sensors optimization, which was described earlier. There are many mechanical and physical variations in the properties of ultrasonic sensors, such as shape, size, type and frequency of waves which can affect the results of tests carried out. Wavelet-based 2D fusing of ultrasonic pulse-echo traces measured from two arrays radiating via orthogonal beams is one example of the complex methods that have been used [43,63-64].

However, there is a simpler and more effective way to solve this problem in which an ultrasonic system with a frequency of less than 1 MHz was used to obtain information about materials and structures. This method can improve the level of penetration due to scattering, attenuation can be reduced when the frequency is low [20]. This in turn will provide advantages when performing a test especially when carrying out tests on multi-layered structure, composites and also very thick and bulky materials.

The transducer is one of the major elements that will be studied in this work. Conventional piezoelectric (PZT) transducers will be used for frequencies below 200 kHz. However, there is also a different type of transducer that will be used in this study, and that is the Macro Fibre Composite (MFC) [65]. Although, they are primarily designed for use at frequencies up to 20 kHz, they can be used at frequencies up to 200 kHz. Even though they do not have the power output of conventional PZT, it is normal for a composite to have a greater natural bandwidth. This makes them ideal for pulse compression technique, where greater bandwidth is a big advantage. An investigation of the different shapes of PZT element will also be described in this project. The PZT with special shapes such as a wedge

and conical random-shape upper surface will be prepared to improve the available bandwidth over conventional designs [26].

Different types of waveforms will be investigated which take advantage of the important features of the transducers chosen (MFC and piezocomposites) both of which can have a wide bandwidth. The aim is to improve signal to noise ratio for inspections conducted. Waveforms such as stepped, linear and non-linear chirps, as well as Golay codes, will be used throughout this study [66]. The idea is to get a high resolution time after cross-correlation operation to improve the axial resolution. The operation is known as pulse compression operation where long-time duration signals are transmitted into the sample while output processing afterwards can show a short pulse. This is particularly important for highly absorbing and scattering materials such as composites, concrete, thick and multi-layer materials.

2.7 Conclusions

Ultrasonic testing has become an important technology, it is used at various stages in many sectors. NDT techniques have made some progress since they were introduced, especially with the progress of computer technology in recent years which has contributed to the rapid progress in research and development. In addition, many ultrasonic techniques and new methods have been introduced such as guided wave, ultrasonic phase array and hybrid (e.g. ultrasonic and laser-ultrasonic-thermography) to improve the ability of the ultrasonic techniques. The same goes for progress in terms of development of ultrasonic transducers which are many latest designs that have been introduced to optimize the ability of the technique. However, there are still many shortcomings and limitation in this ultrasonic technique which requires constant study so as to further enhance its capabilities. Materials such as composites, polymers, concrete and large components present challenges when

tested using ultrasonic techniques. Understanding the properties and behaviour of these materials, particularly in response to ultrasonic wave propagation should be reviewed effectively so that good and convincing results can be obtained when ultrasonic testing is conducted on these materials. The study will be focused on the production of an ultrasonic system for use on materials that have a high attenuation such as polymer, concrete, composite multi-layered and bulky material. It will emphasise the use of ultrasonic low frequency ultrasound below the MHz range. The work will also be devoted to the use of piezo composite transducers and will be combined with coded waveforms such as chirps and bipolar Golay that will provide advantages when used in conjunction with cross correlation techniques of signal procession. In addition, other signal processing and image reconstruction technique will also be exploited so that all the data and the result obtained from the results of this study can be analysed and displayed effectively.

References

[1] I. G. Scott and C. M. Scala, "A review of non-destructive testing of composite materials," *NDT Int.*, vol. 15, no. April, pp. 75–86, 1982.

[2] L. H. Lee, R. Rajkumar, L. H. Lo, C. H. Wan, and D. Isa, "Oil and gas pipeline failure prediction system using long range ultrasonic transducers and Euclidean-Support Vector Machines classification approach," *Expert Syst. Appl.*, vol. 40, no. 6, pp. 1925–1934, 2013.

[3] R. Raišutis, E. Jasiūnienė, R. Šliteris, and A. Vladišauskas, "The review of non-destructive testing techniques suitable for inspection of the wind turbine blades," vol. 63, no. 1, pp. 26–30, 2008.

[4] A. M. T. Hassan and S. W. Jones, "Non-destructive testing of ultra high performance fibre reinforced concrete (UHPFRC): A feasibility study for using ultrasonic and resonant frequency testing techniques," *Constr. Build. Mater.*, vol. 35, no. 0, pp. 361–367, 2012.

[5] M. Motozawa, Y. Iizuka, and T. Sawada, “Experimental measurements of ultrasonic propagation velocity and attenuation in a magnetic fluid.,” *J. Phys. Condens. Matter*, vol. 20, no. 20, p. 204117, 2008.

[6] H. Lowery, “Industrial Radiography,” *Optom. Vis. Sci.*, vol. 18, no. 11, p. 535, 1941.

[7] Anonymous, “NDT Procedure for Liquid Penetrant Inspection,” in *European Conference of Nondesructive Testing*, 2008, vol. 22, no. V, pp. 1–9.

[8] J. J. Van Vaals and A. H. Bergman, “Optimization of eddy-current compensation,” *J. Magn. Reson.*, vol. 90, no. 1, pp. 52–70, 1990.

[9] D. Francis, R. P. Tatam, and R. M. Groves, “Shearography technology and applications: a review,” *Meas. Sci. Technol.*, vol. 21, no. 10, p. 102001, 2010.

[10] Y. Y. Hung, Y. S. Chen, S. P. Ng, L. Liu, Y. H. Huang, B. L. Luk, R. W. L. Ip, C. M. L. Wu, and P. S. Chung, “Review and comparison of shearography and active thermography for nondestructive evaluation,” *Materials Science and Engineering R: Reports*, vol. 64, no. 5–6. pp. 73–112, 2009.

[11] A. Kylili, P. A. Fokaides, P. Christou, and S. A. Kalogirou, “Infrared thermography (IRT) applications for building diagnostics: A review,” *Applied Energy*, vol. 134. pp. 531–549, 2014.

[12] D. L. Novak and B. F. Bates, “Digital radiography: uses and limitations of the method.,” *Am. J. Roentgenol.*, vol. 152, no. 4, pp. 870–872, 1989.

[13] Y. Y. Hung and H. P. Ho, “Shearography: An optical measurement technique and applications,” *Materials Science and Engineering R: Reports*, vol. 49, no. 3. pp. 61–87, 2005.

[14] Y. Fan, S. Dixon, R. S. Edwards, and X. Jian, “Ultrasonic surface wave propagation and interaction with surface defects on rail track head,” *NDT E Int.*, vol. 40, no. 6, pp. 471–477, 2007.

[15] X. Jian, S. Dixon, R. S. Edwards, and J. Morrison, “Coupling mechanism of an EMAT,” *Ultrasonics*, vol. 44, no. SUPPL., 2006.

[16] I. Lillamand, J.-F. Chaix, M.-A. Ploix, and V. Garnier, “Acoustoelastic effect in

concrete material under uni-axial compressive loading," *NDT E Int.*, vol. 43, no. 8, pp. 655–660, Nov. 2010.

[17] Y.-M. Cheong, D.-H. Lee, and H.-K. Jung, "Ultrasonic guided wave parameters for detection of axial cracks in feeder pipes of PHWR nuclear power plants.," *Ultrasonics*, vol. 42, pp. 883–8, Apr. 2004.

[18] Z. Liu and Y. Kleiner, "State-of-the-art review of technologies for pipe structural health monitoring," *IEEE Sens. J.*, vol. 12, no. 6, pp. 1987–1992, 2012.

[19] O. Kaynakli, "Economic thermal insulation thickness for pipes and ducts: A review study," *Renewable and Sustainable Energy Reviews*, vol. 30. pp. 184–194, 2014.

[20] S. Martini, C. Bertoli, M. L. Herrera, I. Neeson, and A. Marangoni, "Attenuation of ultrasonic waves: Influence of microstructure and solid fat content," *J. Am. Oil Chem. Soc.*, vol. 82, no. 5, pp. 319–328, May 2005.

[21] T. H. Gan, P. Pallav, and D. A. Hutchins, "Non-contact ultrasonic quality measurements of food products," *J. Food Eng.*, vol. 77, no. 2, pp. 239–247, 2006.

[22] P. Pallav, D. A. Hutchins, and T. H. Gan, "Air-coupled ultrasonic evaluation of food materials," *Ultrasonics*, vol. 49, no. 2, pp. 244–253, 2009.

[23] K. Komloš, S. Popovics, T. Nürnbergerová, B. Babál, and J. S. Popovics, "Ultrasonic pulse velocity test of concrete properties as specified in various standards," *Cem. Concr. Compos.*, vol. 18, no. 5, pp. 357–364, 1996.

[24] S. Popovics, J. L. Rose, and J. S. Popovics, "The behaviour of ultrasonic pulses in concrete," *Cem. Concr. Res.*, vol. 20, no. 2, pp. 259–270, 1990.

[25] H. Choi and J. S. Popovics, "NDE application of ultrasonic tomography to a full-scale concrete structure.," *IEEE Trans. Ultrason. Ferroelectr. Freq. Control*, vol. 62, no. 6, pp. 1076–85, 2015.

[26] B. C. Kim and J. Y. Kim, "Characterization of ultrasonic properties of concrete," *Mech. Res. Commun.*, vol. 36, no. 2, pp. 207–214, 2009.

[27] Y. Akkaya, "Nondestructive measurement of concrete strength gain by an ultrasonic wave reflection method," *Mater. Struct.*, vol. 36, no. 262, pp. 507–514, 2003.

[28] G. Trtnik, F. Kavčič, and G. Turk, “Prediction of concrete strength using ultrasonic pulse velocity and artificial neural networks,” *Ultrasonics*, vol. 49, no. 1, pp. 53–60, 2009.

[29] A. Nishikawa, N. Nagahama, K. Umeda, T. Sakai and S. I. Oya, “Industrial Applications of Ultrasonic Time-of-Flight-Diffraction (TOFD) Techniques for Various Field Targets” Welding in the World, Vol. 49, no 9, pp 68–74, 2005.

[30] G. V Blessing, J. a Slotwinski, D. G. Eitzen, and H. M. Ryan, “Ultrasonic measurements of surface roughness.,” *Appl. Opt.*, vol. 32, no. 19, pp. 3433–7, 1993.

[31] U. King-, “Ultrasonic Wave Scattering from Rough , Imperfect Interfaces . Part II . Incoherent and Coherent Scattered,” vol. 14, no. 3, 1995.

[32] Z. Liu, J. Oswald, and T. Belytschko, “XFEM modeling of ultrasonic wave propagation in polymer matrix particulate/fibrous composites,” *Wave Motion*, vol. 50, no. 3, pp. 389–401, 2013.

[33] K. Nakahata, G. Kawamura, T. Yano, and S. Hirose, “Three-dimensional numerical modeling of ultrasonic wave propagation in concrete and its experimental validation,” *Constr. Build. Mater.*, vol. 78, pp. 217–223, 2015.

[34] V. Bucur and I. Böhnke, “Factors affecting ultrasonic measurements in solid wood,” *Ultrasonics*, vol. 32, no. 5, pp. 385–390, 1994.

[35] H. Kim and J. W. Lee, “Effect of ultrasonic wave on the degradation of polypropylene melt and morphology of its blend with polystyrene,” *Polymer (Guildf).*, vol. 43, no. 8, pp. 2585–2589, 2002.

[36] J. Chang, C. Zheng, and Q. Q. Ni, “The ultrasonic wave propagation in composite material and its characteristic evaluation,” *Compos. Struct.*, vol. 75, no. 1–4, pp. 451–456, 2006.

[37] R. Kažys, A. Voleišis, and B. Voleišienė, “High temperature ultrasonic transducers : review,” vol. 63, no. 2, 2008.

[38] F. Lionetto and A. Maffezzoli, “Polymer Characterization by Ultrasonic Wave Propagation,” *Adv. Polym. Technol.*, vol. 27, no. 2, pp. 63–73, 2008.

[39] A. A. T. Grattan K T V, *Ultrasonic sensors*. IOP Publishing Ltd., 1997.

[40] S. K. Verma, S. S. Bhadauria, and S. Akhtar, "Review of Nondestructive Testing Methods for Condition Monitoring of Concrete Structures," vol. 2013, no. 2008, 2013.

[41] J. R. Lee, H. J. Shin, C. C. Chia, D. Dhital, D. J. Yoon, and Y. H. Huh, "Long distance laser ultrasonic propagation imaging system for damage visualization," *Opt. Lasers Eng.*, vol. 49, no. 12, pp. 1361–1371, 2011.

[42] J. a Scales and A. E. Malcolm, "Laser characterization of ultrasonic wave propagation in random media.," *Phys. Rev. E. Stat. Nonlin. Soft Matter Phys.*, vol. 67, no. 4 Pt 2, p. 046618, 2003.

[43] V. Matz, R. Smid, S. Starman, and M. Kreidl, "Signal-to-noise ratio enhancement based on wavelet filtering in ultrasonic testing.," *Ultrasonics*, vol. 49, no. 8. pp. 752–9, Dec-2009.

[44] Y. Zhu, J. P. Weight, and A. A. Filter, "Ultrasonic Nondestructive Evaluation of Highly Scattering Materials Using Adaptive Filtering and Detection," *IEEE Trans. Ultrason. Ferroelectr. Freq. Control*, vol. 41, no. 1, pp. 26–33, 1994.

[45] F. Mielentz, "Phased arrays for ultrasonic investigations in concrete components," *J. Nondestruct. Eval.*, vol. 27, no. 1–3, pp. 23–33, Jun. 2008.

[46] C. Li, D. Pain, P. D. Wilcox, and B. W. Drinkwater, "Imaging composite material using ultrasonic arrays," *NDT E Int.*, vol. 53, pp. 8–17, Jan. 2013.

[47] Z. Yang, W. Zhang, Y. Tian, J. Li, and L. Li, "Nonlinear ultrasonic testing technique for micro-damage of TATB based Polymer Bonded Explosive," *Ndt.Net*, no. 18 WCNDT, pp. 16–20, 2012.

[48] S. Yashiro, J. Takatsubo, and N. Toyama, "An NDT technique for composite structures using visualized Lamb-wave propagation," *Compos. Sci. Technol.*, vol. 67, no. 15–16, pp. 3202–3208, 2007.

[49] W. N. Reynolds and S. J. Wilkinson, "The propagation of ultrasonic waves in CFRP laminates," *Ultrasonics*, vol. 12, no. 3, pp. 109–114, 1974.

[50] S. Zhong, Y. Yan, and Y. Shen, “Non-destructive testing of GFRP materials by Fourier-domain infrared optical coherence tomography,” *Int. Conf. Autom. Control Artif. Intell. (ACAI 2012)*, vol. 1, pp. 1407–1410, 2012.

[51] M. Krause, M. B, R. Frielinghaus, F. Kretzschmar, O. Kroggel, K. J. Langenberg, C. Maierhofer, W. Muller, J. Neisecke, M. Schickert, V. Schmitz, H. Wiggenhauser, and F. Wollbold, “Comparison of pulse-echo methods for testing concrete,” vol. 30, no. 4, pp. 195–204, 1997.

[52] R. Kazys, a Demcenko, E. Zukauskas, and L. Mazeika, “Air-coupled ultrasonic investigation of multi-layered composite materials.,” *Ultrasonics*, vol. 44 Suppl 1, pp. e819–22, Dec. 2006.

[53] J. R. Berriman, D. a Hutchins, A. Neild, T. H. Gan, and P. Purnell, “The application of time-frequency analysis to the air-coupled ultrasonic testing of concrete.,” *IEEE Trans. Ultrason. Ferroelectr. Freq. Control*, vol. 53, no. 4, pp. 768–76, Apr. 2006.

[54] M. Fink, D. Cassereau, A. Derode, C. Prada, P. Roux, M. Tanter, J.-L. Thomas, and F. Wu, “Time-reversed acoustics,” *Reports Prog. Phys.*, vol. 63, no. 12, pp. 1933–1995, 2000.

[55] A. V. Osetrov, “Non-linear algorithms based on SAFT ideas for reconstruction of flaws,” *Ultrasonics*, vol. 38, pp. 739–744, 2000.

[56] G. Doctor S R, Collins H D, Crawford S L, Hall T E, Baldwin A J, Bowey R E, “Developement and Validation of Real-Time SAFT-UT System for Inservice Inspection of LWR,” *Nucl. Eng. Des.*, vol. 89, pp. 357–369, 1985.

[57] C. J. Martín, O. Martinez, L. G. Ullate, A. Octavia, and G. Godoy, “Reduction of grating lobes in SAFT images,” in *Proceedings - IEEE Ultrasonics Symposium*, pp. 721–724, 2008.

[58] Q. Li, H. Ma, C. Lu, and L. Shi, “Experimental research on ultrasonic 2-D SAFT of concrete elements,” in *International Conference in Electrics, Communication and Automatic Control*, pp. 429–436, 2012.

[59] C. J. Martin-Arguedas, D. Romero-Laorden, O. Martinez-Graullera, M. Perez-Lopez, and L. Gomez-Ullate, “An ultrasonic imaging system based on a new SAFT approach

and a GPU beamformer," *IEEE Trans. Ultrason. Ferroelectr. Freq. Control*, vol. 59, no. 7, pp. 1402–1412, 2012.

[60] D. Lévesque, A. Blouin, C. Néron, and J. P. Monchalin, "Performance of laser-ultrasonic F-SAFT imaging," *Ultrasonics*, vol. 40, no. 10, pp. 1057–1063, 2002.

[61] a Blouin, D. Levesque, C. Neron, D. Drolet, and J. P. Monchalin, "Improved resolution and signal-to-noise ratio in laser-ultrasonics by SAFT processing.," *Opt. Express*, vol. 2, no. 13, pp. 531–539, 1998.

[62] B. Scrosati, F. Croce, and L. Persi, "Impedance Spectroscopy Study of PEO-Based Nanocomposite Polymer Electrolytes," *J. Electrochem. Soc.*, vol. 147, no. 5, p. 1718, 2000.

[63] B. H. A. Kalpenson, "Collimating and wide-band ultrasonic piezotransducers." NDT. Net, pp. 1–5, 2004.

[64] G. M. Zhang, C. G. Hou, Y. W. Wang, and S. Y. Zhang, "Optimal frequency-to-bandwidth ratio of wavelet in ultrasonic non-destructive evaluation," *Ultrasonics*, vol. 39, no. 1, pp. 13–17, 2001.

[65] R. Pullin, M. J. Eaton, M. R. Pearson, C. Featherston, J. Lees, J. Naylon, A. Kural, D. J. Simpson, and K. Holford, "On the development of a damage detection system using macro-fibre composite sensors," in *Journal of Physics: Conference Series*, , vol. 382, p. 012049,2012.

[66] P. Pallav, T. H. Gan, and D. A. Hutchins, "Elliptical-Tukey Chirp Signal for Ultrasonic Imaging," *IEEE Trans. Ultrason. Ferroelectr. Freq. Control*, vol. 54, no. 8, pp. 1530–1540, 2007.

Chapter 3

Determination of Experimental Design

3.1 Introduction

In this Chapter, different types of waveform will be investigated to take advantage of the wide bandwidth transducers used in this research. Chapter 4 will then describe how this system has been developed with some adjustable parameters that can suit these type of materials, together with a brief discussion of additional signal processing.

3.2 Ultrasonic coded signals

The aim of using coded signals is to improve the signal to noise ratio (SNR) for NDE inspections. Waveforms such as linear Frequency Modulated (FM) chirps, random noise and Golay codes can be manipulated in order to boost the SNR in ultrasonic testing [1]. A chirp has certain advantages when compared to other modulation schemes, and is very popular in signal processing [2-3]. A chirp (also known as a "swept signal [4]) is a signal in which the frequency is swept continuously over a predetermined range where the frequency increases or decreases with time [5-6]. The idea of using this signal is to get a high-resolution in time after cross-correlation operation to improve the axial resolution. Thus, it is suitable to use with pulse compression operation.

One of the main elements of the present work is the use of piezocomposite ultrasonic transducers that are capable of generating a signal with a broad wavelength. Characteristics such as centre frequency, bandwidth, amplitude (power) and the time duration can be adjusted

according to the needs and the ultrasonic transducers used. Coded waveforms can be listed by their type of encoding. Typically, there are three families of coded waveforms:

i. Frequency Modulation which modulates proportionally the transmitted signal frequency (e.g. Chirp Signals).

ii. Phase Modulation also known as binary sequences are the waveforms that shifts in phase transmitted signals proportionally to the signal's amplitude, e.g. MLS, Legendre Sequences, Golay Sequences, Bipolar Golay and Chaos Sequences.

iii. Amplitude Modulation where the signal is modulated in amplitude without any phase changing.

The two main families of waveforms that have been used throughout this study are the Frequency Modulation waveforms (chirp) and Phase Modulation waveforms namely Golay Complementary Sequences (GCS).

3.2.1 Chirp

A chirp signal can be represented as:

$$C(t) = sin(\omega_s t + \frac{\pi\beta}{T}t^2) \qquad 0 \leq t \leq T, \tag{3.1}$$

where ω_s is the starting angular frequency, β is the bandwidth of the signal, and T is the duration of the signal. Figure 3.1(a) illustrates a typical chirp waveform generated using equation (3.1). For this particular waveform, T was 150 µs, and the start and finish frequencies were 100 kHz and 500 kHz respectively. That meant that the bandwidth, β was 400 kHz and the central frequency was 300 kHz. The good thing about chirp is the fact that the start and finish frequencies can be defined to suit the profile of a transducer.

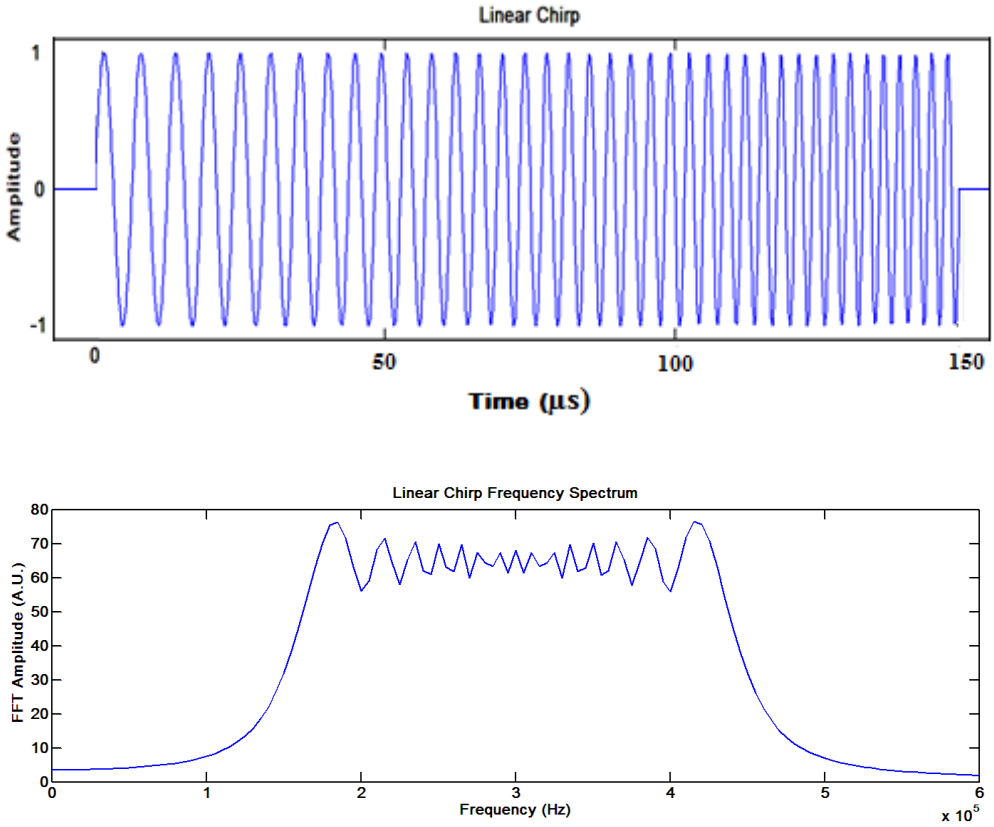

(a)

(b)

Figure 3.1 A chirp showing (a) the time waveform and (b) the frequency spectrum

Figure 3.1 (b) shows the general shape of the frequency spectrum of the corresponding Linear Chirp. It can be seen that the signal has a broad bandwidth which is around 400 kHz but there are some ripples at the top at the band-edge which are known as Fresnel ripples [7]. This is undesirable because it causes artefacts, namely clipping from the overshoot and undershoot, and ringing artefacts or ripples from the oscillations. The ripples as in Figure 3.1(b) above are not good for signal processing because it can become a source of unwanted high-frequency noise. This can be reduced or eliminated by using different types of filters such as low pass or band pass filter.

3.2.2 Golay Complementary Sequences

Another type of waveforms that are often used for pulse compression application is binary sequences. Binary sequences are waveforms generated from a list of 1 and -1 values

[8]. There are a variety of binary sequences that have been used such as Maximum Length Sequences (MLS), Chaos Sequences and Legendre Sequences. But in this study, it is focused on Golay Complementary Sequences (GCS). GCS consist of two binary sequences, $\delta_{GCS}^{A}[n]$, $\delta_{GCS}^{B}[n]$, defined by recursion from two seeds sequences, in which it has a strange property that their autocorrelation coefficients sum to zero:

$$\delta_{GCS}^{A}[n] = -\delta_{GCS}^{B}[n],\ n \neq 0,\ \ \delta_{GCS}^{A}[n] + \delta_{GCS}^{B}[n] = 2L \times \delta[n] \qquad (3.2)$$

Where L is the length sequences. Although it requires 2 seeds of sequences, GCS is the only theoretically coded waveforms that exhibit a perfect pulse compression at the end of the overall procedure [9]. This is due to the perfect shape when the rectification process is carried out. This is why they are popular in ultrasonic measurements [10-11].

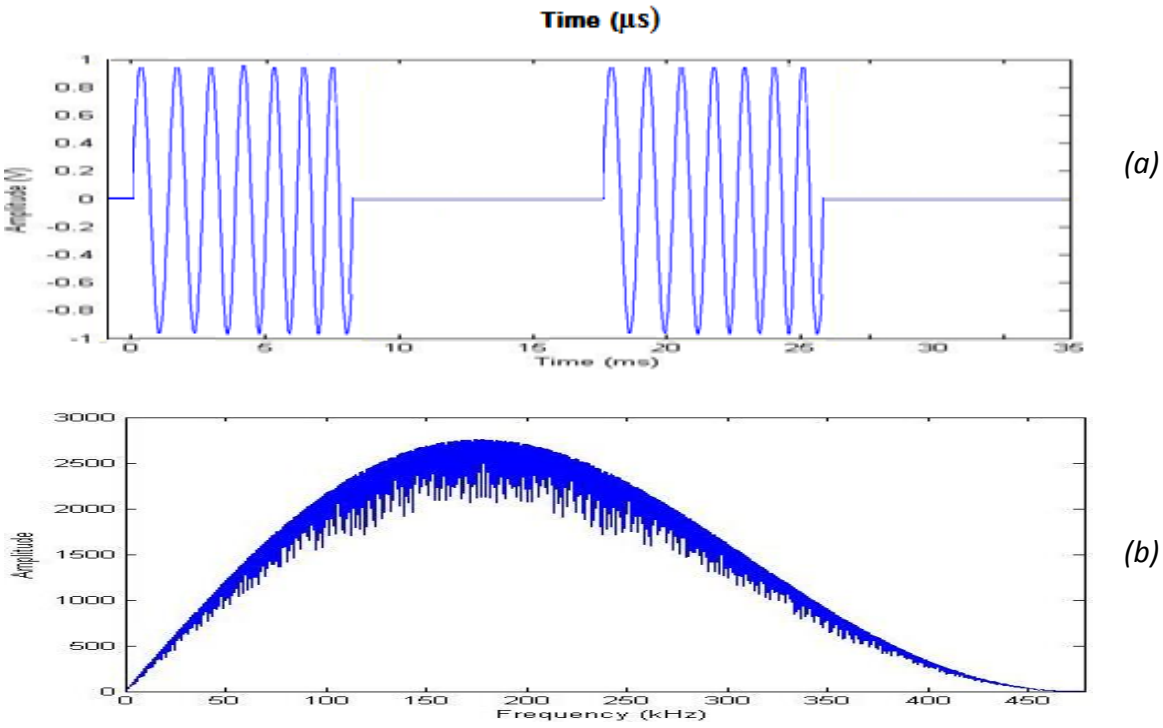

(a)

(b)

Figure 3.2 (a) Bipolar Golay signal and (b) frequency spectrum

3.3 Windows functions

In signal processing, the window function is an important element that can help to produce the best results. It is a mathematical function that can improve the signal by making the output zero-valued outside of some chosen interval [13]. In signal analysis, there are some applications where the window function is used, such as spectral analysis, designing filters and beam forming. Among the main functions of the window function in signal processing is to reduce artefacts or ripples in the signal, as described in section 3.2.1 above [7,14]. There are several types of windows commonly used in ultrasonic testing, such as rectangular, Hanning, Hamming, Blackman, Flat Top and Tukey. Figure 3.3 shows some commonly-used windows.

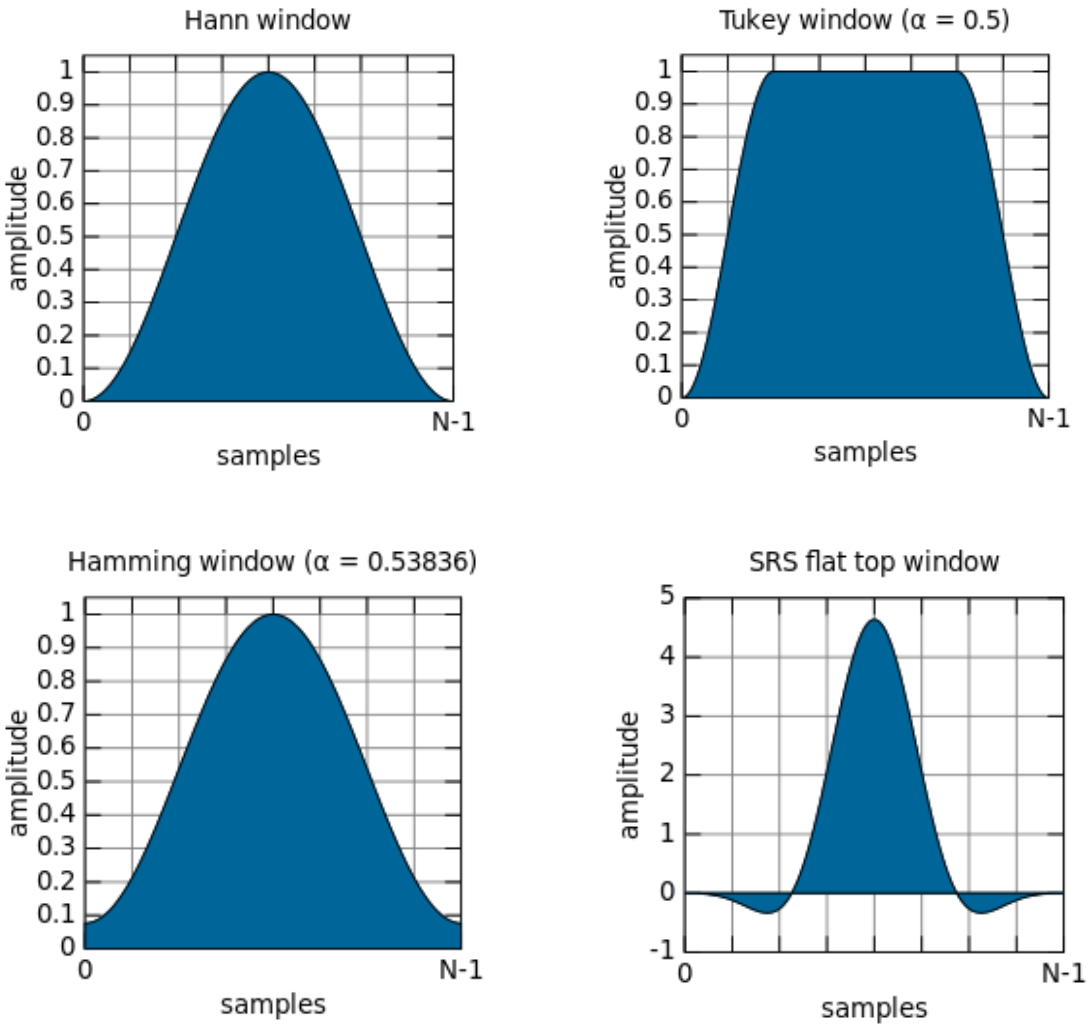

Figure 3.3 some commonly used windows in ultrasonic testing [15]

A window is selected according to the suitability of the waveforms to be used (either chirp or binary codes such as Golay) and also the type of transducer used. For example, Hamming window was applied to the chirp signal of equation 3.1 (Figure 3.1(a)) above. The signal can now be described as:

$$C(t) = H(t)\sin\left(\omega_s t + \frac{\pi B}{T}t^2\right) \quad 0 \leqslant t \leqslant T \tag{3.3}$$

where *H(t)* is the Hamming window that is given by:

$$H(t) = \frac{1}{2}\left[1 - \cos\left(\frac{2\pi t}{T}\right)\right] \tag{3.4}$$

Multiplication of the Hamming window with the chirp has resulted in a bell-shaped envelope which is also known as Hamming chirp as shown in Figure 3.4 below. Although ripples have been reduced, it can be seen that the amplitude has also decreased when a comparison is made to the original signal in Figure 3.1(b).

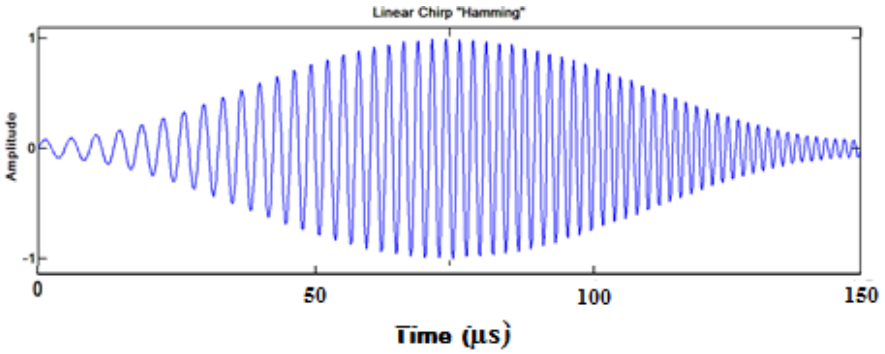

(a)

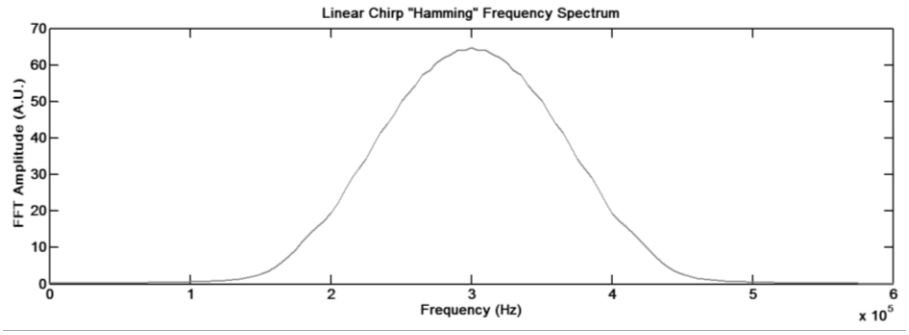

(b)

Figure 3.4 (a) Hamming chirp signal which is a chirp product after the Hamming window; (b) frequency spectrum showing that the ripples have been reduced

3.4 Transducer response

The transducer response must be taken into account when determining the selection of transducers, signal type and frequency range to be used [16-17]. The response of the piezo-composite transducers that were supplied by the manufacturer (EOFE Ultrasonic Co. Ltd) are shown in Figure 3.5. Such piezo-composite transducers were used throughout the study (refer to section 4.3.2 for more details). Figure 3.5 shows the frequency response of devices that were designed to have a center frequency of 170 kHz, and it can be seen that both provide a response of the same bandwidth.

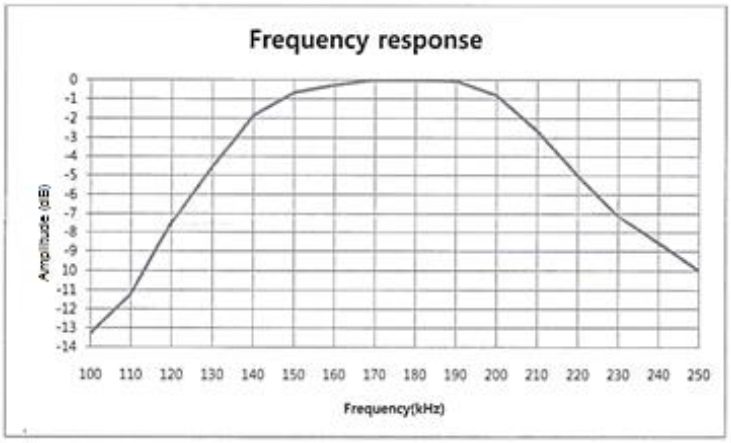

(a)

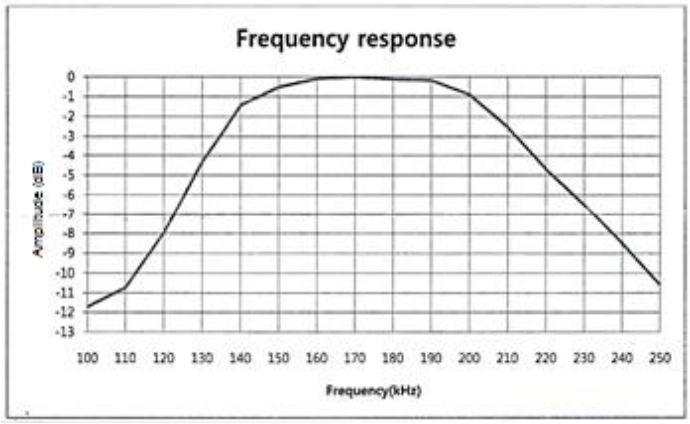

(b)

Figure 3.5 Frequency responses of two Piezocomposite transducers ((a) and (b)) each with a nimonal 50 mm diameter and 170 kHz center frequency (source: EOFE Ultrasonic Co. Ltd)

Figure 3.6 shows the chirp and Bipolar Golay signals that were used in a comparative test, using the same drive voltage level of 2V peak to peak. From Figure 3.6 (a) it can be seen that the linear chirp was windowed so as to have a smooth transition in the power spectrum density. This ensured that the autocorrelation of the chirp signal had a low level of side lobes. It can also be seen from the FFT that the spectrum amplitude of the Golay code was higher than that of the chirp. This is because the Golay uses a pair of waveforms to obtain its characteristics [11] and also due to the fact that the power available from binary sequences were double that of the chirp signal, so in this case the energy from the Golay code was four times larger than of the windowed chirp signal.

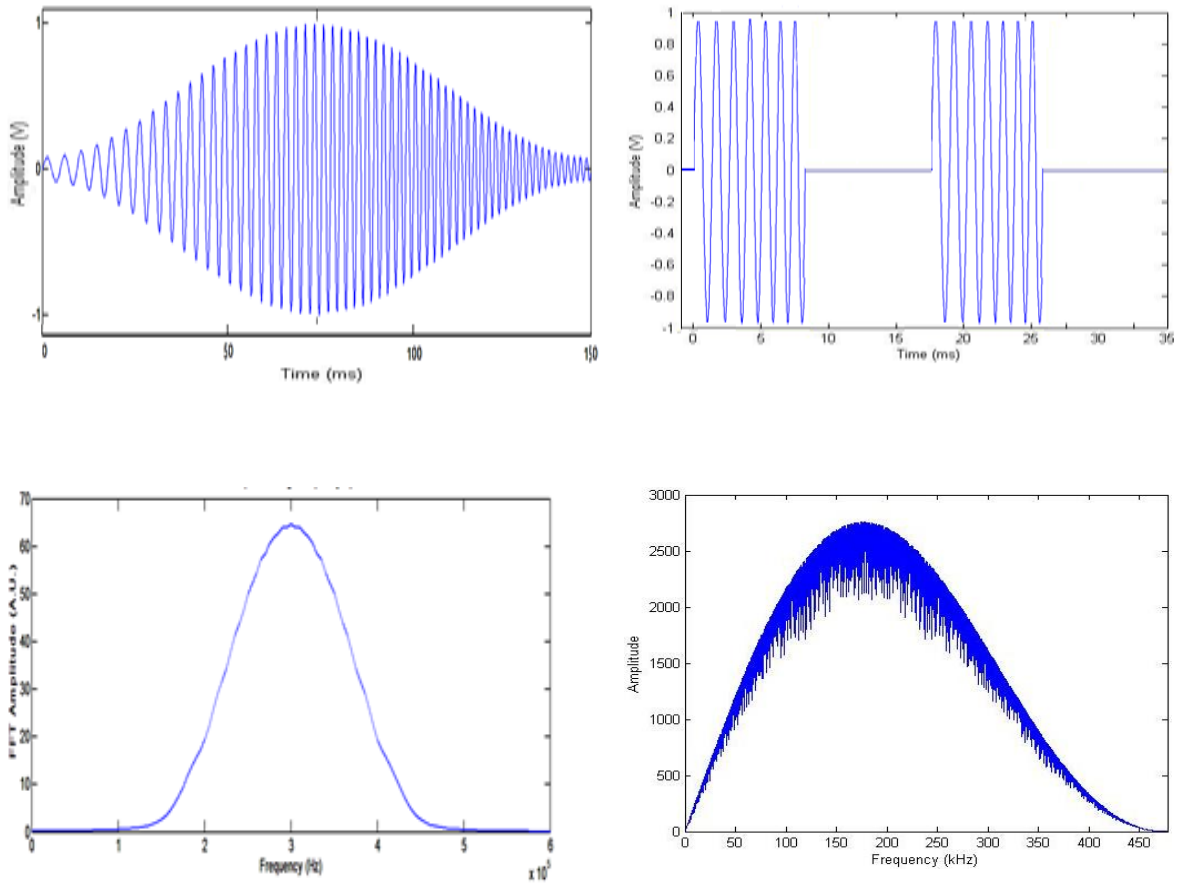

(a) *(b)*

Figure 3.6 Voltage drive signals, and their spectra obtained using an FFT, for (a) a Chirp signal and (b) Bipolar Golay code

In addition, the bandwidth of the Bipolar Golay was greater and extended almost to DC. Note that this traditional Bipolar Golay code waveform would be expected to be better suited to wide bandwidth transduction systems, whereas the chirp could be tuned to suit a narrower, more resonant transduction system for maximum effect. However, the Bipolar Golay scheme allows a center frequency to be selected while noting that it is not completely symmetrical in the frequency spectrum. It thus has to be chosen carefully, so that it produces a maximum output from a given transducer. Figure 3.7 shows the autocorrelation output of chirp and Bipolar Golay signals after they have been cross-correlated. Although electrical coupling modified the frequency spectrum, the results were still within the design range.

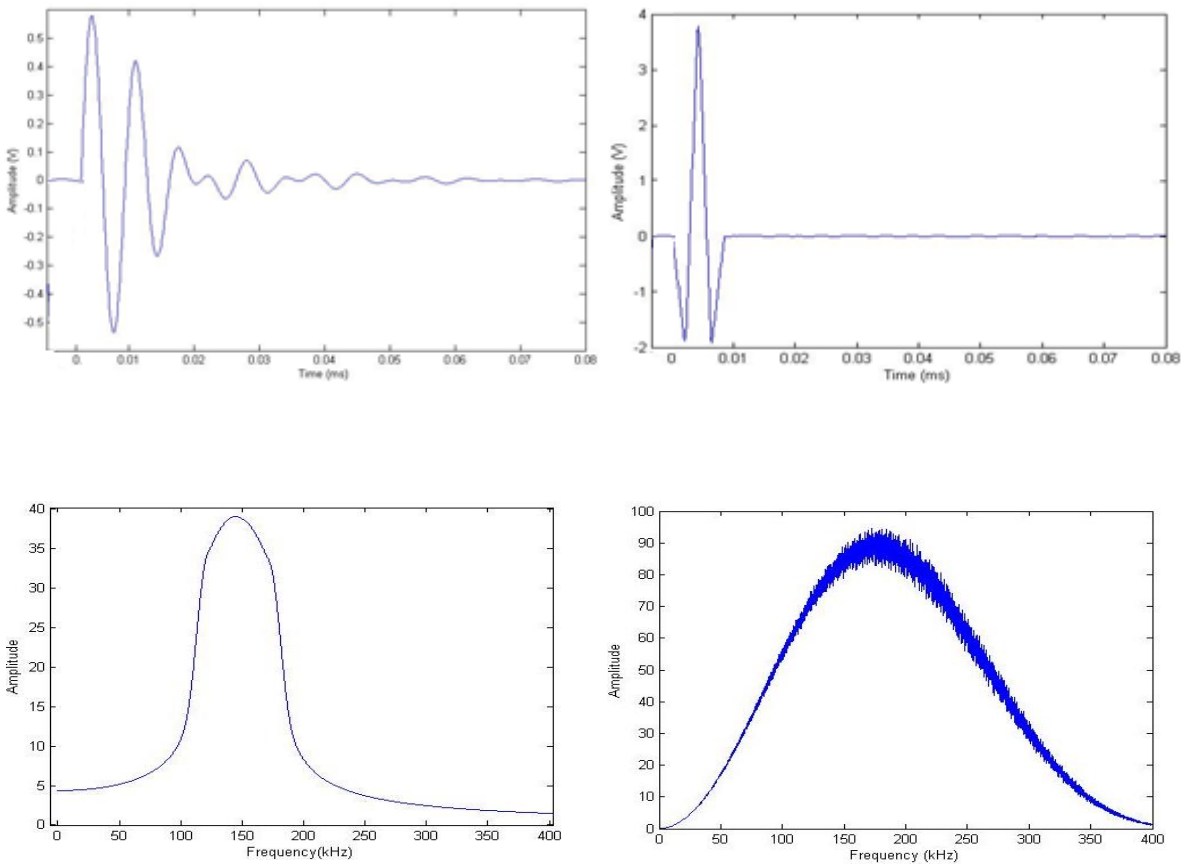

(a) *(b)*

Figure 3.7 Output of cross-correlation of the drive signals and the corresponding frequency spectrum for (a) a Chirp and (b) a Bipolar Golay

3.5 Signal processing techniques

Signal processing is one of the important stages in a NDT test because at this stage all the results from the tests carried out will be analyzed using specific methods to produce more meaningful data and the result can be presented in a certain format. There are a variety of signal processing techniques that are used today, whether it is used during the measurement or carried out after the experiment (post-processing). For equipment that can function in real-time, it is also likely to run signal processing during the measurement or even before a measurement is carried out; such as pulse compression, filtration, and cross-correlation. But

most of the signal processing techniques are carried out after the measurement such as filtering and Synthetic Aperture Focusing Technique (SAFT) imaging.

3.5.1 Pulse compression

The transducers used in conventional ultrasonic NDE are limited in terms of average power and the resolution by the pulse width [19]. In order to get an adequate signal in highly attenuating materials, a high transmitted average power is required. The maximum peak voltage that can be used is normally limited by the transducer construction [20]. In addition, drive voltages have to be limited for some ultrasonic applications in volatile and highly sensitive environments such as oil and gas industry and biomedical investigation. To overcome the problem of peak-power limitation, a lower voltage with a longer time-duration signal is required. Nevertheless, the use of longer signals would affect the spatial resolution of the test. Such difficulties can be overcome through the use of pulse compression [21-23].

Pulse compression techniques involve the transmission of a long coded pulse and the processing of the received signal to obtain a relatively narrow pulse, thus preserving spatial resolution [23]. These techniques resolve the range-resolution problem by means of long-duration and wideband waveforms, which can be compressed into narrow pulses by appropriate processing at the receiving end. Most of the NDT pulse compression systems perform the required pulse compression through cross-correlation [24]. Because cross-correlation systems have the advantages of a high signal to noise ratio, they allow the pulse compression system to be used on more highly attenuating materials and to detect smaller flaws at longer distances than are possible with a system without pulse compression.

$$P(t) = C(t) * [C_T(t)] \tag{3.4}$$

A clear explanation regarding this technique is described in a model produced by Gan *et al*. [24]. Figure 3.10 shows the process in which Hamming chirp has been shifted by 40 μs in time and subsequently mixed with a random signal which has a high noise as shown in Figure 3.8(a). To obtain a compressed pulse signal, the received signal was filtered using a bandpass filter with a bandwidth equal to the bandwidth chirp subtracted as shown in Figure 3.8(b). In this stage, the bandpass filter filtered out most of the noises frequencies outside the band frequency (Figure 3.8(b)). The signal was then cross-correlated with a reference signal and finally the results were smoothed and rectified in order to get the end product as in Figure 3.8(c). This process can be represented using equation 3.4. above. Where the compressed signal, *P(t)* is the product of cross-correlation of the received signal, $C_T(t)$ and the reference signal, *C(t)*. The final stage in this process is a smoothing and rectification, resulting in pulse compression, as shown in Figure 3. 8(c).

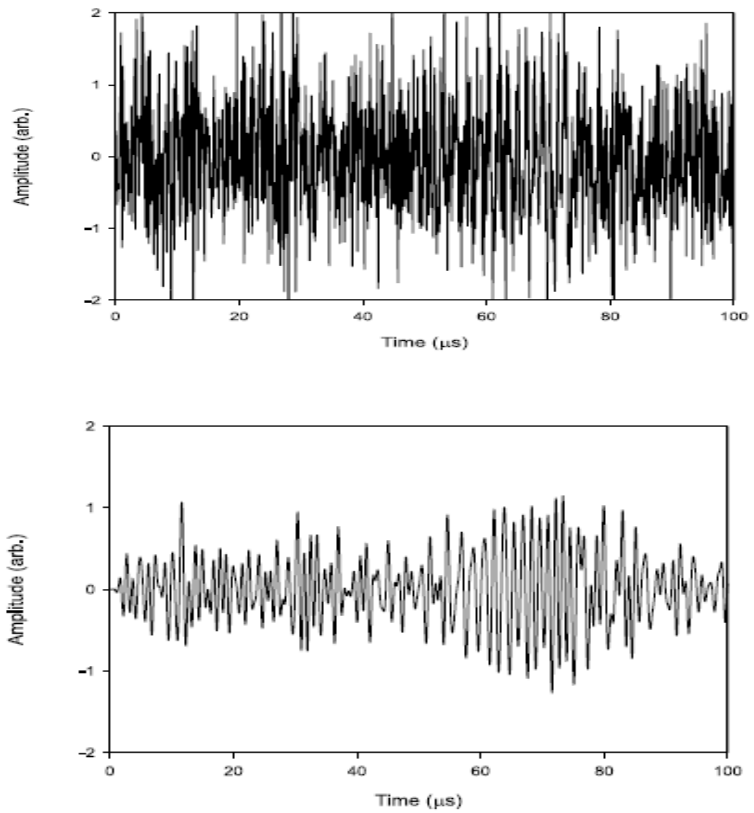

Figure 3.8 (a) An unprocessed chirp signal buried in noise. (b) A compressed pulse signal, where the

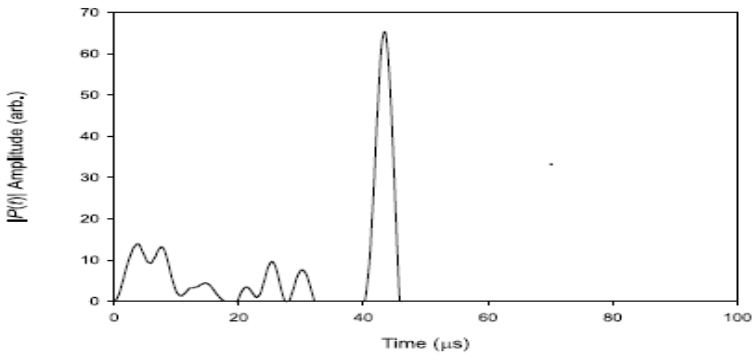

(c)

Received signal was filtered using a bandpass filter with a bandwidth equal to the bandwidth chirp; (c) final result of the pulse compression technique after smoothing and rectification.

3.5.2 Synthetic aperture focusing technique (SAFT)

An ultrasonic echo can be represented by a number of properties such as frequency, bandwidth, amplitude or energy. All these characteristics provide valuable information on defect size, material type, and other properties. But when it comes to the defect location, time of flight or phase are the most important parameter. A single A-scan measurement is not sufficient to determine the location of a defect accurately because a given time of flight can only provide information about the relative distance between the transducer and the defect. However, successive A-scan measurements from several different locations can generate images that give an indication of the location of the defect, depending on the ultrasonic beam parameters.

One way of using A-scan data from multiple locations is SAFT where the technique was originally used in radar technology in the 1950s [25]. This technique was later introduced into the ultrasonic technique in the 1970s when it became known as Ultrasonic SAFT [26-28]. Ultrasonic SAFT reconstruction is an imaging technique that uses information from multiple pulse echo measurements that are combined to produce an image. In its simplest form, a transducer emitting ultrasonic waves is swept along the sample in pulse-echo mode to create a

scanned aperture. If a defect is present in the aperture, echoes can be generated from multiple scanning positions, allowing an estimate of the defect location to be made.

SAFT is a technique that has been introduced to improve the accuracy of ultrasonic imaging, thus enhancing the ability to determine the size of the defect. SAFT imaging provides detailed information about the material being tested. The process of delay and sum used in some versions of the SAFT algorithm acts as an averaging process, and this can improve the SNR of the measurement [29].

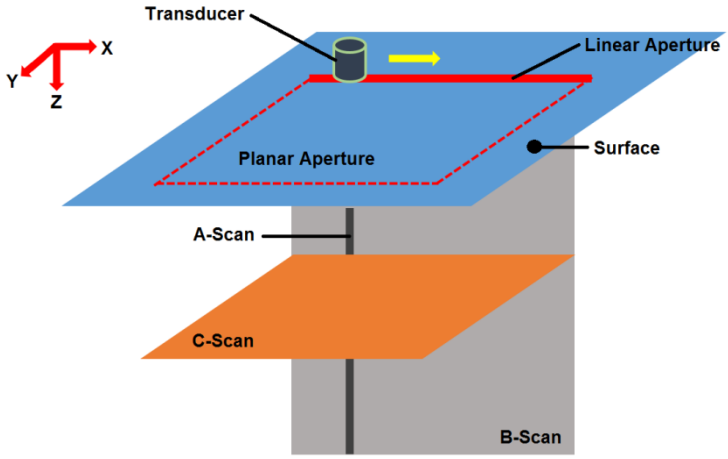

Figure 3.9 Scanning apertures of SAFT technique

In the SAFT measurements reported in this thesis, data was recorded from the surface of the test object in the form of a one or two-dimensional grid, called the aperture, as illustrated in Figure 3.9 above. The basic algorithm coherently superimposes the signals for each element, thus approximating the effect of a transducer of the size of scanning aperture. As in many types of imaging, a bigger aperture leads to a higher imaging resolution, and this is the whole point of the SAFT approach. SAFT can be applied using arrays, although large area scanning using a single array is often not possible. Thus, one or more transducers need to be moved to scan the grid as in Figure 3.10 to create virtual whole aperture. The effect can also be explained by

thinking of multiple locations of small aperture transducers acting as one big aperture, producing a more directional beam. The set of measured signals obtained at the receivers from numerous reflections and scattering of the source pulse inside the material (acquired by Impact-echo measurement) is then processed using SAFT reconstruction.

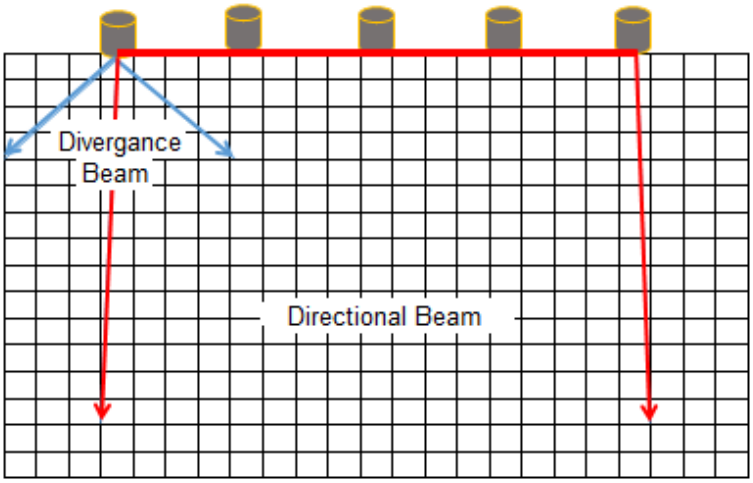

Figure 3.10 An array of single transducers with a small aperture, each with a divergence beam, is scanned over the surface to create a virtual larger aperture with a more directional beam

As stated above, data can be collected in pulse-echo mode, but it is more common to use a pitch-catch configuration, using a set of Transmitters (Tx) and receivers (Rx). Such a situation is shown in Figure 3.11, using a static transmitter and four receiver positions (Rx1 – Rx4). In SAFT image reconstruction, the area under inspection (in this case a vertical slice through the material due to a linear scan, leading to a Linear SAFT (LSAFT) image reconstruction) will be divided into single independent pixels. The geometrical location of every pixel (e.g. pixel A in Figure 3.11) will be used to calculate the path length that would be present if the signal was scattered from that pixel to a given receiver location. This can be repeated for each pixel and each transmitter/receiver location.

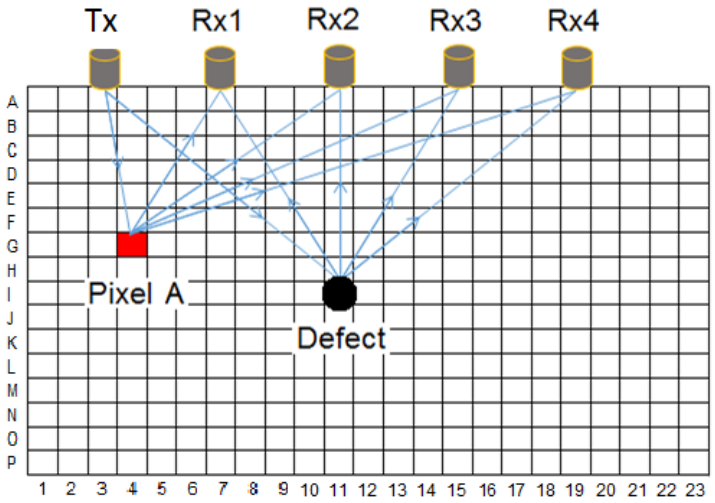

Figure 3.11 LSAFT image reconstruction

The aim of the process is to use this known geometrical information to form an image, and various SAFT algorithms use different ways of achieving this, although they are all based on the same general principles [30-32]. The SAFT algorithm take these hyperbolic patterns into account when reconstructing an image. Basically what it does is that it goes through all the pixels in a B-scan image and calculates how the hyperbolic pattern would look if the pixel were to contain a defect or scatterer. Then the resulting pattern is compared with the surrounding pixels to ascertain if indeed there is a defect within the pixels. When a transducer scans over a point scatterer, the scatterer will be smeared out into a hyperbola in the B-scan, due to the difference in transit time for the transmitted pulses at different locations.

3.6 Conclusions

This chapter has discussed a number of important elements that have been used throughout this study, such as waveforms composed of chirps and binary codes. In addition, the importance of the transducer response. The relationship between the signal, its frequency spectrum, the effect of signal clipping on the results and the use of windowing has been

described. The Chapter that follows will explain how these concepts were applied in actual NDE experiments.

References

[1] P. Pallav, D. A. Hutchins, and T. H. Gan, "Air-coupled ultrasonic evaluation of food materials," *Ultrasonics*, vol. 49, no. 2, pp. 244–253, 2009.

[2] J. R. Berriman, D. a Hutchins, A. Neild, T. H. Gan, and P. Purnell, "The application of time-frequency analysis to the air-coupled ultrasonic testing of concrete.," *IEEE Trans. Ultrason. Ferroelectr. Freq. Control*, vol. 53, no. 4, pp. 768–76, Apr. 2006.

[3] D. Hutchins, P. Burrascano, L. Davis, S. Laureti, and M. Ricci, "Coded waveforms for optimised air-coupled ultrasonic nondestructive evaluation," in *Ultrasonics*, 2014, vol. 54, no. 7, pp. 1745–1759.

[4] S. Martini, C. Bertoli, M. L. Herrera, I. Neeson, and A. Marangoni, "Attenuation of ultrasonic waves: Influence of microstructure and solid fat content," *J. Am. Oil Chem. Soc.*, vol. 82, no. 5, pp. 319–328, May 2005.

[5] R. A. Carmona, W. L. Hwang, and B. Torrésani, "Identification of Chirps with Continuous Wavelet Transform," *Wavelets Stat. A Antoniadis G Oppenheim Eds Lect. Notes Stat.*, vol. 103, pp. 95–108, 1995.

[6] P. Pallav, T. H. Gan, and D. A. Hutchins, "Elliptical-Tukey Chirp Signal for Ultrasonic Imaging," *IEEE Trans. Ultrason. Ferroelectr. Freq. Control*, vol. 54, no. 8, pp. 1530–1540, 2007.

[7] P. D. Lax, "Gibbs phenomena," *J. Sci. Comput.*, vol. 28, no. 2–3, pp. 445–449, 2006.

[8] S. W. Huang and P. C. Li, "Arbitrary waveform coded excitation using bipolar square wave pulsers in medical ultrasound," *IEEE Trans. Ultrason. Ferroelectr. Freq. Control*, vol. 53, no. 1, pp. 106–116, 2006.

[9] M. G. Parker, K. G. Paterson, and C. Tellambura, "Bipolar Golay Complementary Sequences," *Wiley Encycl. Telecommun.*, vol. 7228, no. 1811, pp. 1–18, 2003.

[10] S. Kounias, C. Koukouvinos, and K. Sotirakoglou, "On Golay sequences," *Discrete*

Math., vol. 92, no. 1–3, pp. 177–185, 1991.

[11] A. V. Alejos, D. Muhammad, and H. U. R. Mohammed, "Ground penetration radar using golay sequences," in *2007 IEEE Region 5 Technical Conference, TPS*, 2007, pp. 318–321.

[12] D. J. G. Mestdagh, P. M. P. Spruyt, and B. Biran, "Effect of amplitude clipping in DMT-ADSL transceivers," *Electron. Lett.*, vol. 29, no. 15, pp. 1354–1355, 1993.

[13] O. M. Solomon, "The effects of windowing and quantization error on the amplitude of frequency-domain functions," *IEEE Trans. Instrum. Meas.*, vol. 41, no. 6, pp. 932–937, 1992.

[14] R. . c S. G. . c c Santi S.a c Rovatti, "Gibbs-like phenomena in chaos-based frequency modulated signals," in *Proceedings - IEEE International Symposium on Circuits and Systems*, 2003, vol. 3, pp. III128–III131.

[15] G. Heinzel, a Rüdiger, R. Schilling, and T. Hannover, "Spectrum and spectral density estimation by the Discrete Fourier transform (DFT), including a comprehensive list of window functions and some new flat-top," *Max Plank Inst.*, pp. 1–84, 2002.

[16] P. G. Kenny, J. J. Gruber, and J. M. Smith, "Ultrasonic transducer characterization," *Mater. Eval. (ISSN 0025-5327)*, vol. 45, pp. 730–735, 1987.

[17] C. S. Desilets, J. D. Fraser, and G. S. Kino, "The design of efficient broad-band piezoelectric transducers," *IEEE Trans. Sonics Ultrason.*, vol. 25, no. 3, pp. 115–125, 1978.

[18] V. Matz, R. Smid, S. Starman, and M. Kreidl, "Signal-to-noise ratio enhancement based on wavelet filtering in ultrasonic testing.," *Ultrasonics*, vol. 49, no. 8. pp. 752–9, Dec-2009.

[19] J. Karki, "Signal Conditioning Piezoelectric Sensors," *Sensors Peterbrgh. NH*, vol. 48, no. September, pp. 1–6, 2000.

[20] A. A. T. Grattan K T V, *Ultrasonic sensors*. IOP Publishing Ltd., 1997.

[21] A. M. T. Hassan and S. W. Jones, "Non-destructive testing of ultra high performance fibre reinforced concrete (UHPFRC): A feasibility study for using ultrasonic and

resonant frequency testing techniques," *Constr. Build. Mater.*, vol. 35, no. 0, pp. 361–367, 2012.

[22] T. Inoue and S. Namiki, "Pulse compression techniques using highly nonlinear fibers," *Laser Photonics Rev.*, vol. 2, no. 1–2, pp. 83–99, 2008.

[23] M. Nisoli, S. De Silvestri, and O. Svelto, "Generation of high energy 10 fs pulses by a new pulse compression technique," *Appl. Phys. Lett.*, vol. 68, no. 20, pp. 2793–2795, 1996.

[24] T. H. Gan, D. A. Hutchins, and D. R. Billson, "Preliminary studies of a novel air-coupled ultrasonic inspection system for food containers," *J. Food Eng.*, vol. 53, no. 4, pp. 315–323, 2002.

[25] S. R. Doctor, T. E. Hall, and L. D. Reid, "SAFT — the evolution of a signal processing technology for ultrasonic testing," *NDT Int.*, vol. 19, no. 3, pp. 163–167, Jun. 1986.

[26] Y. Du and S. Jin, "Synthetic aperture ultrasonic imaging in pipeline inspection," in *2009 International Conference on Measuring Technology and Mechatronics Automation, ICMTMA 2009*, 2009, vol. 1, pp. 368–370.

[27] K. J. Langenberg, M. Berger, T. Kreutter, K. Mayer, and V. Schmitz, "Synthetic aperture focusing technique signal processing," *NDT International*, vol. 19. pp. 177–189, 1986.

[28] C. J. Martin-Arguedas, D. Romero-Laorden, O. Martinez-Graullera, M. Perez-Lopez, and L. Gomez-Ullate, "An ultrasonic imaging system based on a new SAFT approach and a GPU beamformer," *IEEE Trans. Ultrason. Ferroelectr. Freq. Control*, vol. 59, no. 7, pp. 1402–1412, 2012.

[29] J. Opretzka, M. Vogt, and H. Ermert, "A synthetic aperture focusing technique with optimized beamforming for high-frequency ultrasound," in *Proceedings - IEEE Ultrasonics Symposium*, 2010, pp. 2303–2306.

[30] Q. Li, H. Ma, C. Lu, and L. Shi, "Experimental research on ultrasonic 2-D SAFT of concrete elements," in *International Conference in Electrics, Communication and Automatic Control*, 2012, pp. 429–436.

[31] T. Stepinski, "Synthetic aperture focusing techniques for ultrasonic imaging of solid

objects," *Synth. Aperture Radar*, pp. 438–441, 2010.

[32] A. Barkefors, "3D Synthetic Aperture Technique for Ultrasonic Imaging," *Uptec F10 017*, 2010.

Chapter 4

Sub-MHz Ultrasonic System for Highly Attenuating Materials

4.1 Introduction

The most important thing in ultrasonic testing of highly attenuating materials, and those showing a high degree of ultrasonic scattering, is to provide an ultrasonic system that is capable of generating a signal of the correct form, so that it is able to pass through the material being tested. There are various mechanisms by which ultrasonic energy can be lost within a given material. The two characteristics of most interest within the types of materials looked at in this thesis (polymers, composites and concrete) are attenuation due to absorption (changing into heat), and scattering mechanisms. When an ultrasonic test is conducted on these types of materials, the ultrasonic signal may have a low signal to noise ratio (SNR), and may reduce in amplitude to below the noise level itself. The parameters of an ultrasonic wave propagating in a solid structure can be influenced by a broad range of factors such as: the physical properties of the substrate [1], the geometrical characteristics of the specimen under test, the environmental conditions (temperature, moisture content, mechanical loading etc.) and the measurement conditions [2].

One method to reduce the attenuation is to lower the signal frequency in order to increase the wavelength of the ultrasound signal, thus reducing its losses by interaction with the material being tested. Nevertheless, there is a tradeoff that needs to be considered because this action will reduce the spatial resolution of the system [3]. Spatial resolution depends on the diameter of the transducer used and also the frequency of the ultrasonic signal. But in the testing of materials with very high attenuation, a low resolution signal is better than no signal at all. The developed system requires a robust combination of hardware,

software and signal processing, and needs to be designed with the specific parameters that will produce optimum signals for different types of industrial samples.

4.2 Sub-MHz Ultrasound

This research will use ultrasonic frequencies below 1 MHz to obtain information about a material or structure. This seems to be a frequency range that is often not investigated, but there are many advantages to using lower frequencies – attenuation and scattering will be lower, penetration depths will increase, and materials that could not be inspected easily (such as multi-layer materials, certain composites, thick sections, concrete etc.) could then be suitable for testing [4]. Approximate wavelengths in steel at frequencies between 100 kHz and 1 MHz are 50-5 mm. Lower frequencies would be used for inspection of thicker sections, but obtaining bandwidth at lower frequencies is sometimes a problem especially using piezoelectric transducer.

Low frequencies have been used for many years for such materials, and yet there is still a need to improve the inspection techniques for the detection of voids and reinforcement bars (rebars), the identification of changes in concrete bulk properties (e.g. in nuclear storage tanks close to the concrete surface), and in other applications [5]. The frequencies of interest are likely to be above 100 kHz, but below the range of conventional ultrasonic NDE, which usually operates at frequencies above 1 MHz.

Lowering the frequency is one of the easiest and effective way of reducing the attenuation of ultrasonic signals during testing [6]. Sub-MHz ultrasound is a terminology that will be used in this thesis when experiments are performed at frequencies below 1 MHz; the frequencies of most interest are between 100 kHz and 500 kHz. Although lower frequencies will further reduce attenuation, it will also lower the spatial resolution of the resulting system. Spatial resolution of any imaging system is defined as its ability to

distinguish two points as separate in space where it can be categorized into axial and lateral resolution as in Figure 4.1. Axial resolution is resolution in the direction parallel to the ultrasound beam. Axial resolution is not affected by the depth of imaging because the resolution at any point along the beam is the same. While, temporal resolution is define as the ability of a system to distinguish two points in the direction perpendicular to the ultrasonic beam direction. Wider beams typically diverge further in the far field and any ultrasound beam diverges at greater depth, decreasing lateral resolution.

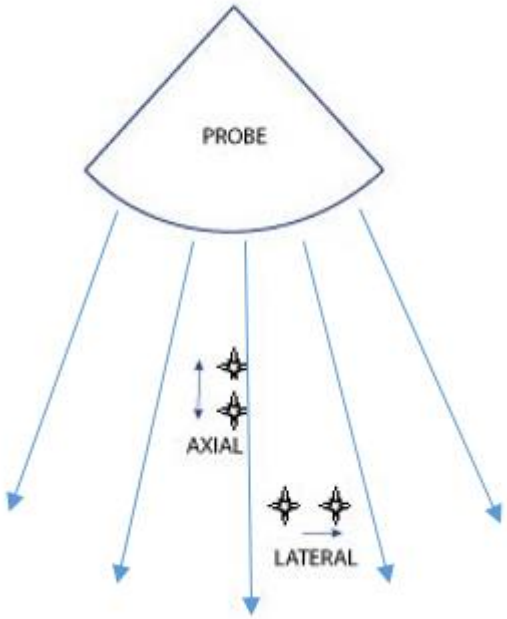

Figure 4.1: Axial and lateral resolution in a divergence beam

In order to produce a good system, the optimum frequency must be determined to ensure that the system can produce an ultrasonic signal with good penetrative power as well as the required spatial resolution. In determining the optimum frequency of the system, other factors such as ultrasound speed in that particular material, homogeneity of the material, composition and other physical properties also need to be considered. This is because all

these factors play a role in determining the SNR of the ultrasonic signal detected during an NDE experiment.

4.3 Hardware

Hardware is an important element in the development of this system. It required a computer for controlling the rest of the system, which could integrate the processor, signal generator, data acquisition and signal processing in real time. Real time measurement is a crucial requirement for the system to ensure the functionality of the system during the measurement and also to make sure that the signals were not clipped and the parameters were selected appropriately [7]. In the testing environment, data quality checks could reduce the risk and expense of retesting, where data visualization is also important for providing a quick review of the results. For visualization, the focus is on both real-time views and the end results.

Besides the computer, transducers also play an important factor in producing a good ultrasonic system. Two important parameters that must be considered in order to have a good system are frequency and bandwidth [8]. The low frequency can be used to improve the SNR in lossy materials and the large bandwidth could be used in conjunction with a pulse compression technique [9] to further improve SNRs. Nevertheless, it is difficult to produce a piezoelectric material that can fulfil these requirements [10], and in particular, to provide the bandwidth needed to make good use of pulse compression techniques. For this reason piezocomposite transducers have been used in this system to further enhance its capabilities in addressing problems in ultrasonic testing of high loss materials. These have the ability to produce an ultrasonic signal with broader bandwidth at low frequency [11].

Figure 4.2 shows a schematic diagram of the system that was used throughout the study. The main components are a method for generating and processing signals suitable for

pulse compression, the transducers, and other electronics and instrumentation for amplification and display. A display unit is also included.

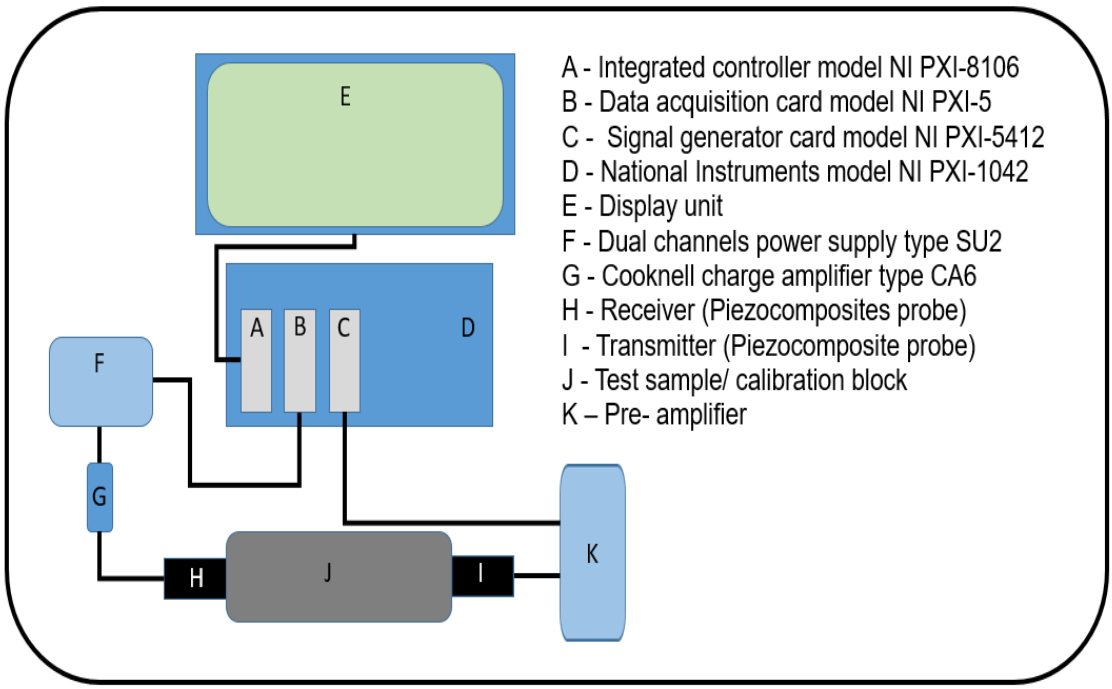

Figure 4.2: Schematic diagram of the developed system

4.3.1 The National Instruments PXI System

In this system, the PXI system from National Instruments model NI PXI-1042 was used as the integral hardware unit, and contains the components A-D in Figure 3.1. A photograph of the front of the unit is shown in Figure 4.3, where the main cards controlling the experiment can be seen. The unit contains an integrated embedded controller model NI PXI-8106 (Figure 4.4 (a)). The embedded controller enables the PXI unit to function as a computer, so as to integrate the signal generator cards and data acquisition card. The controller card also consists of communications ports that can be utilised for data transfer and connection for further data processing. These ports such as few Universal Series Bus (USB) ports, Digital Visual Interface (DVI) port, display port, serial port and internet port

are crucial for the system. This internet connection is important to keep the machine updated especially for antivirus updates.

The PXI system is also equipped with a signal generator card model NI PXI-5412 as well as data acquisition card model NI PXI-5105 with 12-bit 60 Ms/s digitizer (Figure 4.4 (b)). The signal generator is a 100 MS/s arbitrary waveform generator featuring 14-bit resolution and up to 256 MB of on-board memory in a compact, one-slot 3U PXI module. Because the NI PXI-5412 uses the PCI bus to communicate with the host computer, it is possible to download waveforms at up to 84 MB/s far faster than traditional GPIB-based instruments. This is useful for generating the type of waveforms needed for pulse compression.

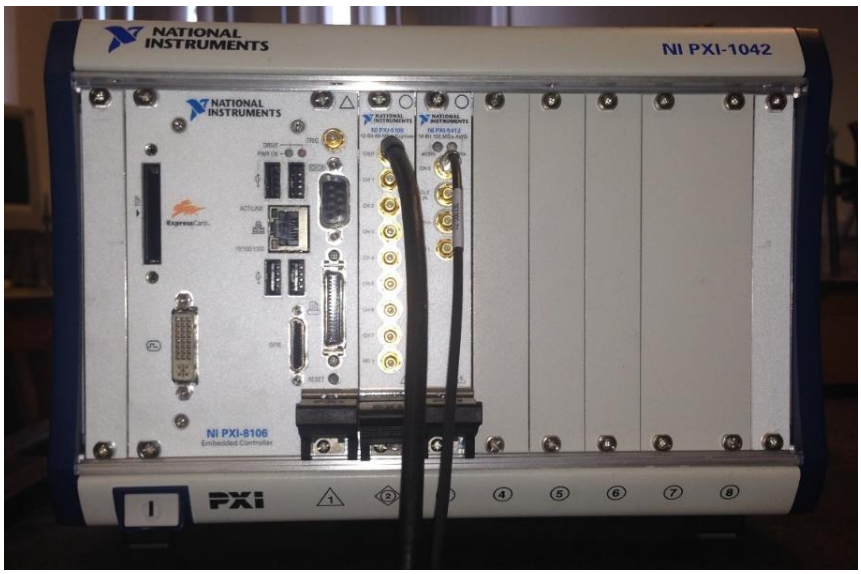

Figure 4.3: PXI system model NI PXI-1042 used through out the study

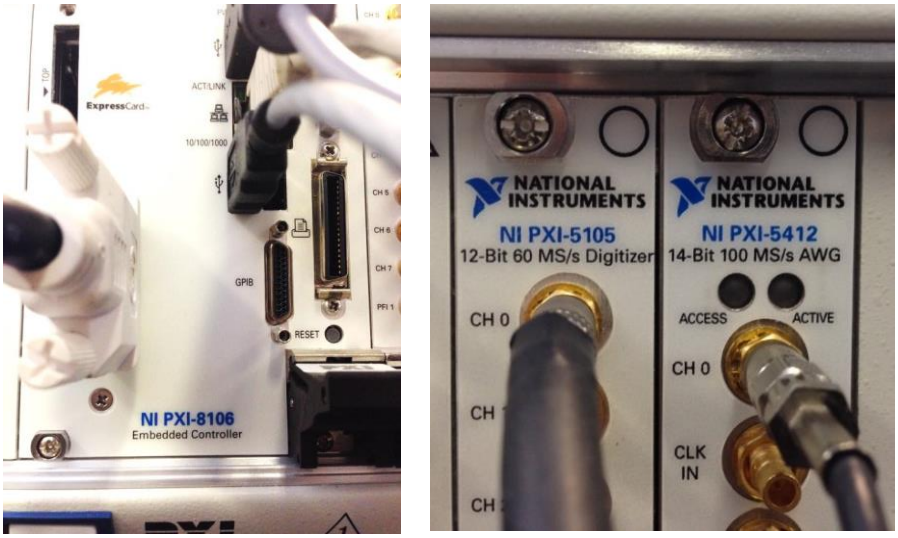

(a) *(b)*

Figure 4.3: (a) Integrated embedded controller; (b) signal generator card and data acquisition card

4.3.2 Piezocomposite transducers

An important feature of any ultrasonic instrumentation system is the transducer [12]. The transducer is one of the major elements that will be studied in this work. There are several different types of transducer that could be used for this study, the main aim being the generation of high amplitude signals with a broad bandwidth at frequencies in the 100-500 kHz range. The transducer types chosen for initial study were two types of piezocomposite transducers - Macro Fibre Composites (MFCs) and 1-3 Piezocomposites. Piezocomposite materials consisting of a piezoelectric active component and a passive matrix usually epoxy resin or other polymers. Such composites combine the piezoelectric properties of the ceramics with lower density and softness of the polymer. The combination of these materials within the composite gives piezocomposite devices an advantage over conventional piezoelectric bulk ceramic material, which has greater natural bandwidth [11]. This makes them ideal for pulse compression, where greater bandwidth is a big advantage. 1-3 piezocomposite materials are made of thin rods of ceramics embedded in a polymer

material. Their properties depend on the ceramic and polymer properties and the microstructure itself.

There are two basic structures of piezocomposite material, namely 1-3 structure and 2-2 structure [13]. The 1-3 structure is so named because the pillars of ceramic are continuous in one dimension, while the Polymer is continuous in all three dimensions. This structure is commonly used in 1-3 piezocomposite transducers. In the 2-2 structure, both the ceramic and the polymer filler are continuous in two dimensions with lengths of ceramic and polymer arranged in parallel. 2-2 structures are the type used in MFC transducers. Various sizes and shapes of 1-3 piezocomposites transducers are available, depending on the application. Figure 4.5 shows an example of both 1-3 and 2-2 piezocomposite structures.

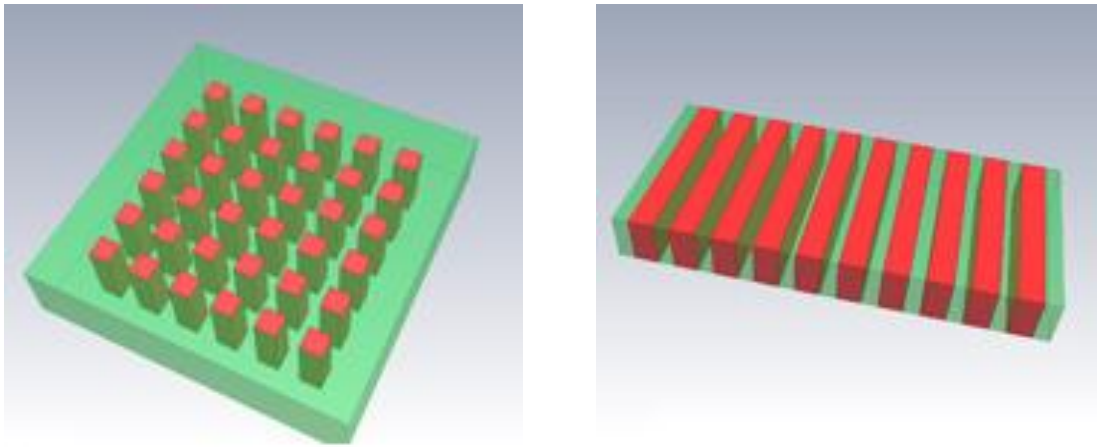

(a) *(b)*

Figure 4.5: (a) Example of piezocomposite materials with 1-3 structure commonly used in 1-3 piezocomposite transducers; (b) piezo ceramic 2-2 structure mainly used in MFC devices [14]

1-3 piezocomposite transducers consist of two basic components, namely a piezoelectric active ceramic in the form of a rod or a fibre and a non-active polymer matrix where the rod is embedded [15]. There are a few techniques that have been used to produce

1-3 piezoelectric materials, but commercially the most used techniques are dice-and-fill technique and soft-mould technique [13]. The dice-and-fill technique is the simplest method involving 6 steps as illustrated in Figure 4.6. It starts with a piezoelectric ceramic plate which is then sliced in two orthogonal directions to a depth of a few hundred micrometers to produce rectangular rods in a square arrangement (Figure 4.6 (c)). After the sawing process, the rod structure is filled with polymer both sides (in Figure 4.6 (d)), then being polish and electrode as in Figure 4.6 (e) and (f). The soft mould technique is quite popular in producing 1-3 piezo-ceramic with cylindrical rod structure. Even though this technique is simpler and doesn't involve many steps as in dice-and-fill technique, but precision and high technology is needed in order to prepare a master mould. Performance of 1-3 piezo transducers depends on the effective material properties of the composites. The effective properties of two component system can be influenced by factors such as density and dielectric and mechanical coefficient of the composites. The aim of these devices is to increase bandwidth, due to the interactions between each PZT pillar.

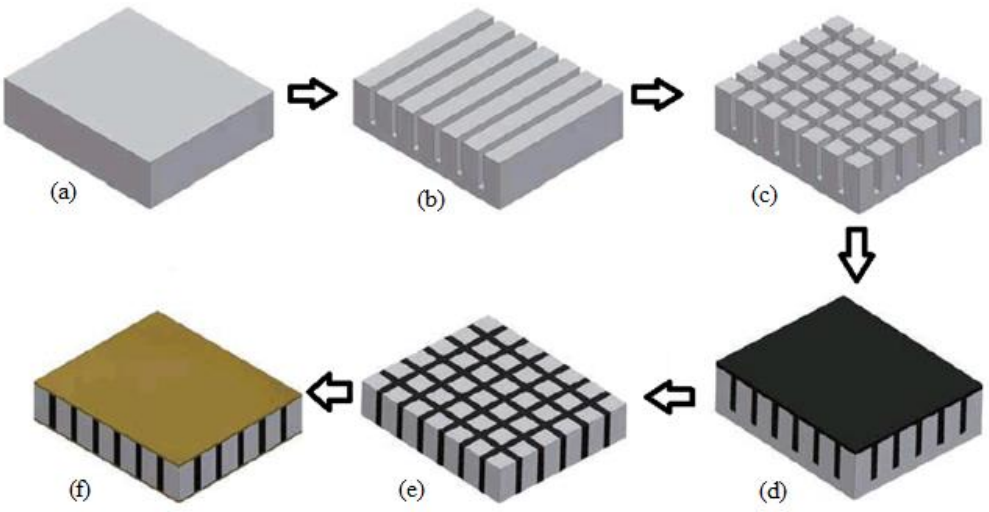

Figure 4.6: Steps that involved in dice-and-fill technique [14]

Macro Fibre Composite (MFC) is a type of piezocomposite material. It is a low profile sensor with high flexibility and durability. MFC is used primarily for frequencies up to 20 kHz, but in certain application they can be used up to 200 kHz. MFC is available in various forms; nonetheless, it can be classified within two basic categories, which are d_{33} and d_{31}. Figure 4.7 (a) shows an example of MFC type d_{33}. Because of the advantages it can offer, MFC has become more popular for various applications recently [16-18]. The main component for an MFC is a sheet of rectangular aligned piezo-ceramic (PZT) fibres that are sandwiched between sheets of structural epoxy, as shown in Figure 4.6 (b). The other two components of the MFC are the polymer matrix and the interdigital electrodes. The electrodes deliver the electric field required to activate the piezoelectric effect in the fibres and allows invoking the stronger longitudinal piezoelectric effect along the length of the fibres. The overall strength of MFC is heavily contributed by the combination of these components that are stacked together in a vacuum heating press process. The main advantage of MFC as compared to other type of ultrasonic transducer is its flexibility that makes it very suitable for use on flat and complex shape samples or structure.

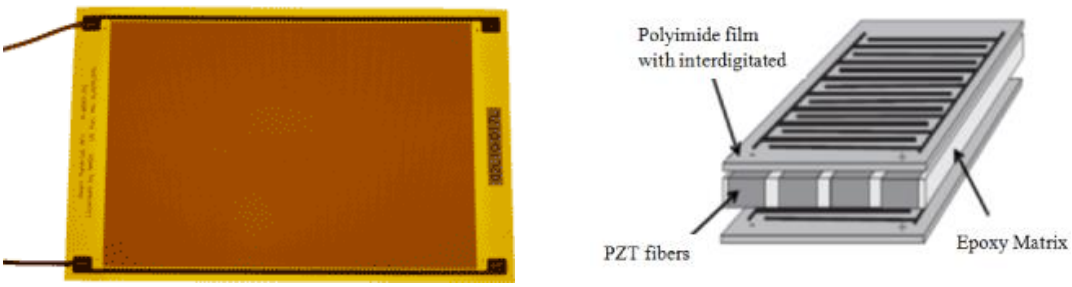

(a) *(b)*

Figure 4.7: (a) Example of MFC type d33; (b) basic components of MFC [19]

As explained earlier, MFC devices are available in d_{33} and d_{31} operational mode. This mode is determined by the order of its basic structure and this mode will determine

how it works. It is actually influenced by the arrangement of stacked metal electrode around the piezoelectric material. Figure 4.8 (a) shows the basic configuration in MFC type d_{33}. Metal electrodes are arranged side by side in opposite charge and the PZT material were sandwiched with electrodes that have the same charge. This type of MFC will produce shear ultrasonic waves rather than longitudinal waves. This is because the electrodes mutually opposite charges will attract each other while the same charge of the electrode that sandwiched the PZT material will repel each other. Alternating current flows continuously causes the piezoelectric composite materials to expand and contract continuously that turn produces a shear wave signal. Meanwhile, Figure 4.8 (b) shows the structure MFC type d_{31} were electrode with the same charge arranged adjacent and electrode with opposite charge are sandwiched the PZT material. This type of MFC is capable of producing longitudinal waves more than the shear waves. Figure 4.9 shows three different piezocomposites transducers that have been used in this study; Figure 4.9(a) are the longitudinal MFC (left) and shear MFC (right), Figure 4.9(b) are 50 mm diameter 1-3 piezocomposite transducers with 170 kHz centre frequency (will be later referred to as Transducer A) and Figure 4.9(c) 17 mm diameter 1-3 piezocomposite transducers with 300 kHz centre frequency (will be later referred to as Transducer B)

(a) *(b)*

Figure 4.8: Structure of (a) shear MFC (d_{33}), (b) longitudinal MFC (d_{31}) [20]

(a) *(b)* *(c)*

Figure 4.9: Piezocomposite transducers that have been used throughout the study; (a) longitudinal MFC (left) and shear MFC (right); (b) 50 mm diameter 1-3 piezocomposite transducers with 170 kHz centre frequency (Transducer A); (c)) 17 mm diameter 1-3 piezocomposite transducers with 270 kHz centre frequency (Transducer B)

4.3.3 Amplifier

The experiments on materials with high levels of scattering and attenuation required the use of amplification on both the input signal generated by the PXI system, and the output from the receiver transducer. The type of amplifier needed was different in each case, and photographs of each type are shown in Figure 4.10.

(a) *(b)*

Figure 4.10: Amplifier devices available with the system; (a) dual-channel power supply type SU2 with Cooknell charge amplifier type CA6; (b) in-house fabricated amplifier

A charge amplifier is a current integrator that might produces a voltage output proportional to the integrated value of the input current [24]. In this kind of amplifier, it counterbalances the input charge and produces an output voltage inversely proportional to the value of the reference capacitor. It can be said that the circuit acts as a charge-to-voltage converter. The gain of the circuit depends on the value of the feedback capacitor. This type of amplifier is commonly used as amplification of signals from piezoelectric sensors and photodiodes, where the charge output from the transducer is converted into a voltage. Besides that, it is also used widely in ionizing radiation, such as the proportional counter or the scintillation counter, where the energy of each pulse of detected radiation due to an ionising event are detected and measured.

The CA6 Charge Amplifier that was used throughout this study was specifically designed for use with ultrasonic transducers. It is an extremely low noise, high gain amplifier with high interference rejection housed in a compact robust casing. The specification of the charge amplifier is described in Figure 4.1 below:

Input	Connector N' type socket fitted as standard Input impedance 100 Ω approx. above 10 kHz.
Output	Connector 'N' type socket fitted as standard
Performance	Charge Sensitivity 250mV/Pico-coulomb nominal. Bandwidth <10kHz to >25MHz
D.C. Supplies	+ve +24V @ ≈80mA. ; -ve -24V @ ≈7mA.
Packaging	Brass box & lid all Gold Plated for interference immunity & potted for atmospheric protection.
Dimensions	77 mm x 26 mm x 41 mm excluding connectors. 123mm x 26mm x 41mm including connectors. Weight: 0.5Kg

Table 4.1: The specification of the charge amplifier

Beside the charge amplifier, there is also another amplifier that was used in the study. It is an in-house fabricated power amplifier (Figure 4.9(a)), normally been used as a pre-amplifier when testing a material with very high attenuation or big lumps of materials like a concrete block.

4.4 Software

In addition to the hardware described above, the software is also an equally important element of this system. This is because the software controls and integrates the hardware so that it can function as intended. Moreover, this software is the backbone of the system functioning a mediator between machine and the user. As the PXI box is driven by an integrated embedded controller from National Instrument, LabVIEW has become the main software used in this system [25]. Lab VIEW was used to design the interface for controlling the ultrasonic signal generation as well as for the data acquisition. The display was in the form as shown in Figure 4.11. Note that the software that was implemented on the PXI system, and which is used in this study, was developed primarily by Dr Marco Ricci and Mr Stefano Laureti, as part of a joint research programme with the University of Perugia. However, the original software has been modified from time to time to suit the experiments that were carried out throughout the study.

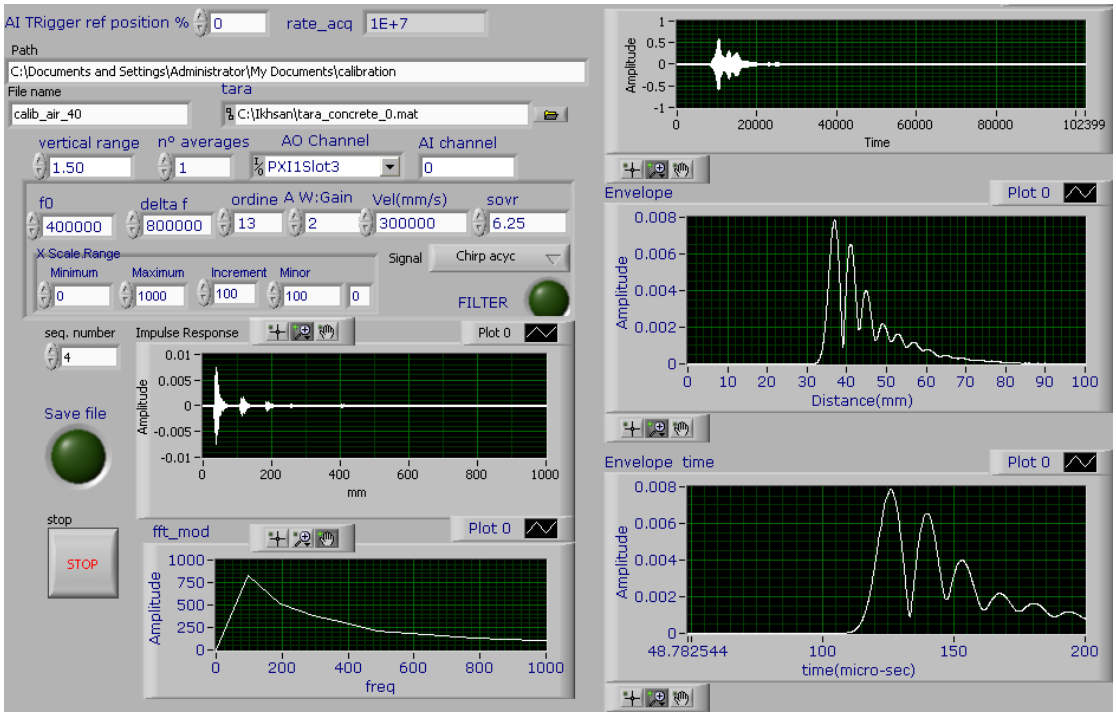

Figure 4.11: Example of a front panel of the lab view interface that has been used for signal generation and data collection

The main parts of the display are as follows:

i. Raw Output: Signal that shows the raw output obtained from the receiver (before any signal processing such as a cross-correlation)

ii. Impulse Response: Showing the output signal that has gone through a cross-correlation process

iii. Impulse response envelope: The result of using pulse compression on the output signal, which has then been subsequently smoothed and rectified. The display is in terms of distance (mm) into the sample

iv. Impulse response envelop time: As in iii, but displayed in time (μs)

v. FFT Mod: Fast Fourier Transform of the output signal to obtain spectral information.

The operating system for the developed software such as saving files, start and stop signals are controlled using the interface as shown in Figure 4.10 above and can be customized according to requirements. Key parameters such as central frequency (f_0), bandwidth (*delta f*), signal amplitude (*gain*) and velocity (*Vel* (mm/s)) can also be adjusted. Since the PXI system was equipped with a signal generation card and a data acquisition card that has an unequal sampling rate as in Figure 4.4 (b), a scaling factor (SOVR) is used to adjust both cards to operate at the same rate, depending on the desired central frequency. This ensures that the acquisition rate is always 10 Msamples/second at all times.

The software also allows users to select the channel for signal generation (channel A0) port and signal acquisition port (channel A1) because both cards consist of a few channels each. As the system is meant to be used with low frequency ultrasound as well as coded waveforms, it has been equipped with the option that allows users to select the type of input signal to be used (whether it is chirps, Golay, bipolar Golay or MLS). In addition, there are also other parameters that can be changed to get the best signal display for easier data interpretation as follows:

i. Vertical range: The vertical range is an option for setting the range in x-axis in the output depending on the amplitude of output signal. It has to be in an optimum value in order to get a visible signal, but cannot be so big that it causes clipping of the signal.

ii. Rate acq: This is the received sampling rate of the data acquisition card. For this system this value should always be 10 Mega-sample/s so that it is equal to generation rate. Based on the sampling theorem: rate of capacity must be at least ½ of the sampling rate.

iii. N_0 average: A filter function provided to smooth out the signal.

iv. X scale range: The range of x scale can be adjusted, thus changing the values of minimum and maximum time/distance to be displayed. This is convenient when trying to gate out electrical pick-up or unwanted direct coupling between two transducers, for instance.

v. Filter: A band pass filter that can filter out low and high frequencies, depending on the pre-determined values.

The LabView block diagram is shown in Figure 4.12. For each measurement to be carried out, it is important to maintain the parameters such as gain, vertical range, velocity and SOVR so that the acquired results are relatively comparable and between each of them. Nevertheless, if forced to be changed, all the results have to be normalized during the analysis process. Before any application, the software has been validated and calibrated by comparing the acquired data with the data gained by PUNDIT.

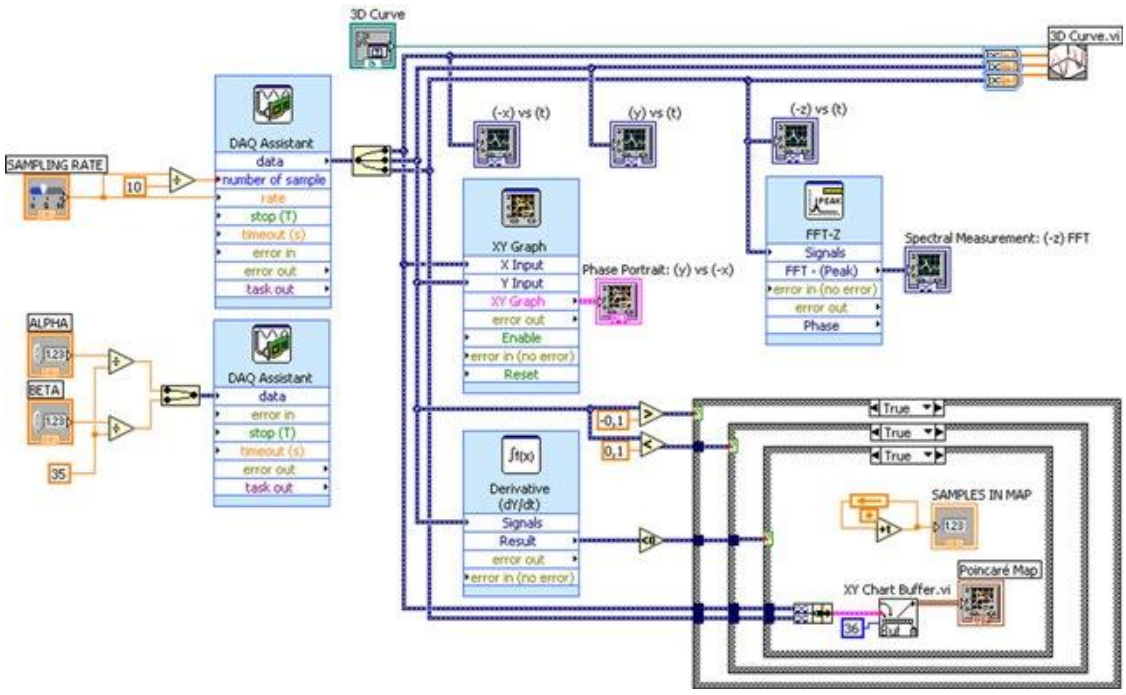

Figure 4.12: Example of LabVIEW block diagram for signal generation and data acquisition

4.5 Calibration

Calibration refers to the act of evaluating and adjusting the precision and accuracy of measurement equipment. In ultrasonic testing, several forms of calibration must occur. First, the electronics of the equipment must be calibrated to ensure that they are performing as designed. It is also necessary for the operator to perform a "user calibration" of the equipment. This user calibration is essential because most ultrasonic equipment can be reconfigured for use in a large variety of applications. The user must calibrate the system, which includes the equipment settings, the transducer, and the test setup, to validate that the desired level of precision and accuracy are achieved. In this particular system, there is another calibration whish should be normally performed once in a while, especially when it involves testing on different sample or when changing the type of transmitting signal.

Calibration of the system is run by bridging the two transducers together. If the system is in a well-calibrated condition, it is supposed to signal that the first peak is at zero position. If the peak is not at zero (Figure 4.13), the value of the x –axis, measured from the peak to the zero is taken and inserted in the MATLAB script at the back panel of the software. After that, validation testing was performed using the known sample where in this case a calibration block made of Plexiglas is used as illustrated in the Figure 4.14. If the calibration has been carried out correctly, the system should give a reading of the transit time as written on the calibration block which is 25.2 μs.

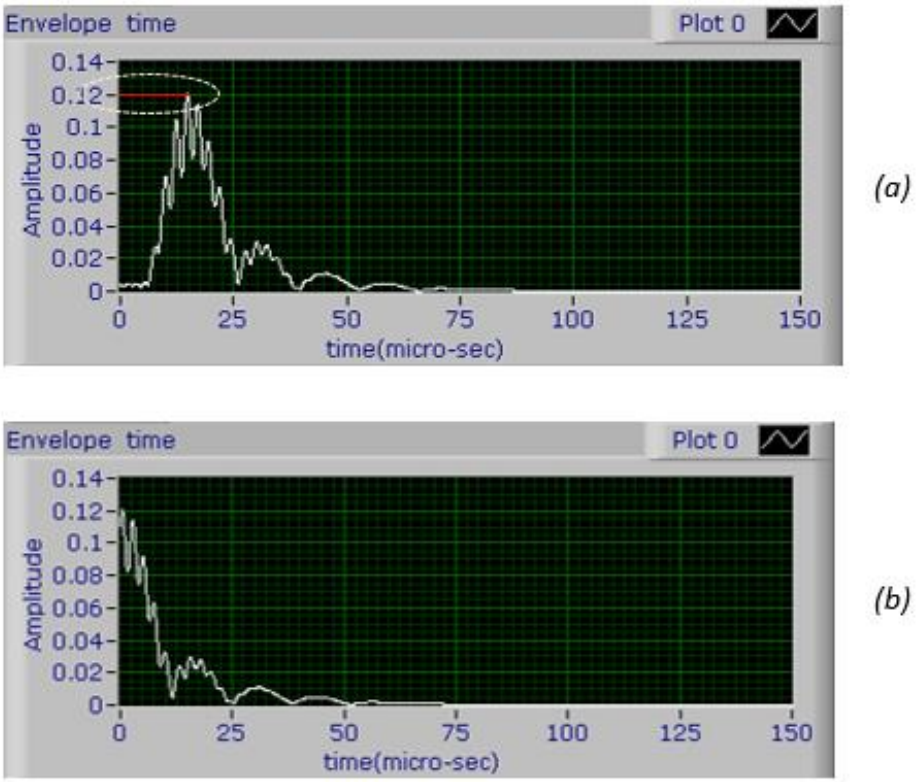

Figure 4.13: (a) Result of uncalibrated figure with the correction value (red line in white doted ellipse mark); result of calibrated figure where the first peak start at zero.

Figure 4.14: A Plexiglas calibration and receiver block with 25.2 µs transit time sandwiched by two piezocomposite transducers of 55 mm diameter operating at a centre frequency of 170 kHz.

4.6 Signal processing

Digital signal processing (DSP) is a branch of signal processing that uses digital systems to operate on signals. It is a process of analysing and modifying a signal to optimize or improve its efficiency or performance. It involves applying various mathematical and computational algorithms to analogue and digital signals to produce a signal that's of higher quality than the original signal. The advantages of digital over analogue signal processing is that memory is more easily employed (so that time may be re-run at different speeds and directions) and that a wider range of arithmetic operations and algorithmic complexity is possible; in addition, DSP allows the implementation of variable bandwidth filters and the like. However, in some instances digital techniques are slower than analogue techniques.

For this system developed, signal processing is divided into two parts, real time signal processing and post processing. Real time signal processing can be carried out using the integrated software within the system. Functions such as vertical range, average N0, x-scale range and filters can be applied accordingly. In addition, this software is also able to display the results in the form of cross correlation or pulse compression in real time. Details about this real time signal processing functions are as explained in section 3.4. Post processing was performed off-line using Matlab.

4.7 Conclusion

This chapter is a very important part of this thesis because it discussed in details the ultrasonic system which has been developed specifically for the testing of materials with high degree of attenuation. The system that has been utilized ultrasound at frequencies below MHz range (sub-MHz frequencies) was designed with a special ability, particularly in terms of penetration ability which is a major problem when conducting ultrasonic testing of high attenuation samples such as concrete, multi-layered composites and thick section of

polymers. In this chapter has described in detail the hardware that was used within the system such as the National Instruments PXI box that has been used as the integral part of the developed system. Besides that, the other important element was the piezocomposite transducers have been an important ingredient to a system that has been developed. The transducer that had played a big part of producing good ultrasonic signal that has been proven to be effective when used in conjunction with pulse compression technique, the signal that has a broad bandwidth at low frequency. In addition, this chapter also discusses the software that has been developed with a research group from the University of Perugia, which is part of our research collaboration. Finally, this chapter has been closed with a discussion of calibration that was used throughout this study as well as image processing techniques are also an important element contributing to the success of this system.

References

[1] S. R. Doctor, H. D. Collins, S. L. Crawford, T. E. Hall, A. J.Baldwin, R. E. Bowey, "Developement and Validation of Real-Time SAFT-UT System for Inservice Inspection of LWR," *Nucl. Eng. Des.*, vol. 89, pp. 357–369, 1985.

[2] V. Bucur and I. Böhnke, "Factors affecting ultrasonic measurements in solid wood," *Ultrasonics*, vol. 32, no. 5, pp. 385–390, 1994.

[3] J. R. Berriman, D. a Hutchins, A. Neild, T. H. Gan, and P. Purnell, "The application of time-frequency analysis to the air-coupled ultrasonic testing of concrete.," *IEEE Trans. Ultrason. Ferroelectr. Freq. Control*, vol. 53, no. 4, pp. 768–76, Apr. 2006.

[4] X. Zhao, H. Gao, and G. Zhang, "Active health monitoring of an aircraft wing with embedded piezoelectric sensor / actuator network : Defect detection , localization and growth," *Smart Mater. Struct.*, vol. 16, no. 5, pp. 1208–1217, 2007.

[5] R. Raišutis, E. Jasiūnienė, R. Šliteris, and A. Vladišauskas, "The review of non-destructive testing techniques suitable for inspection of the wind turbine blades," vol. 63, no. 1, pp. 26–30, 2008.

[6] Y. Zhu, J. P. Weight, and A. A. Filter, “Ultrasonic Nondestructive Evaluation of Highly Scattering Materials Using Adaptive Filtering and Detection,” *IEEE Trans. Ultrason. Ferroelectr. Freq. Control*, vol. 41, no. 1, pp. 26–33, 1994.

[7] T. Olofsson, “Deconvolution and Model-Based Restoration of Clipped Ultrasonic Signals,” *Instrum. Meas. IEEE Trans.*, vol. 54, no. 3, pp. 1235–1240, 2005.

[8] G. M. Zhang, C. G. Hou, Y. W. Wang, and S. Y. Zhang, “Optimal frequency-to-bandwidth ratio of wavelet in ultrasonic non-destructive evaluation,” *Ultrasonics*, vol. 39, no. 1, pp. 13–17, 2001.

[9] M. Nisoli, S. De Silvestri, and O. Svelto, “Generation of high energy 10 fs pulses by a new pulse compression technique,” *Appl. Phys. Lett.*, vol. 68, no. 20, pp. 2793–2795, 1996.

[10] C. S. Desilets, J. D. Fraser, and G. S. Kino, “The design of efficient broad-band piezoelectric transducers,” *IEEE Trans. Sonics Ultrason.*, vol. 25, no. 3, pp. 115–125, 1978.

[11] R. Pullin, M. J. Eaton, M. R. Pearson, C. Featherston, J. Lees, J. Naylon, A. Kural, D. J. Simpson, and K. Holford, “On the development of a damage detection system using macro-fibre composite sensors,” in *Journal of Physics: Conference Series*, 2012, vol. 382, p. 012049.

[12] Y. C. F. Hayward G, Hutchins D A, Papadakis E P, Smith W L, Thomson R B, Wagner J W, *Ultrasoic Measurement Methods*. Academic Press Ltd., 1990.

[13] S. Gebhardt, A. Schönecker, R. Steinhausen, T. Hauke, W. Seifert, and H. Beige, “Fine scale 1-3 composites fabricated by the soft mold process: Preparation and modeling,” *Ferroelectrics*, vol. 241, no. 1, pp. 67–73, 2000.

[14] P. Dumas, J. Poguet, and G. Fleury, “Piezocomposite technology An innovative approach to the improvement of N . D . T . performance using ultrasounds,” in *European Conference on Nondestructive Testing*, 2002, no. 8, pp. 20–21.

[15] T. J. Clipsham and T. W. Button, “1-3 Piezocomposites realised from small feature size, high aspect ratio, hot embossed moulds. Part II: piezocomposite fabrication,” *Microsyst. Technol.*, vol. 16, no. 11, pp. 1983–1988, 2010.

[16] I. D. Park G, Cudney H, “Impedance-based health monitoring of civil structure components,” *J. Infrastruct. Syst.*, vol. 6, no. 4, pp. 153–1670, 2000.

[17] H. M. Matt and F. L. Di Scalea, “Macro-fiber composite piezoelectric rosettes for acoustic source location in complex structures,” *Smart Mater. Struct.*, vol. 16, no. 4, pp. 1489–1499, 2007.

[18] B. A. Hagood N, “Development of piezoelectric fiber composites for structural actuation,” *strucutures, Struct. Dyn. Mater.*, vol. 93, no. 12, pp. 3625–3638, 1993.

[19] W. K. Wilkie, D. J. Inman, J. W. High, and R. B. Williams, “Recent Developments in NASA Piezocomposite Actuator Technology,” *Smart Materials Corp. Publications*. pp. 1–4, 2005.

[20] A. L. Bernassau, D. Hutson, C. E. M. Démoré, and S. Cochran, “Characterization of an epoxy filler for piezocomposites compatiblewith microfabrication process,” *IEEE Trans. Ultrason. Ferroelectr. Freq. Control*, vol. 58, no. 12, pp. 2743–2748, 2011.

[21] A. A. T. Grattan K T V, *Ultrasonic sensors*. IOP Publishing Ltd., 1997.

[22] G. M. L. Svilainis, “Power amplifier for ultrasonic transducer excitation,” *Issn 1392-2114 Ultragarsas*, vol. 1, no. 58, pp. 30–36, 2006.

[23] R. Senani, D. R. Bhaskar, A. K. Singh, and V. K. Singh, *Current Feedback Operational Amplifiers and Their Applications*. Springer, 2013.

[24] E. Quantistica, S. E. Cnr, and F. Ring, “feedback charge amplifier integrated on the detector water,” *Nucl. Instrum. Methods Phys. Res.*, vol. 288, no. 288, pp. 168–175, 1990.

[25] G. R. A. and M. C. J. M. Ferreira, R. Costa, “The PEARL digital electronics Lab : Full access to workbench via the WEB,” 2002, no. 2016, pp. 1–6.

Chapter 5

Pulse Compression Ultrasonic Non Destructive Evaluation of Thick Industrial Polymer Samples

5.1 Introduction

Polyurethane is a polymer composed of a chain of carbamate (urethane) links [1]. It has been widely used in many industries and is an important polymer due to its uses in manufacturing in many different products. The properties of the polymer can be adjusted during manufacturing to give a wide range of mechanical properties. For example, in the form of a foam it can be used as: nonflexible and high-resilience foam seating; rigid foam insulation panels and microcellular foam seals and gaskets. It can also be used in durable elastomeric wheels and tires (e.g. escalator wheels), automotive suspension bushings, synthetic fibers and many other areas [2-3]. Because of its special properties such as high load capability, flexibility, tear resistance and resistance to water, it has been used in the oil and gas industry for many years. Of particular interest here is its use in the sea bed oil logging, as part of a flexible riser system [4] or as a bend stiffener [5]. Figure 5.1 shows some applications of polyurethane material in seabed oil logging. While it can offer many advantages, problems arise under certain situations. Obviously, following the Gulf of Mexico oil spill, it is very important that the structural integrity of such structures can be maintained in such a complicated and hostile environment [6]

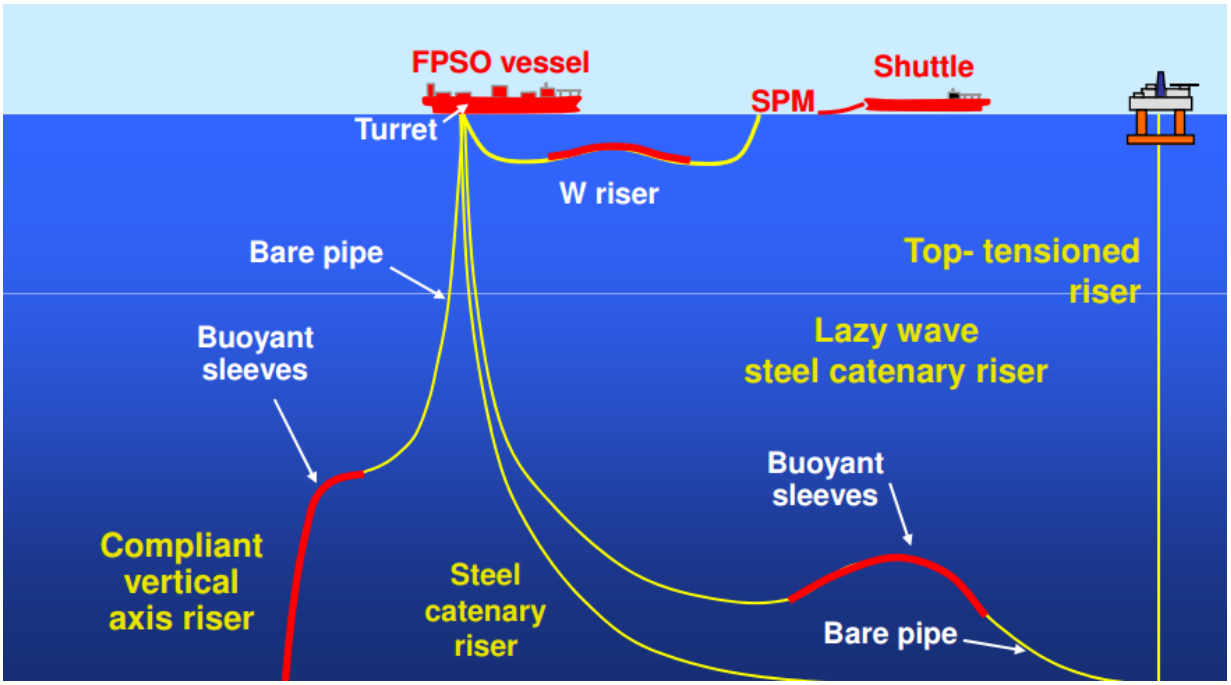

Figure 5.1: Example of the applications of flexible riser [7]

The flexible riser allows the oil platforms to move with wind and tides while remaining connected to the sea bed. A diagram of the internal structure of such a riser is shown in Figure 5.2, where the complicated structure can be seen. It is important how these risers are connected together in sections, and also how they connect to larger structures (the platform, sea bed etc.). In such cases, a bend stiffener is used, which restricts motion of the riser so as to avoid catastrophic failure due to fatigue or excessive motion of the riser at the connection point. The stiffener often has a hollow conical shape, with additional steel components to allow the riser and stiffener to be connected together. This is visible in the photographs shown in Figure 5.3(a), where the polyurethane material is visible. The BP material, shown in Figure 5.3(b), is similar to that tested in this thesis.

Since its application is the sea or seabed that has a very high pressure and unpredictable current, flexible riser must be meticulously designed with special properties suitable for its use. Typical flexible riser has several layers that have a very high strength while it has flexibility to suit the movement of the erratic water flow. Figure 5.2 shows an

example of a flexible riser available in the market, comprising of 10 layers in total. It can be seen that the core layer which is the carcass, made of metal materials (normally stainless steel) has a high strength to resist external pressure from collapse and was also designed for flexibility. This layer was covered with a pressure sheath usually made of nylon or high density polyethylene (HDPE), which works to absorb pressure by transferring the internal pressure to the pressure layer. Next is the vault layer to resist the internal and external pressure which is made of metal material. In the middle, there are two layers of armour wire to give an extra strength to the structure particularly to resist tensile load. In between the armours layers, there are a few layers of anti-wear tapes to ease abrasion between armours as well as the pressure layer. Outside of the structure, there is an external sheath made of HDPE which usually serves to protect abrasion, seawater penetration and steel corrosion to the internal layers. Sometimes, there is also a layer of protective sheath (but is optional) in which it serves to protect the external sheath. All of the layers contained in the flexible riser has its own function which eventually form a strong and flexible structure to suit its applications.

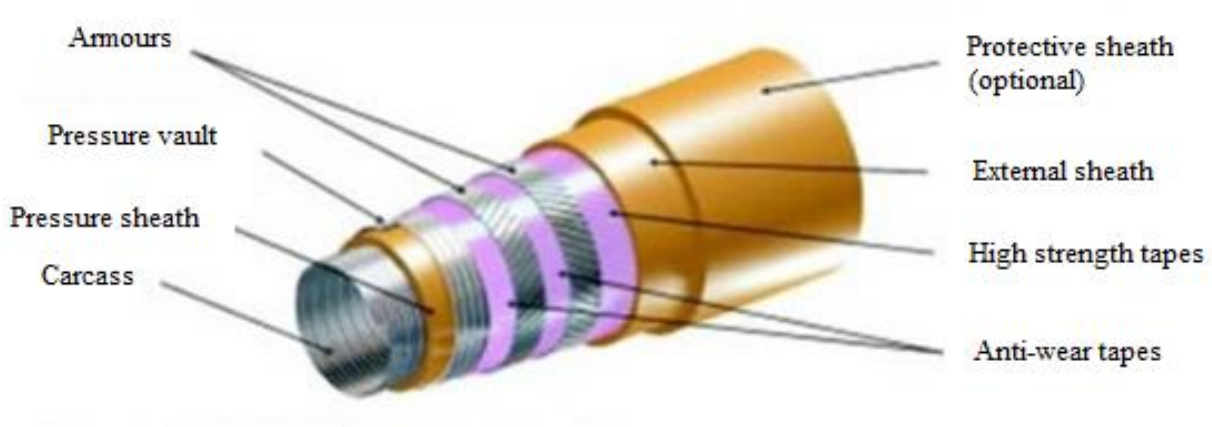

Figure 5.2: Typical flexible riser structure [8]

Although the flexible riser was designed to be flexible, there is a limit to its flexibility because the main characteristic of the structure is its strength. So to protect the riser reaching its elastic limit and to extend the life of the structure, bend stiffeners are used. Basically, bend stiffeners provide additional stiffness to the riser to limit bending stresses and curvature to acceptable levels. There are various sizes and specification for bend stiffeners. Each bend stiffener is specifically tailored to suit a particular application. Properties such as fatigue resistance, creep resistance, tensile strength and tear resistance are very important in the construction of a bend stiffener. Therefore, the polyurethane polymer materials are used as the basis for the construction of a bend stiffener. Figure 5.3 shows an example of bend stiffeners produced by Trelleborg Ltd. (Figure 5.3 (a)) and British Petroleum (BP) in Figure 5.3(b).

Because it is an important component, there is a need to ensure they are always safe to use at all time. Therefore, structure integrity inspection should be carried out especially during the manufacturing process to prevent the installation of bad components. Besides that, the process of replacing defective components is expensive because everything needs to be carried out offshore and sometimes at the seabed. So a testing technique (especially NDT) is required for this structure and ultrasonic testing is one of the suitable techniques. But Polyurethane material which is the base polymer for the construction of a bend stiffener is quite extenuative to ultrasonic signal and the fact that it's a huge and thick structure, makes it more difficult for testing. Therefore, an ultrasonic system with low frequency and pulse compression technique that has been developed, was used to investigate if it could penetrate this material and produce information highlighting any defects therein, especially to detect the presence of air bubbles.

(a)

(b)

Figure 5.3: (a) Polyurethane bend stiffener as used in the oil and gas industry by Trelleborg Ltd [9];(b) BP bend stiffeners for use in North Sea oils and gas platforms [10]

5.2 NDE polyurethane material as used in riser stiffeners

Measurement of the ultrasonic properties of polyurethane in bulk solid form has only received limited study. In most cases, it is used only in small thicknesses. For example, it has been tested with ultrasound when used for the strengthening of composite structures

[11]. Also, when used as a coating, its attachment to the substrate can be estimated [12]. As a foam product, air-coupled ultrasonic techniques can be used, due to the low acoustic impedance of the material which is better-matched to air than many materials [13-14]. The use of polyurethane paint coatings has also been observed to affect laser-based ultrasonic NDE systems [15]. However, the NDE of large bulk polyurethane material, as used in bend stiffeners, seems not to have been described in any literature.

5.3 Initial measurements of riser stiffener samples.

Because of the above, it was necessary to perform some initial experiments to characterise the material in terms of ultrasonic propagation. In particular, the attenuation within the sample was found to be sufficiently high that testing in thick sections could not be performed using conventional ultrasonic frequencies at frequencies higher than 1 MHz. This is due to the large attenuation of signals within the material.

At the initial stages of the experiment, the ultrasonic system needed to be flexible in design, so as to achieve the best set up that can be used on a polyurethane sample. This is because there are certain parameters such as the type of waveforms, center frequency, frequency bandwidth, time duration and many others that need to be determined for that particular type of material and the type of transducers used [16]. Figure 5.4 shows the sample chosen for this study. It is a polyurethane section, which was part of a larger structure used within a riser stiffener in the underwater oil and gas industries. The sample shown is 1.20 m long, and 0.16 m thick at its thicker end. The material is very attenuating as such conventional signals could not be used to detect defects within the sample.

In the early stages, few types of ultrasonic transducers have been considered to be used in this study including MFC, piezocomposite and piezoelectric transducers. MFC was chosen because of their physical form that is thin and flexible allowing it to be integrate

with the surface or shape of the structure to be tested. Besides, MFC is capable of producing shear wave ultrasound which its properties can be applied in the polarization technique. But after running a series of tests using MFC, it was found that the energy is much lower than the energy generated from other ultrasonic transducers such as piezocomposite as well as the normal piezoelectric transducer. Therefore, the use of MFC in this study had been stop and focused on the use of piezocomposite and piezoelectric transducers throughout the study.

A comparison (reported later in this Chapter) was carried out between the narrow and broad bandwidth transducers and their impact on the chirps and bipolar Golay. For this purpose, two types of transducer were used to study the effect of centre frequency and bandwidth on the pulse compression system, noting that the choice of modulation scheme will depends heavily on the available bandwidth. The transducers were a narrow bandwidth conventional piezoelectric transducer with a nominal centre frequency of 200 kHz, and a broader bandwidth piezocomposite transducer with a maximum output at ~300 kHz. These two transducers are shown in Figure 5.5. Measurements were taken in either through transmission, so as to measure the attenuation properties of the material, or in pitch-catch for imaging purposes. The waveforms (either chirp or binary) were generated using an arbitrary waveform generator within a National Instruments PXI system, details about the PXI system were explained in chapter 4.

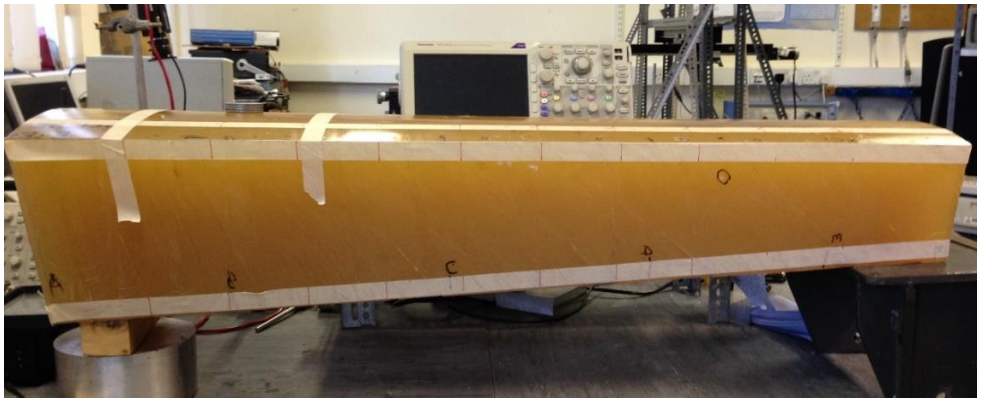

Figure 5.4: One of the polyurethane samples that were used in the study

Figure 5.5: Photograph of the narrow bandwidth conventional piezoelectric transducer (right) and the, broad bandwidth piezocomposite transducer (left)

Initial tests were carried out to determine what frequencies could penetrate the material using conventional pulse-echo inspection. Figure 5.6 shows the frequency response of the piezoelectric and piezocomposite transducers, which represent the narrow and broad bandwidth transducers respectively. It was found that the piezocomposite transducer gave a better result because it produced a higher amplitude while also generating a broader signal useful for pulse compression technique. It was thus decided that pulse compression could be used quite effectively in this material. However, it also meant that this had to be performed at frequencies below 1 MHz.

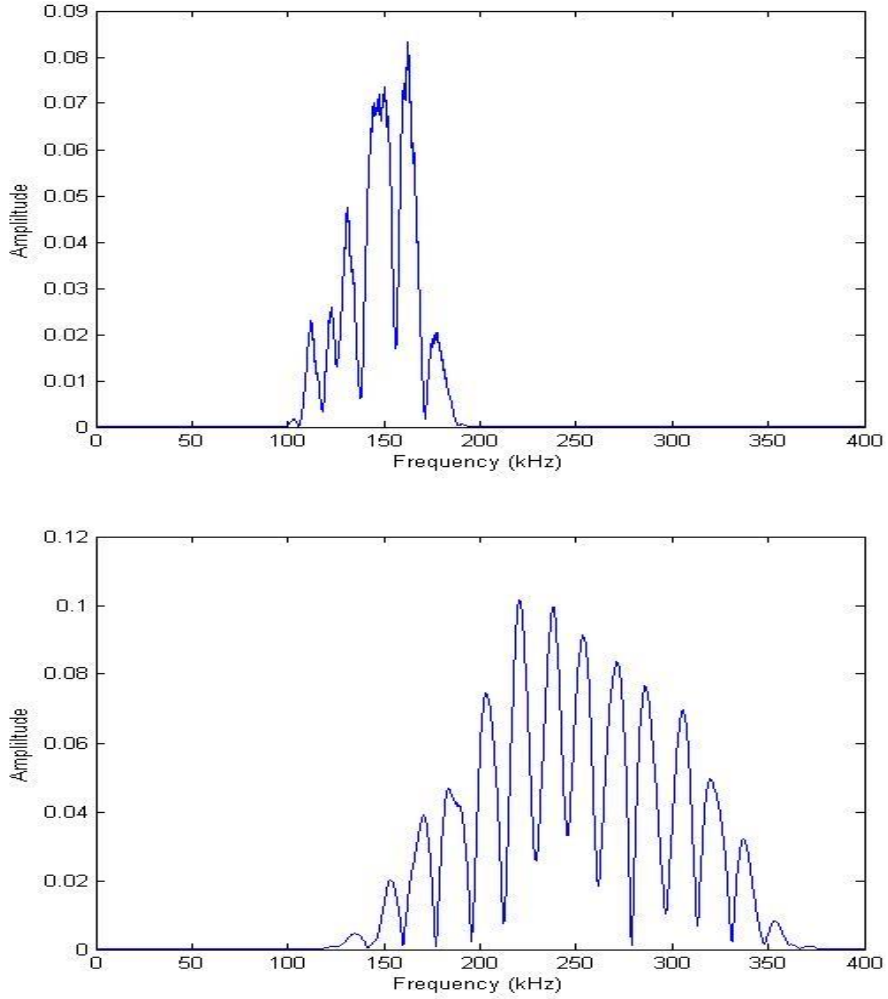

(a)

(b)

Figure 5.6: (a) Frequency response of the chirp obtained from the polyurethane sample of (a) narrow band transducer (piezoelectric); (b) broad band transducer (piezocomposite)

Following these measurements, it was decided that a centre frequency of 250 kHz with 100 kHz bandwidth would be used for NDE tests on polyurethane. This used piezocomposite transducers shown earlier in Figure 3.8(c) which were obtained from (EOFE Ultrasonic Co. Ltd), and were designed primarily for high frequency SONAR. They had a diameter of 17 mm. Tests were carried out to determine the bandwidth of these transducers, with the results being shown in Figure 5.7. Initial tests were performed with a chirp signal where the range of frequencies ($f_2 - f_1$) covered by the chirp could be adjusted, as could the total time duration (T) and the centre frequency (f_0). In this case the values were T = 0.07 ms, $f_2 - f_1$ = 250 kHz and

f_0 = 275 kHz. Figure 5.8 shows a typical waveform received in pitch-catch measurement on a 120 mm thickness of polyurethane, demonstrating good transmission. Attenuation within the material using such a system could then be determined. Generally, attenuation coefficient test requires different thickness for its measurement. The shape of this sample (tapered) gave advantages in this situation (Figure 5.3).

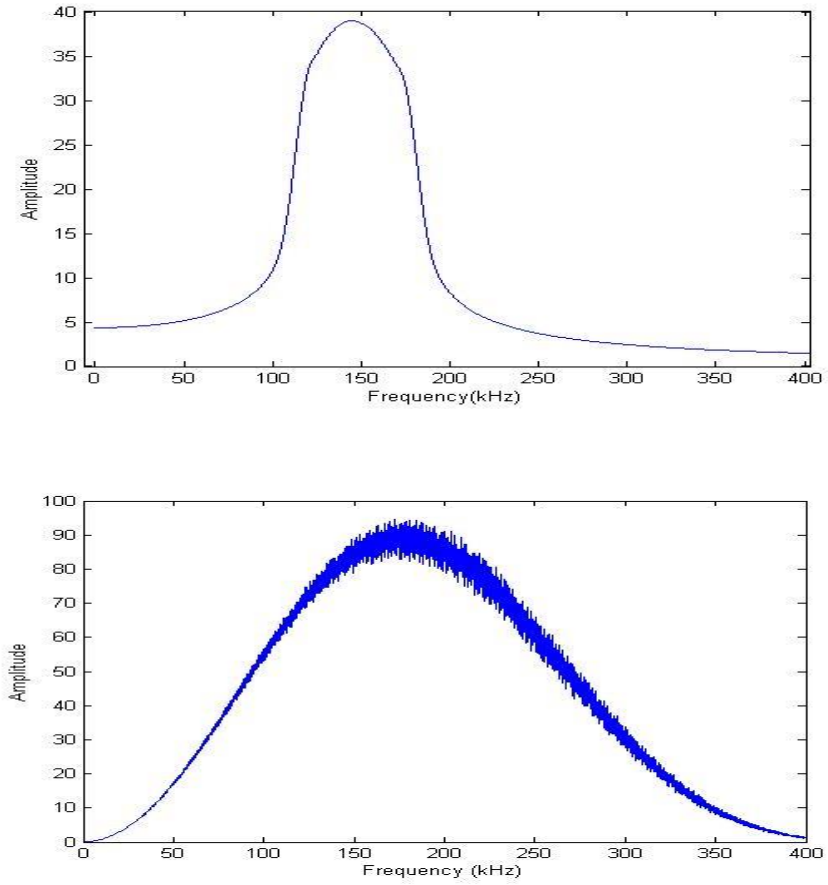

(a)

(b)

Figure 5.7: Frequency response of the 300 kHz piezocomposite transducers from direct coupling of (a) narrow band transducer (piezoelectric); (b) broad band transducer (piezocomposite)

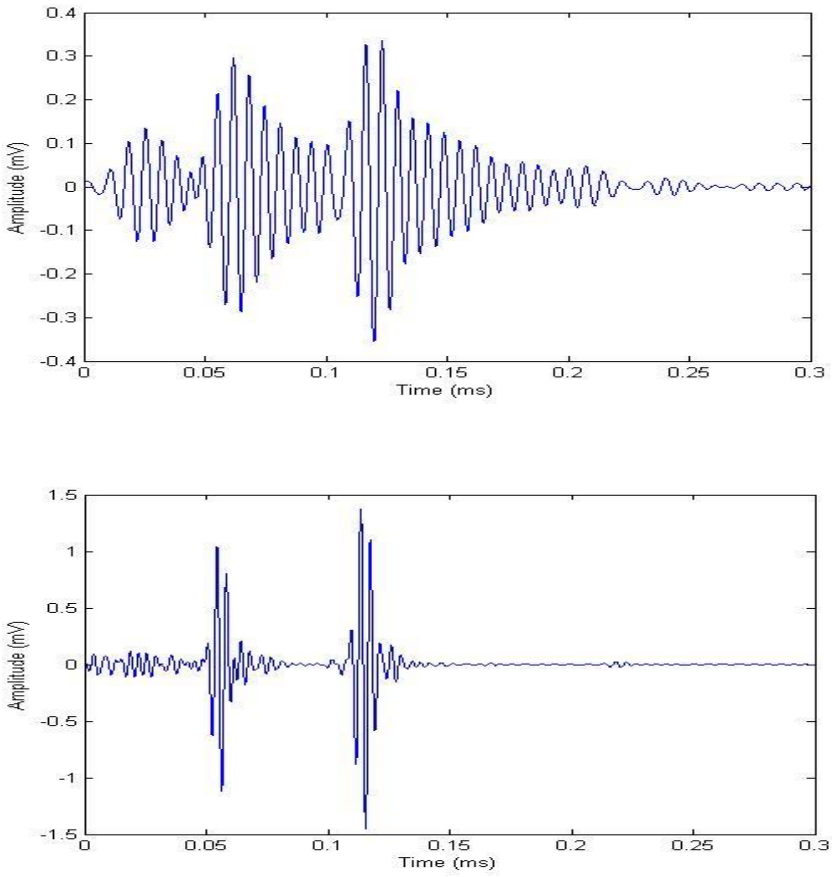

Figure 5.8: Pulse compression received signal obtained from the defect area of polyurathane sample of (a) narrow band transducer (piezoelectric); (b) broad band transducer (piezocomposite)

From Equation 1.3, it can be seen that the slope of a graph of amplitude vs thickness gives a measure of the attenuation coefficient of the material. For this test, 10 locations (with different thicknesses) were selected and marked as locations for a through-transmission measurement, as shown in Figure 5.9. Surface preparation was not necessary for this sample because the surface was already smooth. Conventional ultrasonic couplant was used between the transducers and the sample surface, noting that the shape of the sample surface was not flat (but was slightly curved with a radius of 0.2 m). The measurement was repeated 10 times at each location, so that a graph of amplitude vs. sample thickness could then be plotted.

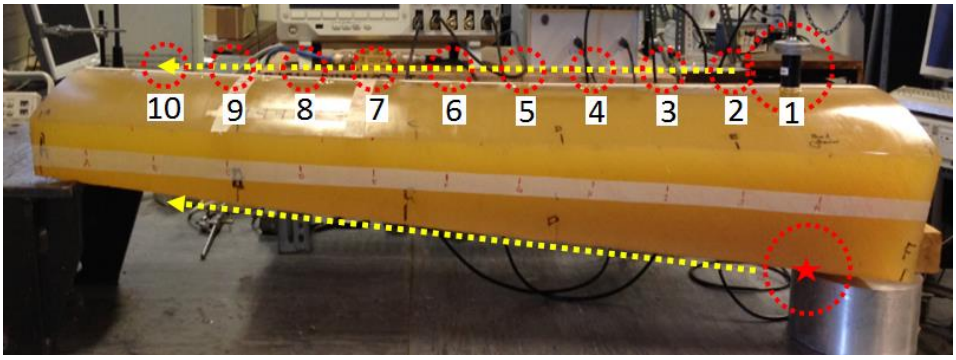

Figure 5.9: Location points on the polyurethane sample for attenuation coefficient measurement

Transducers were attached to the sample in a through transmission mode, as shown in Figure 5.10 in which a transducer was placed on the top surface of the sample while the other transducer was placed underneath the sample.

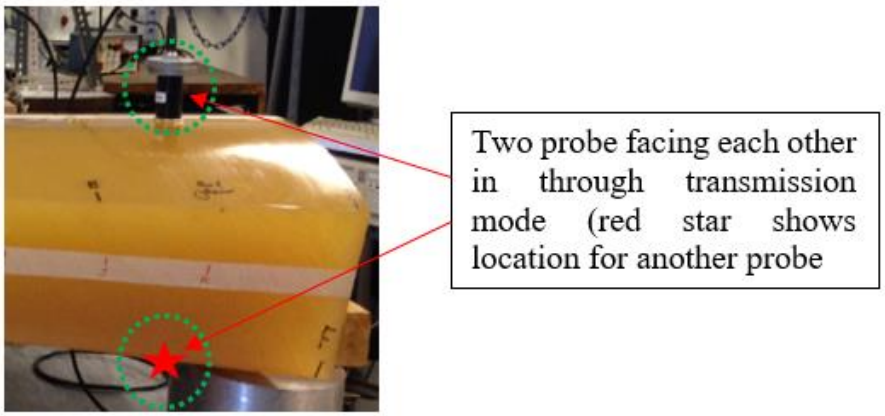

Figure 5.10: Through transmission mode on the polyurethane sample

Measurements were taken at 10cm intervals along the length of the sample, the thickness varying from 8.8 cm to 15 cm. At each point, measurements were repeated 10 times and all waveforms were recorded. Data was processed using MATLAB, where the peak amplitude and frequency were documented. A graph of amplitude (in dB) vs thickness is shown in Figure 5.11. Here, the slope of the graph gave the attenuation coefficient of the Polyurethane sample, which was estimated to 1 ± 0.1 dB/cm at 250 kHz. This value is considerably higher than the value published earlier by other researchers [17-18], but is lower than that observed in other studies that used a higher frequency [19]. Note that the

present results have not been corrected for diffraction effects, and hence do not consider the transducer characteristics clearly. However, they do give an indication of the level of signal loss in the polyurethane material.

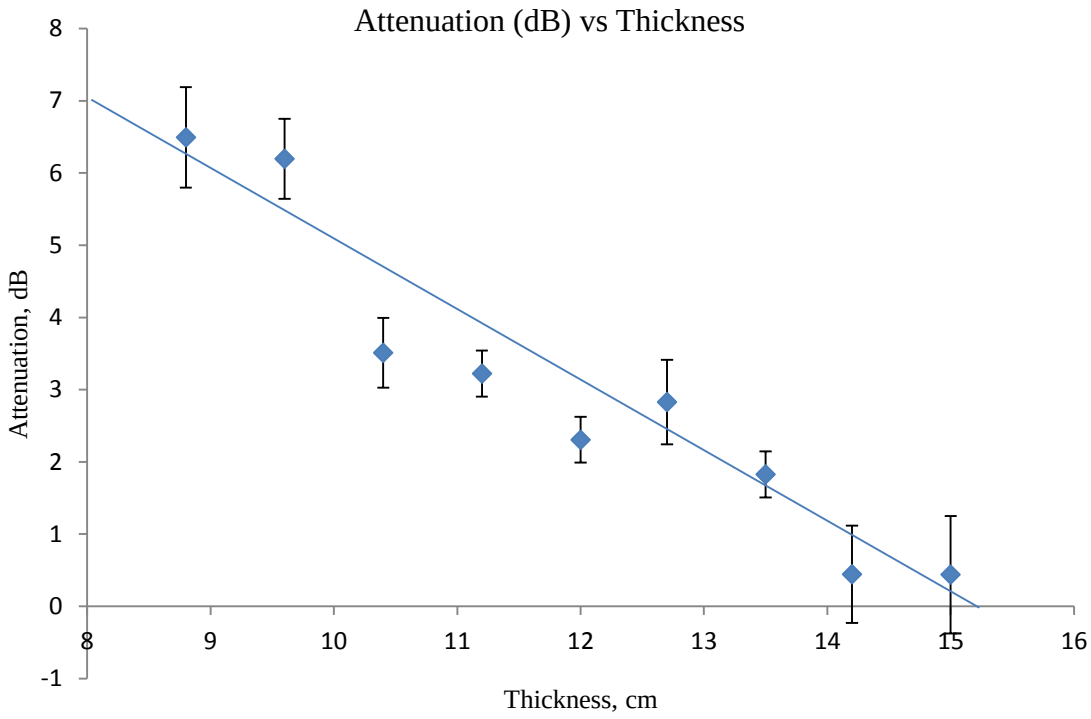

Figure 5.11: Graph of received amplitude (dB) vs thickness at a frequency of 300 kHz for the polyurethane material. Draw a best-fit line through the data.

Another important aspect involved the choice of the best pulse compression scheme for polyurethane samples. Chapter 4 discussed the different choices was used throughout the study. Piezocomposite transducers appeared to be a good choice transducer (refer to section 3.3.2 for details about the transducer), mainly because their ability in generating broad bandwidth ultrasonic signal at lower frequency. For the experiment involving polyurathane polymer, small-sized transducer was chosen because of the curved sample surface. Following the discussion of Chapter 3, chirps and bipolar Golay signals were compared so as to determine the best type of signal to be used in this situation. At the start

of the experiment, the center frequency for both types of signal was set at 300 kHz. From the data sheet supplied by the manufacturer (EOFE Ultrasonic Co. Ltd) of the piezocomposite transducers (Figure 4.9), the most effective range for the transducer is between 260 kHz to 420 kHz. But the transducer can still produce ultrasonic frequencies as low as 220 kHz. The use of low frequencies is important for this application in order to transmit as much possible signal into the tested object. Therefore, for the purposes of determining this frequency, the frequency range between 250 kHz to 450 kHz for both types of signal (chirp and bipolar Golay) was applied to the sample. From the analysis, the frequency range suitable for this polyurethane samples was determined. Two types of transducer were used to study the effect of centre frequency and bandwidth on the pulse compression system, namely a conventional piezoelectric transducer and broader bandwidth piezocomposite transducer. The choice of modulation scheme will depend heavily on the available bandwidth.

5.4 Area scanning for defect detection and characterization

NDE practitioners often encounter problems in the testing of large industrial infrastructures, especially when the materials involved are difficult to test (such as composites, concrete etc.)[20-21]. Often, the problem arises because the ultrasonic signal is either attenuated or scattered, leading to a poor signal to noise ratio (SNR). For these reasons, ultrasonic frequencies below 1 MHz are often used for high attenuation and scattering materials. Studies have shown that this frequency region can provide low scattering and low attenuation in measurements, and also can increase the level of penetration [22-23]. However, such low frequencies will also reduce the resolution of the resulting image or measurement, because of the longer wavelengths with respect to tests in the MHz range. Approaches including pulse compression [24] and signal processing [25]

have thus been investigated to try and lessen these problems. Other methods include modification of transducer shape, size, and frequency. The use of larger synthetic apertures (leading to SAFT imaging [21,26]) has also been reported as a means of increasing resolution and SNR values. As stated above, the use of ultrasound at low frequencies can provide many advantages. Nevertheless, it is important to choose the correct signal processing method that also takes into account the characteristics of the transducers. It is extremely difficult to construct piezoelectric transducers with wide bandwidths at lower frequencies [27]. It is thus important to design the excitation to use the available bandwidth to maximum effect, so as to optimise the SNR.

5.4.1 Experimental set-up

The main aim of this study was to develop an area scanning procedure for detection of defects, anomalies or flaws within the sample. For this purpose, a section of the polyurethane was selected and marked to be scanned. An area of 22 cm by 12 cm was marked and a scanning grid determined, as shown in Figure 5.12. The scans were performed on the marked area in a direct contact method where both transducers were in pulse echo mode. The scanning was carried out with two transducers where the transmitter (Tx) and receiver (Rx) were placed side by side. In order to manage the scanning process better, two transducer holders were designed and fabricated (Type A and Type B).

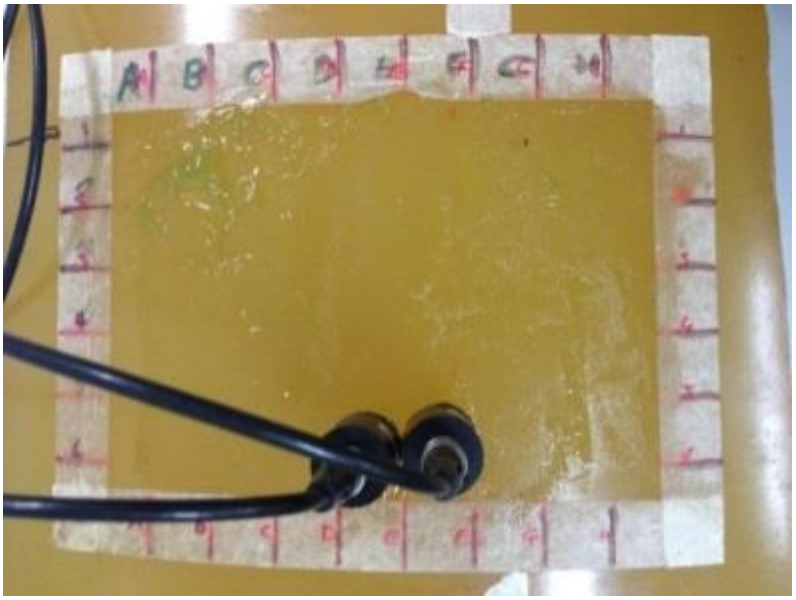

Figure 5.12: Marked location for the scanning area

In a set up where the transducers were arranged perpendicular to the length of the polyurethane sample, transducer holder type A was used (Figure 5.13 (a)). While in the case where the transducers were arranged in parallel to the length of the sample (both transducers in a flat position) a transducer holder type B was used (Figure 5.13 (b)).

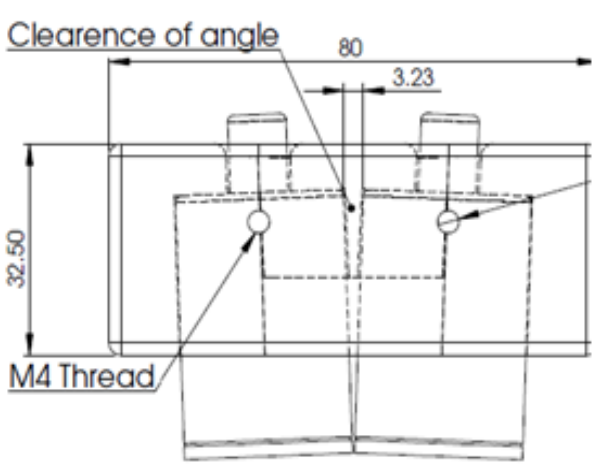

Type A

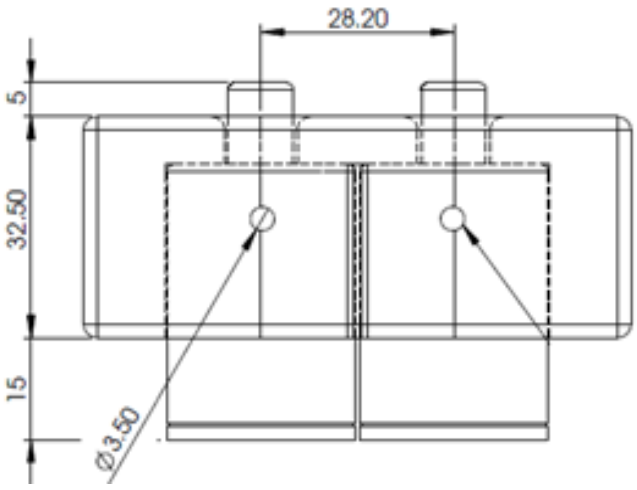

Type B

(a) *(b)*

Figure 5.13: Transducer holders that have been used in the study; (a) Curved transducer holder for 17 mm diameter piezo-composites transducer for scanning purposes of curved samples; (b) flat transducer Holder for 17 mm diameter piezo-composites transducer for flat surface samples.

To ensure the scanning could be done accurately, especially due to the movement of the transducers, a scanning stage was used to position and move the transducers as in Figure 5.14. An X-Y scanning stage was used to scan in X and Y direction. As the measurement was carried out by direct contact, some water based couplant was used as the coupling. To ensure a consistent contact between the transducer and the sample surface, a spring was used (Figure 5.14 (a)) and was placed in the transducer holder as in the Figure 5.14 (b). The selection of spring must be done with caution because they cannot be too stiff or too loose to obtain sufficient pressure for the scanning. Figure 5.15 show the position of the transducer holder and the scanning procedure that was used.

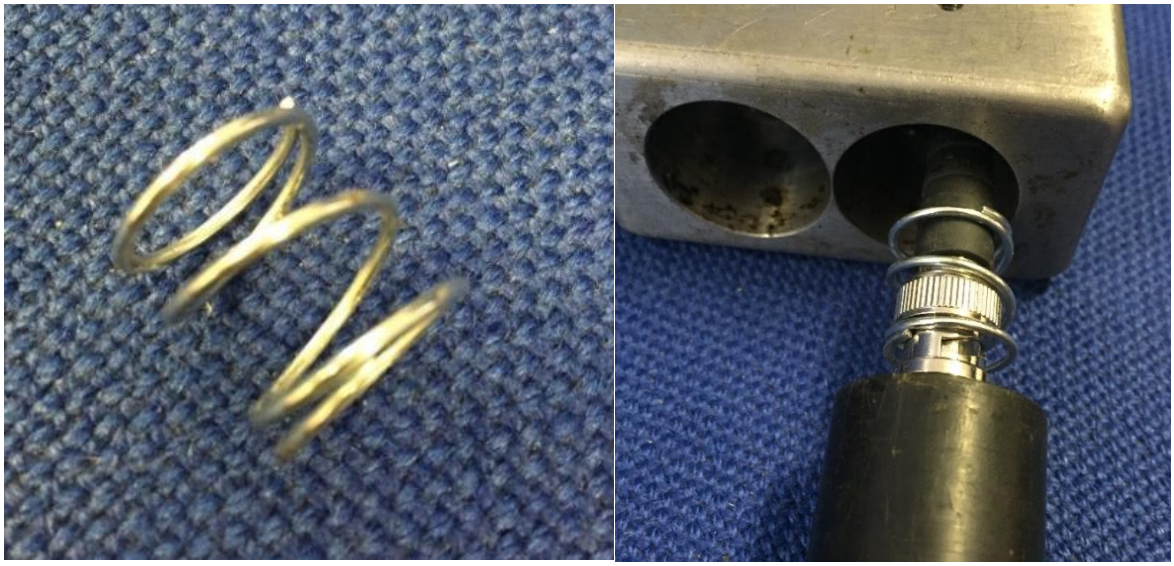

(a) *(b)*

Figure 5.14: (a) Spring that was used as the suspension; (b) arrangement of the spring and the transducer holder

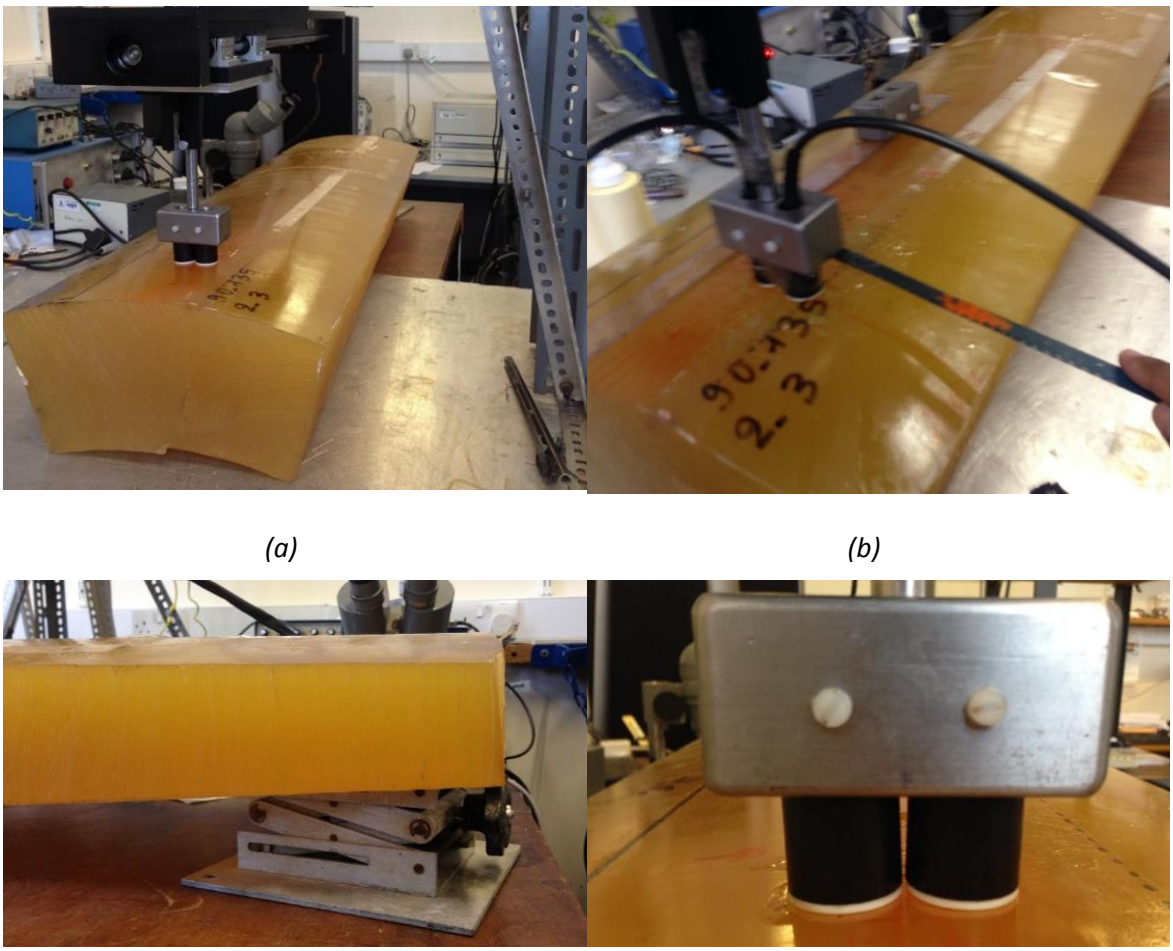

(a) *(b)*

(c) *(d)*

Figure 5.15: Scanning stage and set up; (a) scanning position of the sample in parallel with the scanning stage; (b) scanning in progress; (c) the jack used to level the sample horizontally so that it is in parallel to the scanning stage; (d) transducers and the sample surface must be properly in contact at all time

A chirp with a frequency range of 150 kHz to 450 kHz was used as the transmitted signal for the scan. The central frequency of the signal was 300 kHz and the duration was 7 ms. An elliptical - Hamming filter was applied to the signal generated during the scanning process as explained in the previous chapter. The parameter of the generated signal was discussed in Chapter 4. As mentioned earlier, two piezocomposite transducers were placed next to each other on the top left of the marked area at the beginning of the scan, then both transducers were moved 5 mm horizontally to the next point. This step was repeated until the end of the first line. Then, the transducers were returned to the original location before moved down 5 mm vertically to begin the scan of the second line and the process was repeated until the whole marked area was fully scanned. During the scanning process, it was important that the couplant was always applied between the transducers and the sample surface to ensure consistency in the data obtained.

5.4.2 Choice of pulse compression scheme

Figure 5.16 shows the output signals of both chirp and bipolar Golay, when used with the narrow bandwidth transducer as the transmitter, and a piezocomposite as the receiver. It shows that the patterns for both types of signal were similar, but the signal from the Golay excitation was more damped in time, and has a wider spectrum. However, in both cases, the narrow bandwidth of the transmitter influenced the response. In this test both signal characteristics were adjusted as close as possible to the transducers profile in order to get maximum output.

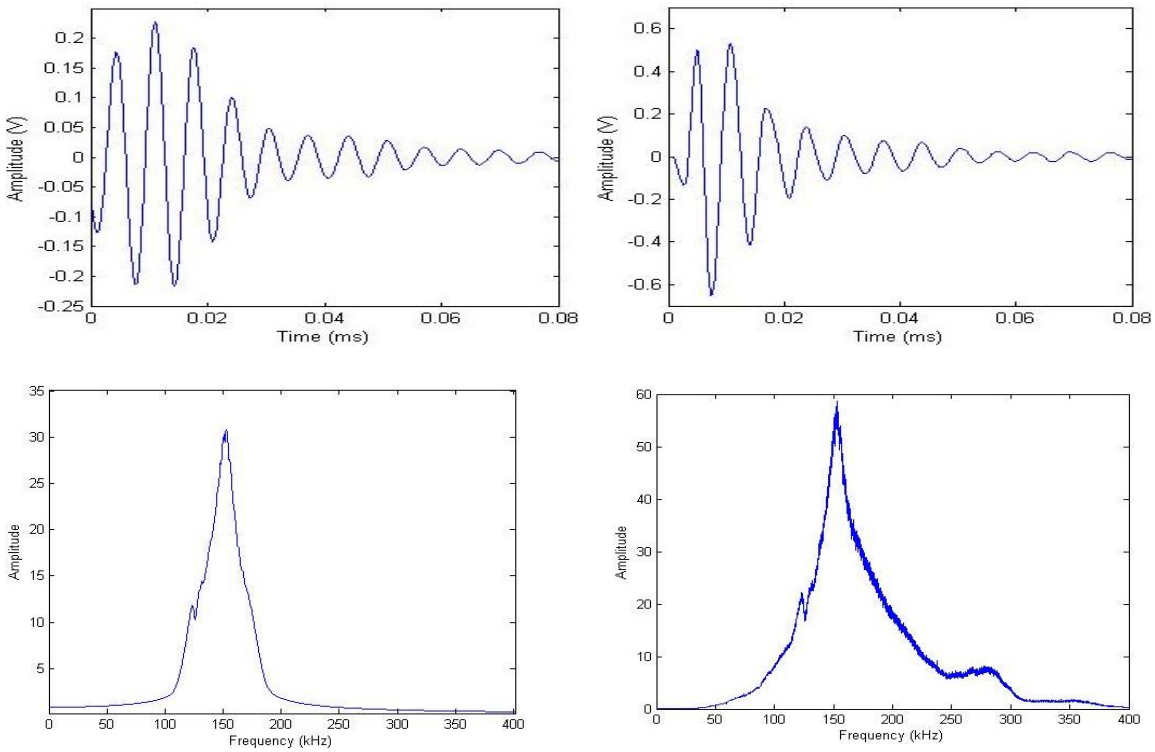

(a) *(b)*

Figure 5.16: Experimental cross-correlation outputs for the narrow bandwidth transducer, showing both the waveform and the spectrum, for (a) the chirp and (b) the bipolar Golay code drive signal.

Figure 5.17 and 5.18 show the results of a pulse echo measurement, in which signals were reflected from an air-bubble defect of ~6 mm diameter, located approximatively at 6 cm below the sample surface. The two figures show the differences in the response when the chirp (Figure 5.17) or the Golay code (Figure 5.18) was used with either the narrow bandwidth transmitter or the pair of broad bandwidth piezocomposites. For chirp excitation (Figure 5.17), the response is as expected – the piezocomposites gave a much wider bandwidth in the Pulse Compression (PuC) output when compared to that from the narrow bandwidth transmitter. It was also clear that a very good signal was obtained with the piezocomposite pair, showing that PuC had worked very well with these transducers in this highly-attenuating material. In particular, the extension of bandwidth up to frequencies of

350 kHz produced an excellent result. For the bipolar Golay code excitation, Figure 5.18, this bandwidth was extended even further.

Although bipolar Golay signals showed better ability (in terms of amplitude and bandwidth) compared to chirps, especially when used with the broad bandwidth transducers, chirps were chosen for this work because they were more easily adapted to the transducers profile. It is chirps characteristic that allows users to specify the parameters such as start and finish frequency, bandwidth and time duration of the signal to be used. Although in terms of amplitude and bandwidth bipolar Golay was better than chirp, both gave almost the same result (in terms of shape and ability to dump the signal in time) when applied to the polyurethane sample. Therefore, chirps were selected as the input signal throughout the study.

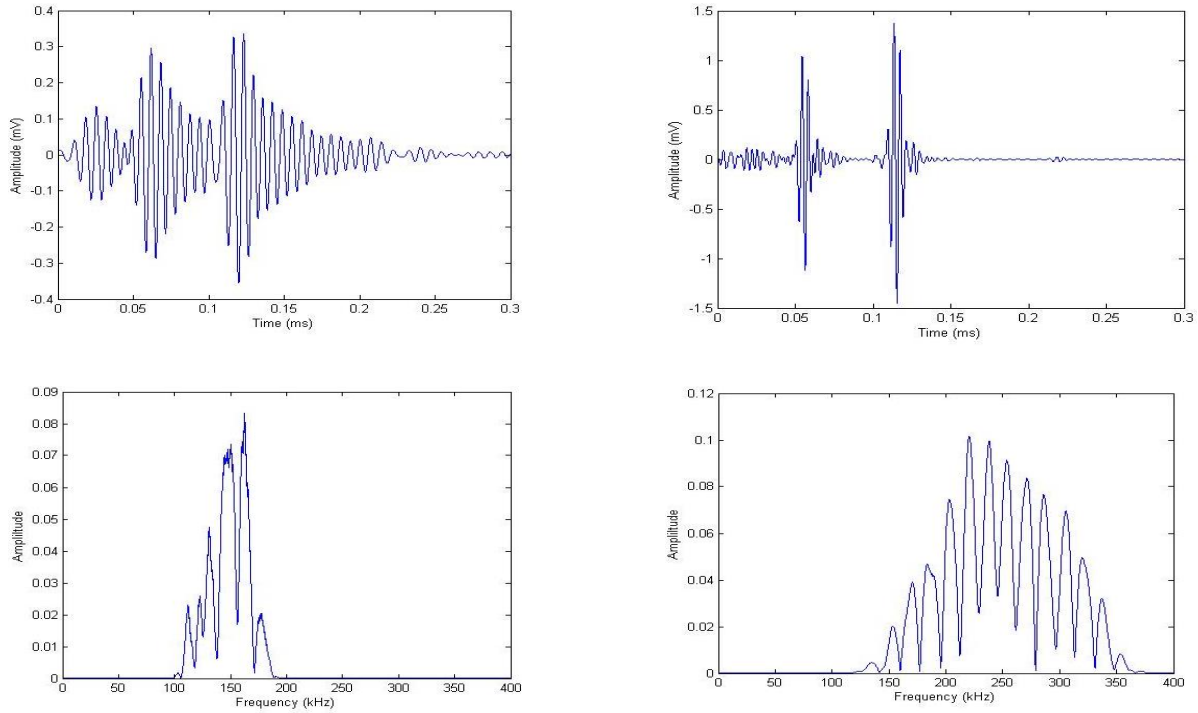

(a) *(b)*

Figure 5.17: Detection of a sub-surface defect using pulse compression and chirp excitation. This is shown for (a) the narrow bandwidth transmitter and (b) a pair of wide bandwidth piezocomposite transducers.

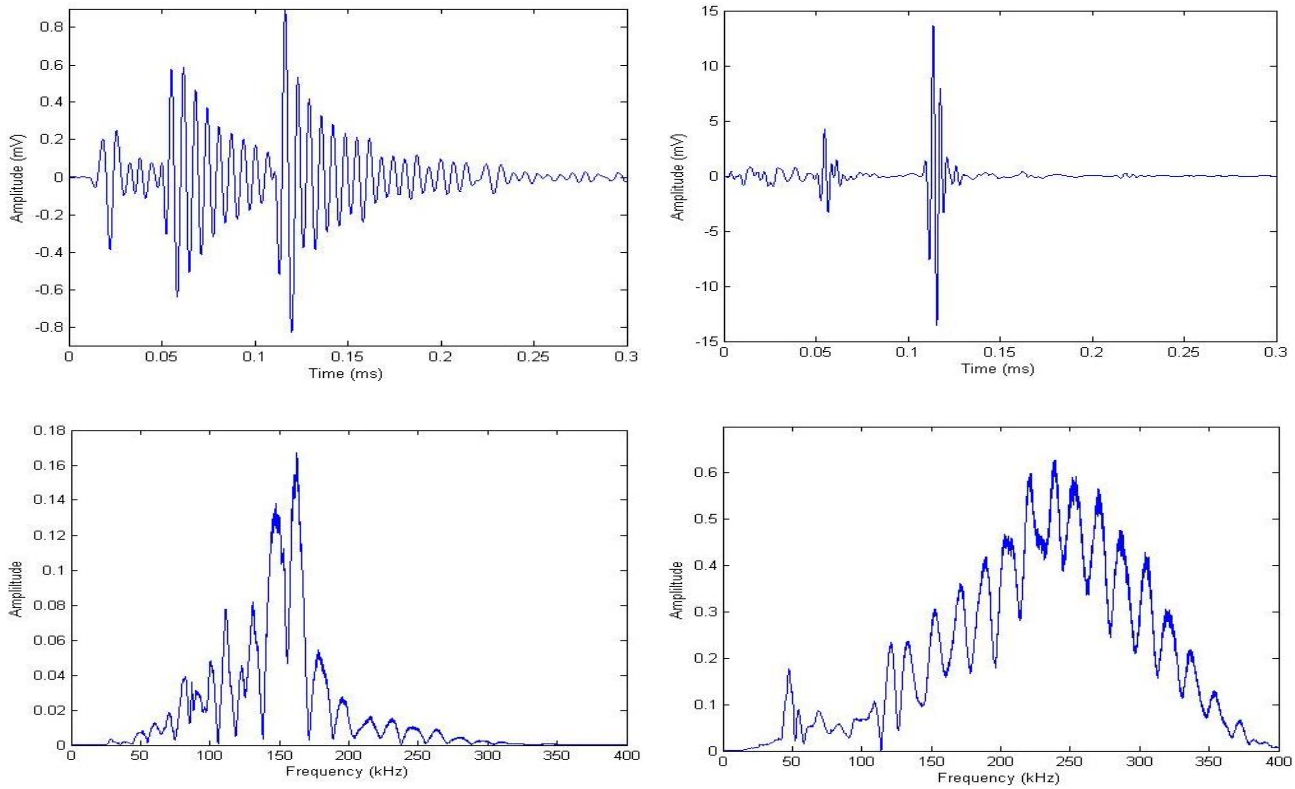

Figure 5.18: Detection of a sub-surface defect using pulse compression and bipolar Golay Code excitation. This is shown for (a) the narrow bandwidth transmitter and (b) a pair of wide bandwidth piezocomposite transducers.

5.4.3 Detection and characterization of air bubble defects

The presence of air bubbles in a riser stiffener arises due to the manufacturing process (see the photograph of Figure 5.19). Their presence causes the potential concentration of stress within the material, and the possibility of premature failure. It is thus important that these defects be located. The sample provided by BP contained such defects. An image obtained using optical imaging is shown in Figure 5.20 where defects were approximately 7 mm and 5 mm in diameter, separated by a distance of approximately 55 mm. The depth of the defects was not known exactly but they were thought to be 85 mm from the top sample surface where the sample thickness was 120 mm.

The collected data were processed further using MATLAB-based software provided by the University of Perugia to provide both 3-D C-scan images, and image reconstruction by a SAFT algorithm. This software was used to plot the images shown in Figures 5.21-5.24. The defect echoes were identified and their peak-to-peak amplitude plotted in a matrix which represents the condition of the scanned area of the polyurethane sample. The resultant C-scan image is shown in Figure 5.21 where the two defects were surrounded by two dotted ellipses. It demonstrates that two defects were detected within the scan area. The results indicate that the detected defect areas were similar, although their amplitudes were different (as also evident in Figure 5.20(b)). However, the C-scan does not contain depth information. A better approach would be to represent the measurements by 3D images, in order to show the defects in more detail and to assess the defect depth beneath the polyurethane surface.

Figure 5.19: Photograph of the bubbles obtained using optical imaging

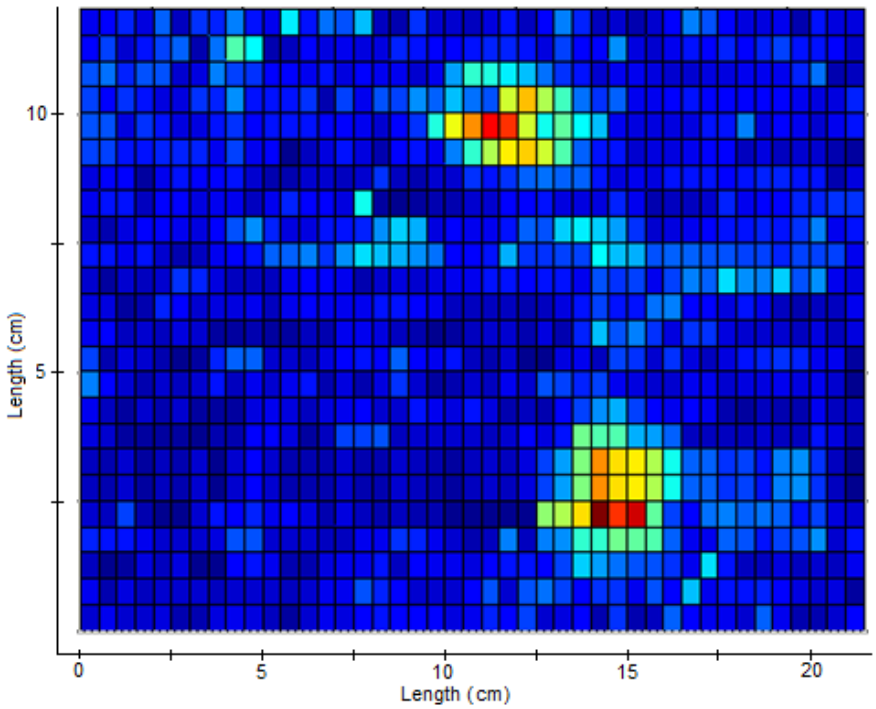

(a)

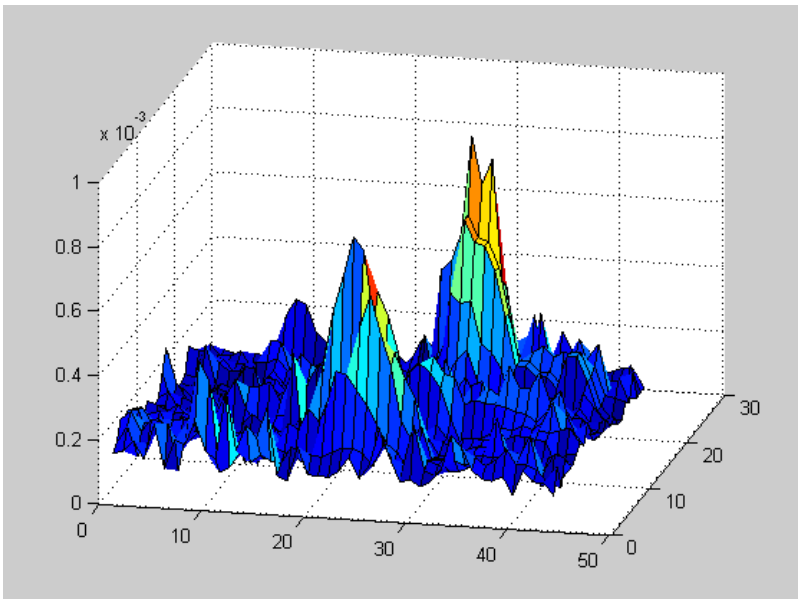

(b)

Figure 5.20: (a) Top view of C- scan image, and (b) surface plot of the data

Figure 5.21 (a) shows that there are two dark spots that can be seen (in red ellipse), which correspond to the defect signal showed in Figure 5.21 (b). In addition, the defects depth can be estimated in the interval between 6-8 cm and 7-9 cm respectively. However, the dark zone on the top of the hypercube corresponding to small depths beneath the

polyurethane surface (< 4cm) implies that the defect imaging process is actually blind in this range. This can be due to many factors; for example, a strong electrical coupling between Tx and Rx that affects each measurement. Other phenomena such as the onset of surface waves that directly travel between the two transducers as well as an abnormal scattering in the first material layer due to inhomogeneous composition of the sample can also contribute to the blind zone (Figure 5.21(a)). In general, it is good to reduce the blind zone to as minimum as possible to get more precise result in the defect depth evaluation.

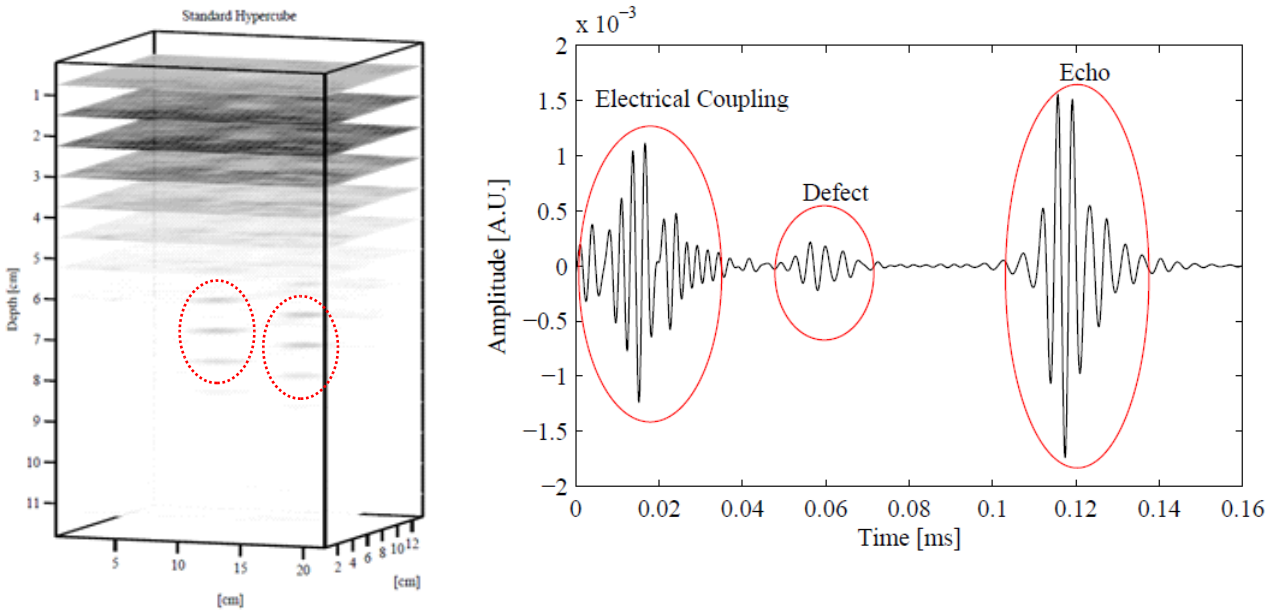

(a) *(b)*

Figure 5.21: (a) 3-Dimensional imaging of the polyurethane sample. As in Figure 5.19 the two red ellipses that appears from 6 cm to 9 cm of depth indicate the defects. (b) Typical impulse response acquired from the polyurethane sample, in the presence of a defect.

To achieve this aim, further post processing techniques were tested both during and after the application of PuC. In contrast to the standard PuC algorithm, where the data recorded by the transducers is cross-correlated with the time replica of the input signal. Ideal

signal namely ‘Normal’ as in the Figure 5.22 (a) was generated numerically. For further study, the data was also cross-correlated with the time replica of the signal recorded from the direct contact of the two transducers (namely ‘Transducer’ as in Figure 5.22(a)) and from a through-transmission measurement on a clean area of the sample (namely ‘Material’ as in Figure 5.22(a)). Thus, the real properties of the transducers and the material and their effect on the frequency spectrum were taken into account.

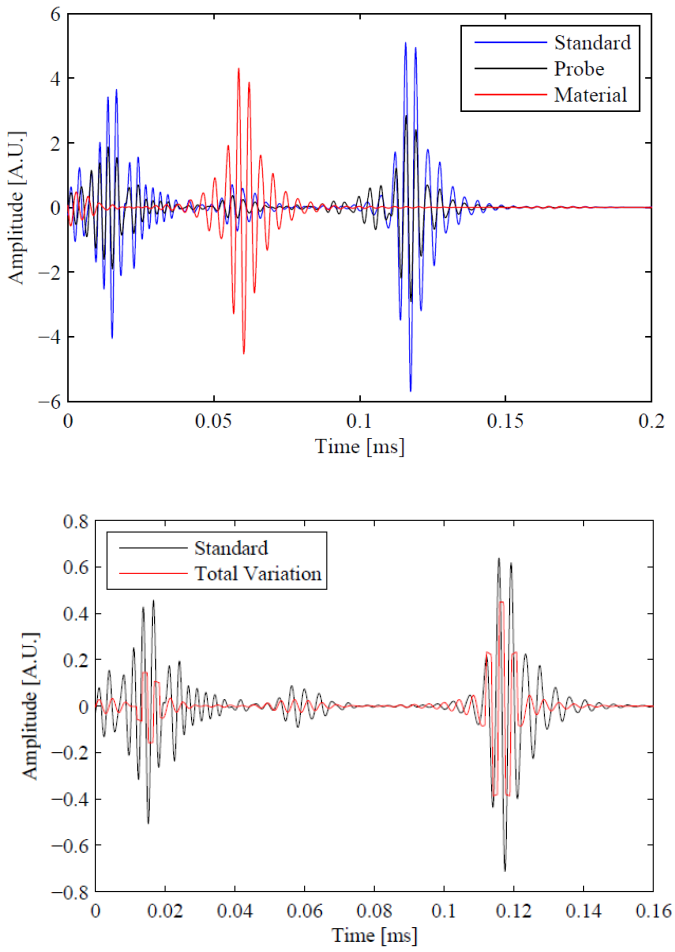

Figure 5.22: (a) Comparison between the standard matched filter technique (blue), the cross-correlation with the signal modified by the transducers spectrum (black) and by the sample+material properties (red); (b) Comparison between the standard matched filter technique (dark) and the Total Variation deconvolution (red).

5.4.4 Detection and characterization of flat bottom hole defect

The aim of this test was to examine the ability of the system in detecting the features of known defects such as the location, shape and size. For this purpose, a drilled-hole was machined into the sample using 10 mm drill bits. This hole was drilled to a depth of 70 mm from the bottom surface of the sample at a region where the sample thickness was 150 mm (i.e. the bottom of the hole was 80 mm from the top surface.

Figure 5.23 shows the 3-D image of the measurement that was carried out to detect the drilled-hole. It was a set of measurement collected over a grid of 23 x 35 points with a grid resolution of 2 mm x 2 mm. The procedure for hypercube image reconstruction is shown in the previous chapter. In Figure 5.23 (a), different visualizations of the C scan data built from the envelope of the single measurements points can be observed. On the top-right, XZ showed a B-scan corresponding to a plane that crosses the defect in its center; on the bottom-right is a XY B-scan at the depth of the defect. Although the defect image obtained was not clear, it appears that the hypercube image shows there is a defect in the position 80 mm from the surface. The 3-D images clearly shows that the thickness of the tested sample was between 150 to 160 mm. From here, it proved that the developed system can be used on polymer materials, especially polyurethane. However, there are drawbacks in the C-scan image generated in terms of its spatial resolution. Thus, a better approach of image reconstruction was made called synthetic aperture focusing technique (SAFT) in order to enhance the spatial resolution of the reconstruction image as shown in Figure 5.24. In this SAFT image, it can be seen that the result was improved vastly where the resolution of the defect was increased. The defect can be clearly seen and the size of the defect (in the reconstructed image) are closer to the real defect (hole) on the polyuretahne sample which is 10 mm.

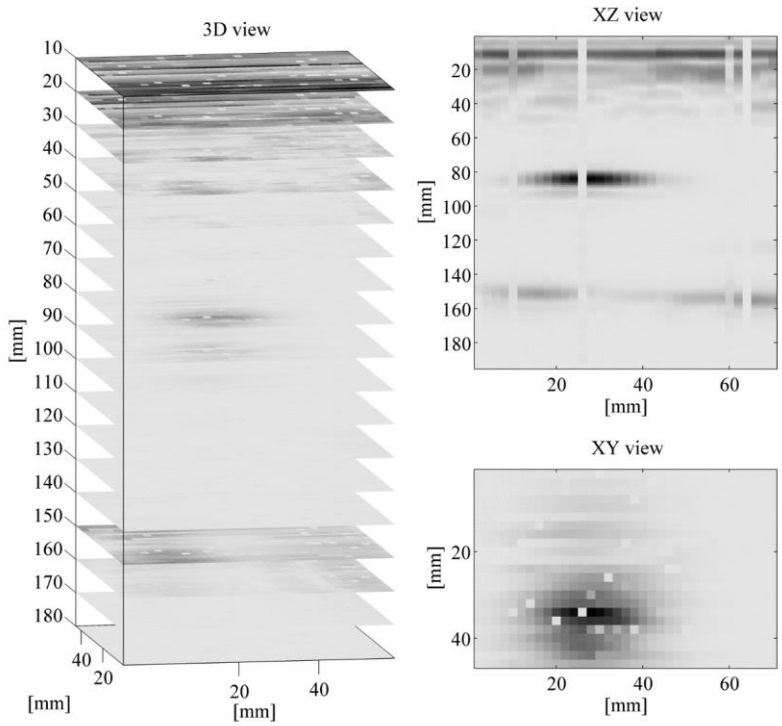

Figure 5.23: 3D reconstruction image of C-scan from the drilled hole measurement

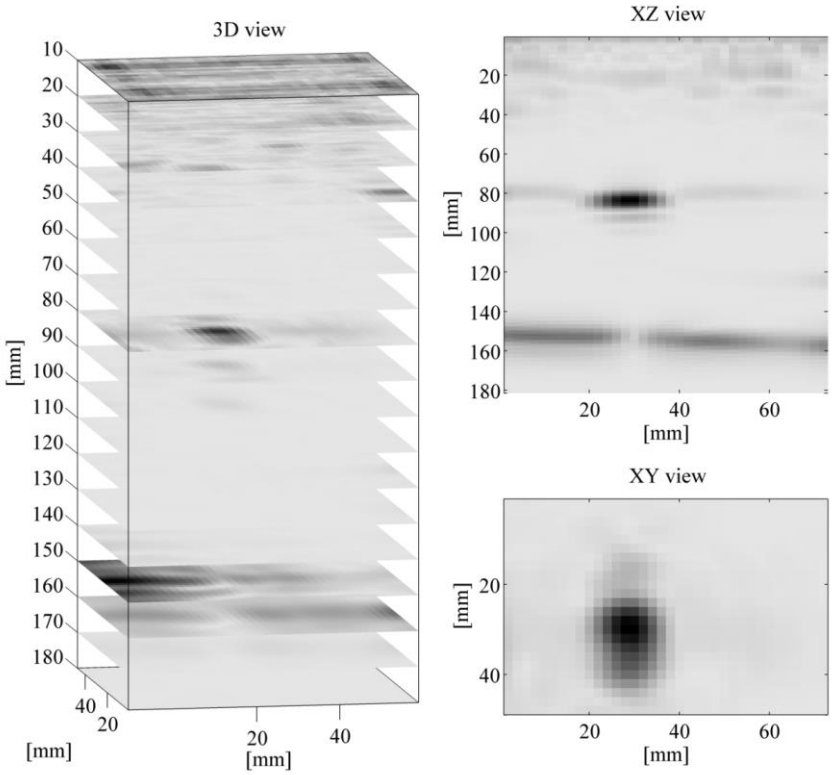

Figure 5.24: 3D reconstruction image of SAFT from the drilled hole measurement

5.5 Conclusions

The results showed that the developed system can be used to investigate materials with high attenuation of ultrasonic signals. The present experiments looked at 15 cm thick polyurethane, where the use of conventional NDT at frequencies >1 MHz would not be possible. Chirp signal and bipolar Golay have proven suitable to be used in conjunction with the PuC technique at low frequencies, where the attenuation is more manageable. It was shown that a broad bandwidth transducer has the advantage when compared to the narrow bandwidth transducer. It is suitable for use with Chirp and bipolar Golay codes, because bandwidth is important in PuC techniques both for assuring high SNR gain and inspection resolution. From the results from the tests on the sample, scan data showed that this technique can be used to detect and reveal defects or flaws that are present in thick and highly-attenuating materials. It is simply a matter of how to increase the capacity in terms of signal processing and image reconstruction in order to get a more precise result, particularly in terms of sizing and locating of the defect. However, several methods of signal processing such as generation of 3-D hypercube C-Scan imaging and 3-D SAFT imaging in which SAFT has shown that it can improve the spatial resolution of the measurement. Besides, it has also shown a number of different methods of performing cross correlation process that could eventually help to reduce the blind and improve the ability of the developed system.

References

[1] K. M. Zia, H. N. Bhatti, and I. Ahmad Bhatti, “Methods for polyurethane and polyurethane composites, recycling and recovery: A review,” *Reactive and Functional Polymers*, vol. 67, no. 8. pp. 675–692, 2007.

[2] T. Romaskevic, S. Budriene, K. Pielichowski, and J. Pielichowski, “Application of polyurethane-based materials for immobilization of enzymes and cells: a review,” *Chemija*, vol. 17, no. 4, pp. 74–89, 2006.

[3] S. Gebhardt, A. Schönecker, R. Steinhausen, T. Hauke, W. Seifert, and H. Beige, "Fine scale 1-3 composites fabricated by the soft mold process: Preparation and modeling," *Ferroelectrics*, vol. 241, no. 1, pp. 67–73, 2000.

[4] F. Moore, "Materials for flexible riser systems: problems and solutions," *Eng. Struct.*, vol. 11, no. 4, pp. 208–216, 1989.

[5] S. F. Badran, A. B. Saddek, and H. W. Leheta, "Ultimate strength of y and T stiffeners subjected to lateral loads with three different levels of initial imperfection," *Ocean Eng.*, vol. 61, pp. 12–25, 2013.

[6] M. H. Patel and F. B. Seyed, "Review of flexible riser modelling and analysis techniques," *Eng. Struct.*, vol. 17, no. 4, pp. 293–304, 1995.

[7] C. Braithwaite, "Developmental Tests On the Underwater Mining System Using Flexible Riser Concept" [Online]. Available: http://www.subseauk.com/documents/Wellstream_Chris_Braithwaite.pdf.

[8] M. Nisoli, S. De Silvestri, and O. Svelto "typical flexible riser structure." [Online]. Available: http://www.offshorerisertechnology.com/.

[9] P. G. Kenny, J. J. Gruber, and J. M. Smith, "Trelleborg bend stiffener," *Mater. Eval. (ISSN 0025-5327)*, vol. 45, pp. 730–735, 1987.

[10] D. Kaye, "Flexible Riser Integrity Management Experience West of Shetland," 2008. [Online]. Available: http://www.hse.gov.uk/pipelines/seminar08/11-managementexperience.pdf.

[11] F. Bastianini, A. Di Tommaso, and G. Pascale, "Ultrasonic non-destructive assessment of bonding defects in composite structural strengthenings," *Compos. Struct.*, vol. 53, no. 4, pp. 463–467, 2001.

[12] L. Czarnecki, A. Garbacz, and M. Krystosiak, "On the ultrasonic assessment of adhesion between polymer coating and concrete substrate," *Cem. Concr. Compos.*, vol. 28, no. 4, pp. 360–369, 2006.

[13] T. H. Gan, D. A. Hutchins, D. R. Billson, and D. W. Schindel, "The use of broadband acoustic transducers and pulse-compression techniques for air-coupled ultrasonic imaging," *Ultrasonics*, vol. 39, no. 3, pp. 181–194, 2001.

[14] R. J. Dewhurst, "Review of Progress in Quantitative Nondestructive Evaluation," *Opt. Acta Int. J. Opt.*, vol. 32, no. 7, pp. 747–747, 1985.

[15] A. D. W. McKie and R. C. Addison, "Laser-based ultrasonic inspection with a fiber-coupled scanning Cassegrain system," *Ultrasonics*, vol. 40, no. 10, pp. 1037–1046, 2002.

[16] P. Pallav, T. H. Gan, and D. A. Hutchins, “Elliptical-Tukey Chirp Signal for Ultrasonic Imaging,” *IEEE Trans. Ultrason. Ferroelectr. Freq. Control*, vol. 54, no. 8, pp. 1530–1540, 2007.

[17] J. E. Browne, K. V. Ramnarine, A. J. Watson, and P. R. Hoskins, “Assessment of the acoustic properties of common tissue-mimicking test phantoms,” *Ultrasound Med. Biol.*, vol. 29, no. 7, pp. 1053–1060, 2003.

[18] H. Chen, M. Zheng, H. Sun, and Q. Jia, “Characterization and properties of sepiolite/polyurethane nanocomposites,” *Mater. Sci. Eng. A*, vol. 445–446, pp. 725–730, 2007.

[19] I. G. Scott and C. M. Scala, “A review of non-destructive testing of composite materials,” *NDT Int.*, vol. 15, no. April, pp. 75–86, 1982.

[20] M. Rossat, J.-F. Chaix, and V. Garnier, “Ultrasonic wave propagation in heterogeneous solid media,” *J. Acoust. Soc. Am.*, vol. 123, no. 5, p. 3844, 2008.

[21] A. V. Osetrov, “Non-linear algorithms based on SAFT ideas for reconstruction of flaws,” *Ultrasonics*, vol. 38, pp. 739–744, 2000.

[22] J. R. Berriman, D. a Hutchins, A. Neild, T. H. Gan, and P. Purnell, “The application of time-frequency analysis to the air-coupled ultrasonic testing of concrete.,” *IEEE Trans. Ultrason. Ferroelectr. Freq. Control*, vol. 53, no. 4, pp. 768–76, Apr. 2006.

[23] T. Planès and E. Larose, “A review of ultrasonic Coda Wave Interferometry in concrete,” *Cem. Concr. Res.*, vol. 53, pp. 248–255, 2013.

[24] T. H. Gan, D. A. Hutchins, and D. R. Billson, “Preliminary studies of a novel air-coupled ultrasonic inspection system for food containers,” *J. Food Eng.*, vol. 53, no. 4, pp. 315–323, 2002.

[25] P. A. Gaydecki, F. M. Burdekin, W. Damaj, D. G. John, and P. A. Payne, “The propagation and attenuation of medium-frequency ultrasonic waves in concrete : a signal analytical approach,” *Meas. Sci. Technol.*, vol. 3, pp. 126–134, 1992.

[26] R. Sicard, J. Goyette, and D. Zellouf, “A SAFT algorithm for lamb wave imaging of isotropic plate-like structures,” *Ultrasonics*, vol. 39, pp. 487–494, 2002.

[27] P. Dumas, J. Poguet, and G. Fleury, “Piezocomposite technology An innovative approach to the improvement of N . D . T . performance using ultrasounds,” in *European Conference on Nondestructive Testing*, 2002, no. 8, pp. 20–21.

[28] L. I. Rudin, S. Osher, and E. Fatemi, “Nonlinear total variation based noise removal algorithms,” *Phys. D Nonlinear Phenom.*, vol. 60, no. 1–4, pp. 259–268, 1992.

Chapter 6

Low Frequency Coded-Waveform Ultrasonic System for Concrete Inspection

6.1 Introduction

The difficulty of performing ultrasonic testing on concrete materials has become a global problem. The main cause is due to scattering resulting from aggregate and any other type of inclusions present in the material [1]. This condition limits the depth of penetration of the ultrasonic signal and also lowers the SNR especially when the measurement is carried out in pulse echo mode or pitch-catch (single sided) [2]. The problem will become worse when the object or structure to be tested is a large and thick sample. Such situations require a system that can penetrate the thickness of this structure in which the signal can propagate deep into the sample. This is difficult to achieve using a conventional ultrasonic system which relies on simple pulsing of a transducer over a reasonable bandwidth [3].

Section 2.3.2 reviewed some of the ultrasonic techniques that have been described for concrete testing, such as adaptive filtering and SAFT imaging. The objective of the present study was to develop a system at low frequencies (100-400 kHz), which had good penetration, but also had a reasonable bandwidth and signal to noise ratio (SNR) that could be used to test industrial concrete samples. This required the correct combination of the transducer, excitation waveform, and an additional signal processing method so that the resolution of the method in terms of defect location and orientation could be optimized. There are many types of concrete-based materials and structures, but this study focuses

particularly on reinforced concrete, as used in the construction industry, and refractory anchor bricks used in refractory furnace linings.

6.2 Structural problems in reinforced concrete

The standard components within a reinforced concrete structure are sand, cement, aggregate and steel reinforcement bars (rebars). The use of rebars is an essential element that contributes to the strength of a concrete structure, and especially the tensile strength. But there are problems associated with the presence of rebars in concrete, such as deterioration of the rebar, lack of thickness of concrete cover (to cover the rebar) and the problems in relation to the size of the rebar (incorrect size). Usually, the problems arising are interrelated with each other. Deterioration of reinforced concrete caused by corrosion of rebars is a well-known problem [4]. Rust will add to the volume of the rebar, thus putting pressure on the concrete structure from inside the material. This situation can eventually cause cracking and spalling of the surrounding concrete (concrete cover), as can be observed in Figure 6.1 [5].

Corrosion rates can also be greatly accelerated when chlorides are present in the concrete [6]. Chlorides may be pooled into the original mix due to their presence in the sand, aggregate or water. Usually, chlorides penetrate through the cover when the external surfaces of the concrete (concrete covers) are exposed to seawater, marine atmospheres or de-icing salts [7]. Although there are several techniques that have been used to reduce the corrosion (such as chloride extraction, removal and replacement of the concrete cover, cathodic protection, increased concrete cover and concrete coatings), there is still no satisfactory method to suppress corrosion [8]. This situation must be dealt with effectively so that the situation does not worsen, which could threaten the lives of many people. So, the best move is to monitor corrosion and deterioration from the early age of the structure.

Therefore, it is crucial to conduct periodic tests on the concrete's critical component as in Figure 6.1 above as well as the testing during the commissioning process. It is very important to create a testing system that can be used to detect and estimate the size of rebars and measure the thickness of the concrete cover of a structure. Up to now, there is no ultrasonic system that has been proven effective for such application [9].

Figure 6.1: Example of problematic concrete structure where the deterioration of rebars and concrete cover spalling occurred [5]

Currently, the most common device for measuring the thickness of the concrete cover and locating rebars is the concrete cover meter. There are various types and forms of concrete cover meter available in the market today [10]. Figure 6.2 (a) shows an example of a concrete cover meter currently available commercially [11-12]. This equipment is based on pulse induction electromagnetic techniques to detect rebars and estimate their depth below the surface. Rebar detectors (Figure 6.2 (b)) are devices that are more compact and less sophisticated, and can only be used to detect and locate metallic objects below the surface. However, there are still weaknesses in these techniques such as limitations in detection range, a minimum bar spacing (depends on cover depth) and lack of penetration (not reliable for thick structures). In addition, most of the data released by this equipment

cannot be manipulated to run further signal processing. Therefore, this area still continuously become the focus of researchers to study methods and techniques more effectively so that the capability and reliability can be improved and further developed.

Figure 6.2: (a) Concrete cover meter [11]; (b) rebar detector [12]

6.3 Refractory bricks

Refractory bricks, also known as firebricks, are used as a lining in high-temperature furnaces [13]. The main function of the furnace lining is to prevent heat from the furnace core transferring to the furnace structure or outer shell. It also improves thermal insulation due to its low thermal conductivity [14], making the furnace more efficient. There are a few different designs of furnace liner, one of which is applied in high-temperature furnaces used in the steel industry. Here, furnace temperatures can be up to 3000 ^{0}F (1,648 ^{0}C). Therefore, a variety of methods and design of refractory bricks are used to obtain the best results - at this high temperature, the furnace liner must not develop cracks or leaks, as this could cause

a catastrophic failure [15]. One of the most popular design is the use of refractory anchor bricks together with a removable concrete shell, as in Figure 6.3(a). With this method, each section of the inner shell (liner) can be opened or replaced when a problem develops without the need to dismantle or demolish the entire structure. In this design, refractory anchor bricks are used to hold the whole liners with the building structure or outer case. Refractory anchor bricks for steel manufacture, for example, are usually made of ceramic silica/alumina material containing up to 60% of alumina which is very good in terms of thermal shock resistance [14]. Anchor brick shapes are shown in Figure 6.3(b) where there are a variety of shapes that can be adapted to the application [16]. The length of the bricks are varies between 20 cm to 40 cm depending on the thickness of the furnace wall, the access area about 10 cm x 10 cm . The claws are attached to the inner shell to ensure that the external shape of the anchor brick offers large retention forces to the structure.

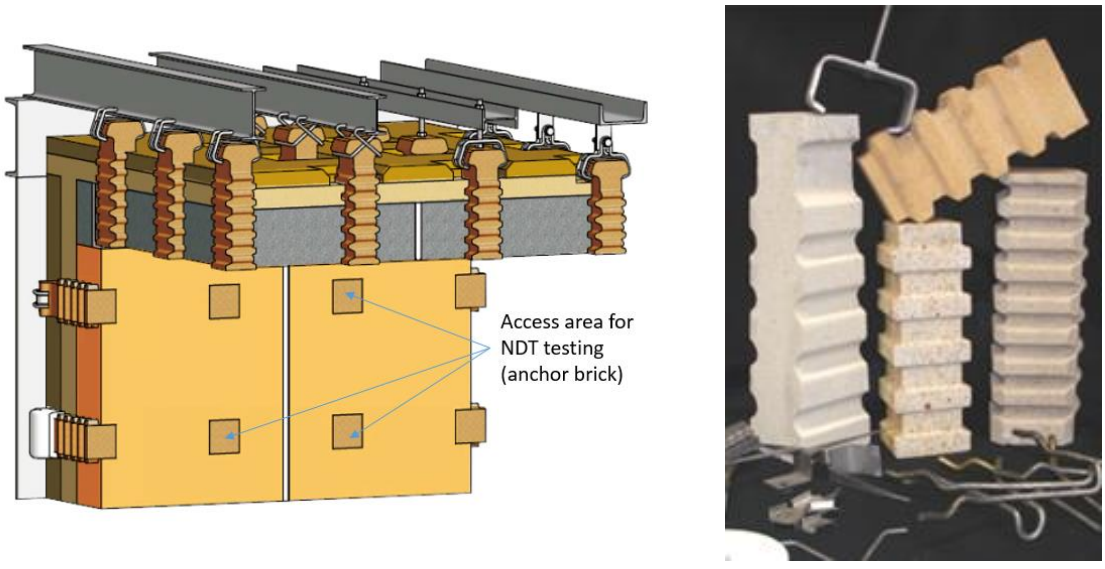

(a) *(b)*

Figure 6.3: (a) sketch of the furnace liner and refractory anchor brick [17]; (b) various type and shape of refractory anchor bricks [16]

In the usage of anchor bricks, there is a problem in which the bricks could crack or break because of the stress concentration at the meeting point between the inner shell and outer shell. This is due to different thermal expansion coefficient of these two materials [18] (see Figure 6.4). This situation causes a tendency for cracking at the interface bewteen the two materials. As the anchor brick is embedded within the refractory brick or concrete, it is impossible to visually detect any cracks or broken parts of the anchor brick. Ultrasound is an obvious approach to use, but there are major problems in applying ultrasonic NDT to such bricks – the material is highly scattering, and the shape means that multiple reflections from the side walls complicate single-sided inspection (the bricks must be tested from the outside of the furnace for major cracking across their width). Until now there were no NDT technique capable of detecting partial or even full fracture of the anchor brick. It is for these reasons that the low frequency technique was appield to this problem.

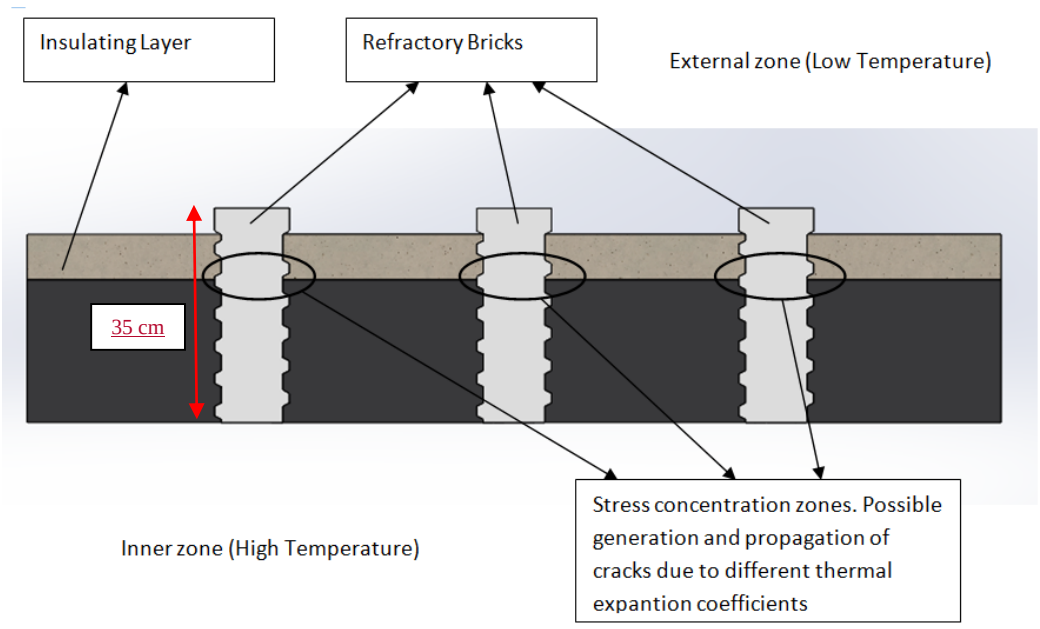

Figure 6.4: Location where the stress concentration zone often causes fracture of the refractory bricks.

6.4 Equipment, materials, and concrete sample preparation

Sample preparation is an important step when performing research on concrete materials. This is because the distribution and composition of materials in concrete is very different depending on types and the way it has been made. In this study, concrete strength is not a primary parameter, so the concrete sample preparation process used standard concrete mixes.

(a) *(b)* *(c)*

Figure 6.5: Equipment for concrete samples preparation (a) Weighing system; (b) Concrete mixer; (c) Concrete mould and vibrating table

The main objective was to manufacture reinforced concrete materials with known properties. In this concrete sample preparation, common equipment such as weighting system, concrete mixers, vibrating table and the concrete molds were used to produce concrete samples in accordance with the British Standard BS 8110-1-1997 (Structural use of concrete. Code of practice for design and construction) and in terms of the selection of raw materials and mix design calculations. The concrete material that was chosen was normal concrete with a 0.5 water to cement ratio. The mix designs used for the calculation

of raw material ratios for different concrete compositions are presented in Table 6.1. There were two types of concrete samples prepared during this study: Type A, a concrete pillar (10 cm x 10 cm x 50 cm) without reinforcement, and Type B, which is a slab containing a reinforcement bar.

Mix No.	Cement	Ratio to cement weight		
		Water	Aggregate	Sand
1	1	0.5	1 (10 mm)	2
2	1	0.5	2 (10 mm)	2
3	1	0.5	1 (10 mm)	1
4	1	0.5	2 (20 mm)	2
5	1	0.5	2 (6 mm)	2
6	1	0.5	0	1
7	1	0.5	0	2
8	1	0.5	0	0

Table 6.1: Composition of the different concrete mixes used in this study.

In the preparation of concrete samples, there were certain raw materials used such as Portland cement and range of aggregate with different sizes (Figure 6.6). For the preparation of Type A samples, a combination of different ratios between aggregates and sand produced eight samples with a different composition as shown in Table 6.1. Two types of aggregates were used in the samples preparation where for sample 1, 2, and , river gravel with maximum size of 10 were used, while river gravel with maximum size of 20 mm were used and for sample 5 granite aggregates of 6 mm maximum size has been used . The correct ratio of the components by weight was achieved using concrete scales (Figure 6.5(a)). Then, a mixture of all raw materials were mixed together using a concrete mixer to obtain a uniform distribution (Figure 6.5(b)) before being poured into the mould for the casting process (Figure 6.5(c)). During this process, a vibrating table (Figure 6.5(c) - under the

mould) was used to ensure that the concrete was well compacted and to reduce trapped air bubbles which could result in unwanted porosity that could affect the measurement. However, excessive use of vibrating table could also be a problem because it can cause segregation of the concrete mix, which ultimately results in uneven distribution of the aggregate in the concrete. All the cast samples were left overnight before being demoulded. Figure 6.7 shows the concrete samples (different ratios) during the casting process and the finish products that were left overnight before demoulding.

(a) *(b)* *(c)* *(d)*

Figure 6.6: the materials used in the concrete samples; (a) sand; (b) 6 mm (max) aggregate; (c) 10 mm (max) aggregate; (d) 16 mm (max) aggregate

Figure 6.7: Concrete samples (different ratios) during the casting process and the finish products that were left overnight before demoulding

In Type A, eight samples were tested. Only five were further selected for Type B (Mix 3, Mix 4, Mix 5, Mix 6 and Mix 8). These samples were concrete slabs with the

dimension of 30 cm x 30 cm x 8.5 cm, containing a reinforcement bar (rebar type deform bars) at a known cover depth (Figure 6.19). Details of these samples are shown in the drawings. The method to prepare this sample was similar to that of Type A and the samples were then cast in wooden moulds which were fabricated specifically for this experiment.

6.5 Ultrasonic testing of concrete samples

6.5.1 Choice of ultrasonic system design

A series of initial test were conducted to determine the choice of pulse compression system design that would be suitable for the experiment on concrete samples. Two types of piezo-composite transducers (Transducer A and Transducer B) as described in section 4.3.2 were considered (refer Figure 4.8 (b) and Figure 4.8 (c)). Finally, it was found that both types of transducers were suitable for use in this application depending on the length and type of the concrete. For long samples (50 cm pillars) Transducer A (Figure 4.8(b)) was used, while Transducer B was used on the thinner sample (80 mm concrete slab with rebar). Initial tests were also done to study the type of waveform and frequency appropriate for this application. It was concluded that Chirps would be used throughout the experiment with the centre frequency of 160 kHz and 100 kHz bandwidth with Transducer A while a centre frequency of 250 kHz (100 kHz bandwidth) was used with Transducer B.

6.5.2 Monitoring of eight concrete pillar samples during cure

As a preliminary study, eight samples with different compositions were prepared (Table 6.1) to study the effects of different concrete mixes on ultrasonic propagation characteristics. The ultrasonic measurements were carried out soon after the samples had been demoulded as shown in Figure 6.8. All the samples were cured in a water tank for 28 days. The measurements were repeated daily during the curing process. They were carried out in through-transmission mode for all eight samples for 28 consecutive days, with the

shape of waveforms, velocity, and frequency profile recorded daily. In addition, measurements were carried out in pulse-echo mode. The data collected as shown in Figure 6.8 was displayed in LabView as shown in Figure 6.9, where the cross-correlation outputs are visible. When they were fully cured (after 28 days), the samples were then cut into 4 different lengths (Figure 6.10) to examine whether the length of the sample affect the measurement, especially when the test was carried out in pitch catch mode.

Figure 6.8: Example of concrete pillar (Mix 1) after demoulding under measurement in through transmission mode

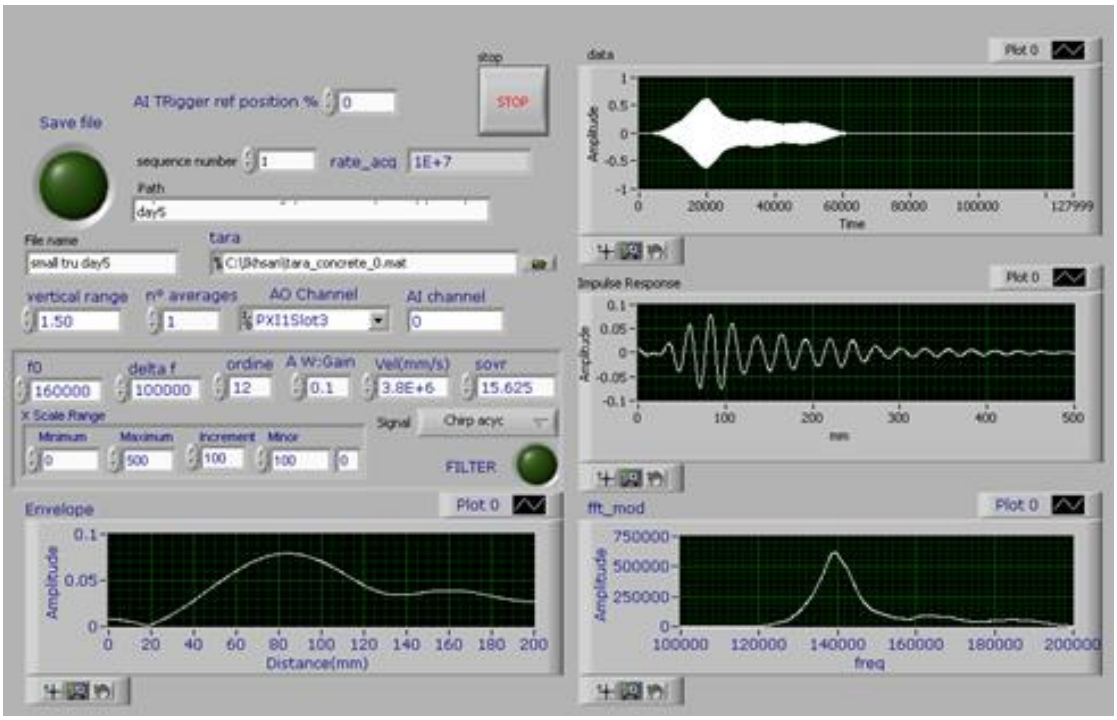

Figure 6.9: Example of LabVIEW window during the measurement in through-transmission mode

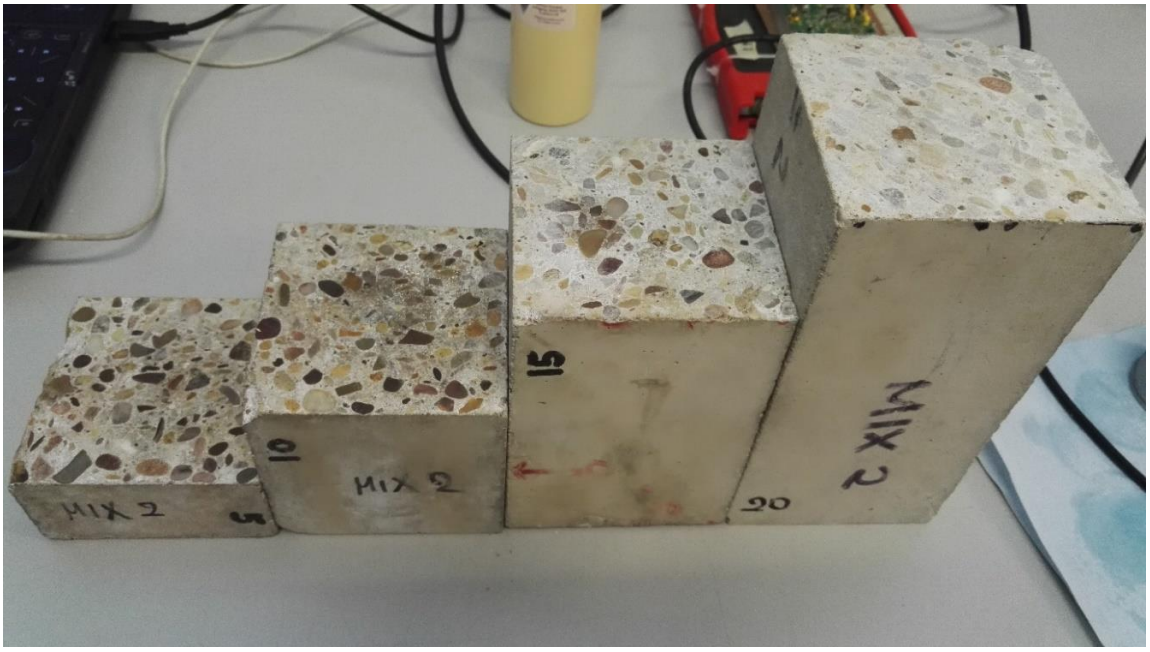

Figure 6.10: The pillars were cut into four different lengths on when it fully cured

Figure 6.11 shows some of the data obtained during the 28 days of measurement on sample Number 1 (Mix 1). From this study, it was found that the system was capable of producing a signal that could penetrate through 500 mm thicknesses of concrete. Initially, the data for Day 1 indicated that the frequency spectrum of the propagated wave through the sample was limited, and with a relatively small bandwidth, but the situation improved from the second day onwards.

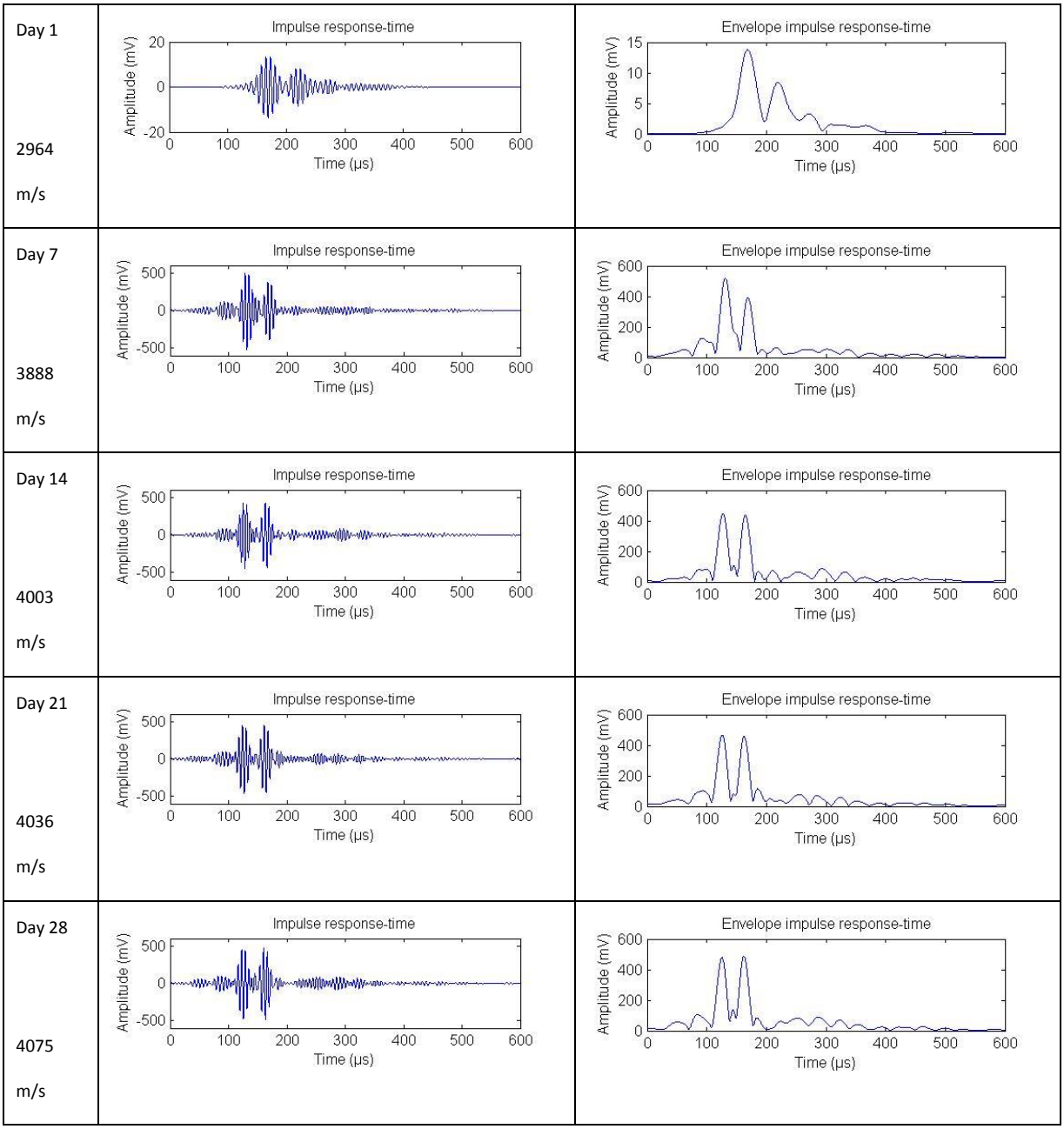

Figure 6.11: Waveform and spectra of signals obtained during the cure process for a pillar sample with Mix 1

Figures 6.12, 6.13 and 6.14 show the waveforms for four different mixes in Day 1, Day 7, Day 14 and Day 28 respectively. All three mixes show the same trend as Mix 1 where the velocity, spectrum and amplitude were at the lowest in Day 1, but started to increase from Day 2 onward. A comparison of the results from different mixes with a different composition also showed differences in terms of velocity and frequency bandwidth for the fully-cured samples.

Mix 1	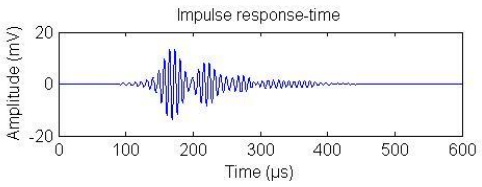	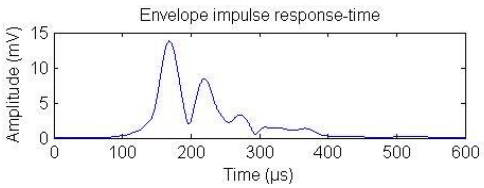
Mix 4	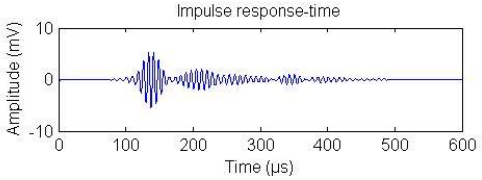	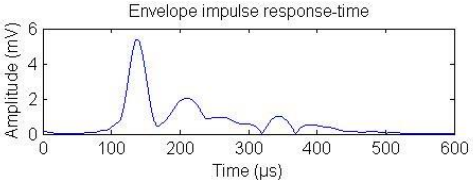
Mix 5	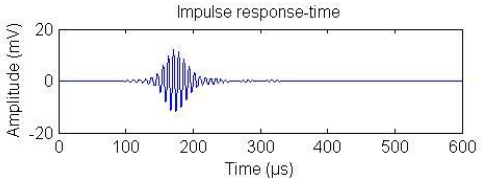	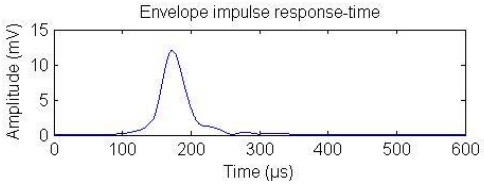
Mix 6	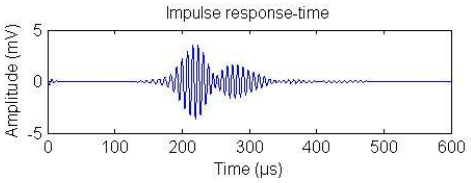	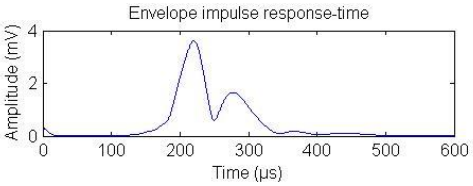

Figure 6.12: Waveforms and frequency spectra of four mixes in Day 1

Mix 1	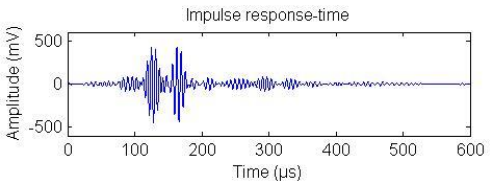	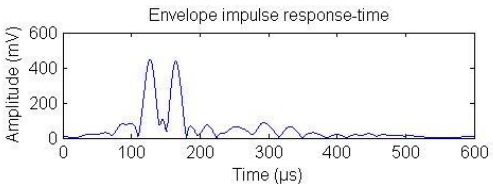
Mix 4	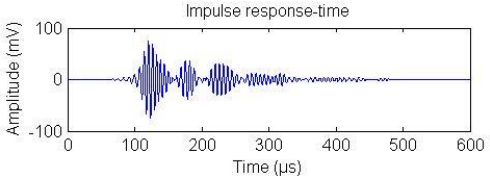	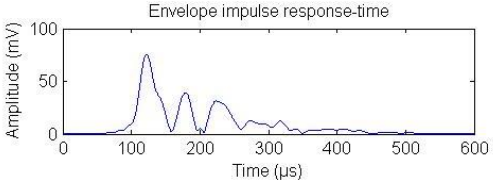
Mix 5	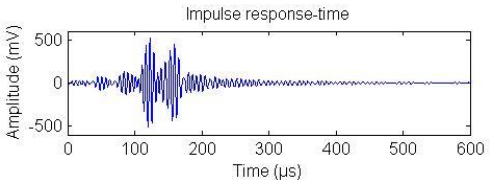	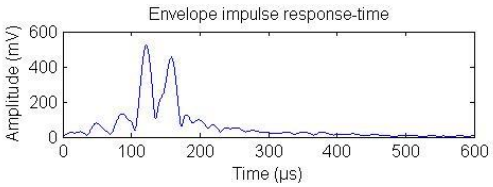
Mix 6	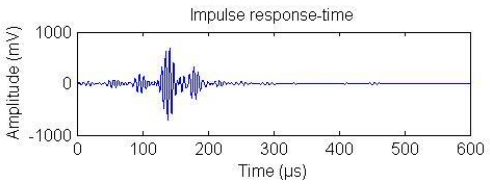	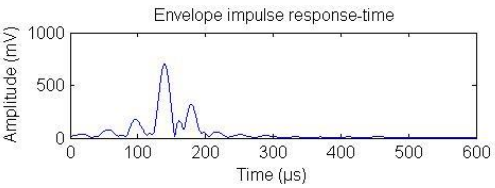

Figure 6.13: Waveforms and frequency spectra of four mixes in Day 14

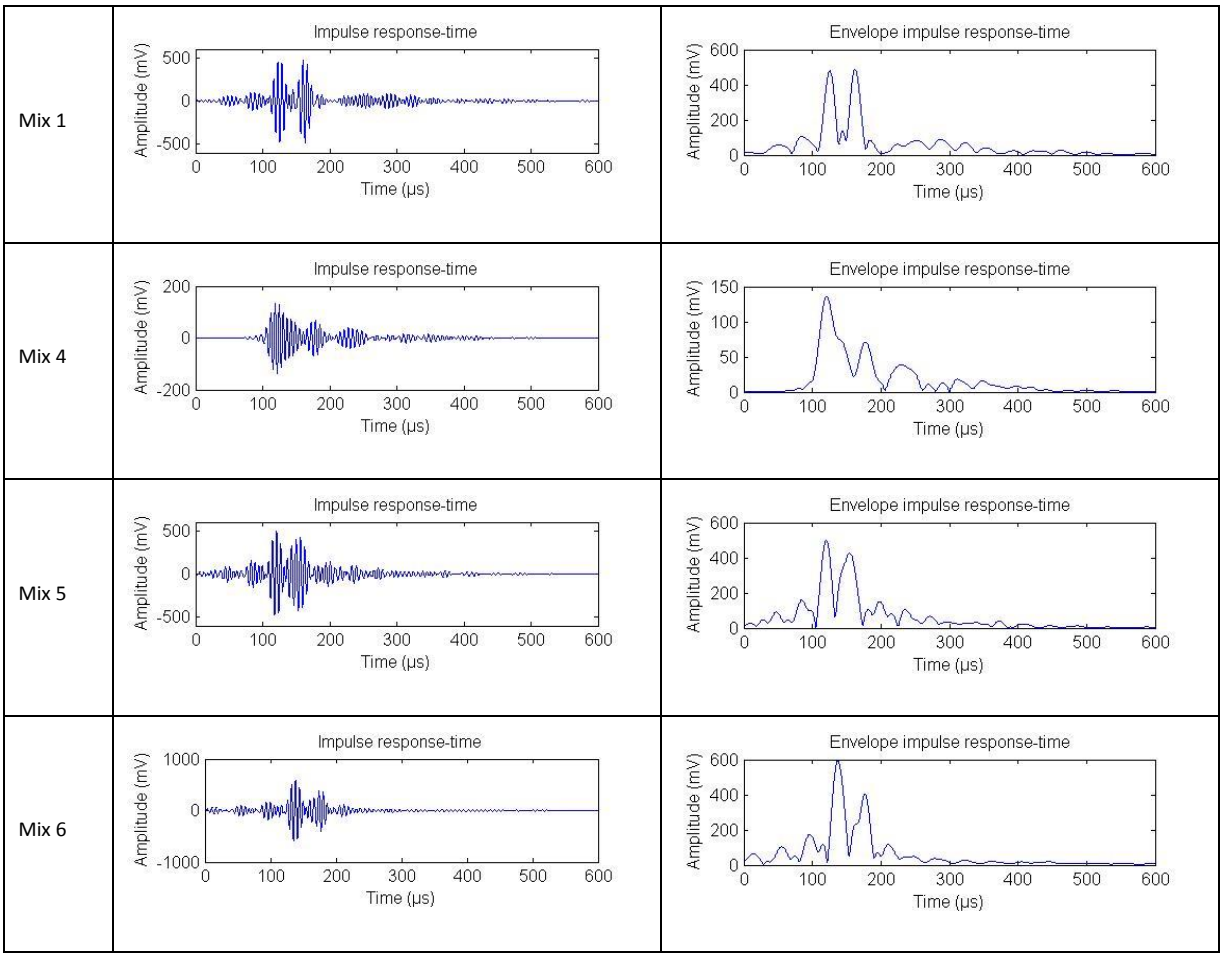

Figure 6.14: Waveforms and frequency spectra of four mixes in Day 28

Figure 6.15 shows the complete longitudinal velocities value for 4 different mixes during 28 days of monitoring. It can be seen that the longitudinal velocity of the ultrasonic signal increased with time from a value of 2,964 m/s for Day 1 as the curing process took place, as shown in Figure 6.15. The increment was quite steep in the first 7 days, then they were increasing minimally until fully cured after 28 days. The difference in the trend for the mixes (Mix 1, Mix 4 and Mix 5) were very little during the monitoring with the exception of Mix 6 where there were no aggregates in the composition. This result proved that the presence of aggregate plays a big role in determining the properties of concrete, particularly the longitudinal velocity which can also be related to other properties.

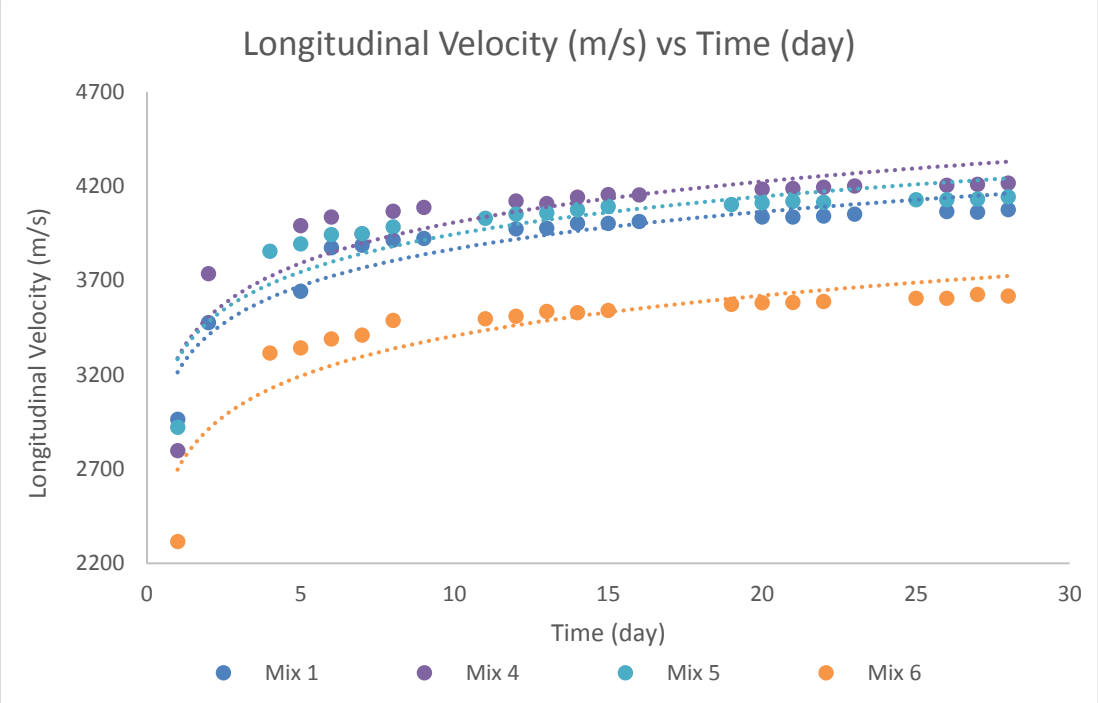

Figure 6.15: Graph of longitudinal velocity vs time during the curing process for a concrete pillar of Mix 1, Mix 4, Mix 5 and Mix 6

Figure 6.16 is a comparison of received signal for four different lengths namely 5 cm, 10 cm, 15 cm and 20 cm of concrete samples (Mix 2) from the cut pillar (Figure 6.10) in pitch catch mode. It shows that the time of flight shifted to the right indicating that it increases with an increase in length of the sample. The result also shows that the system was capable of detecting changes for a concrete sample as thick as 20 cm.

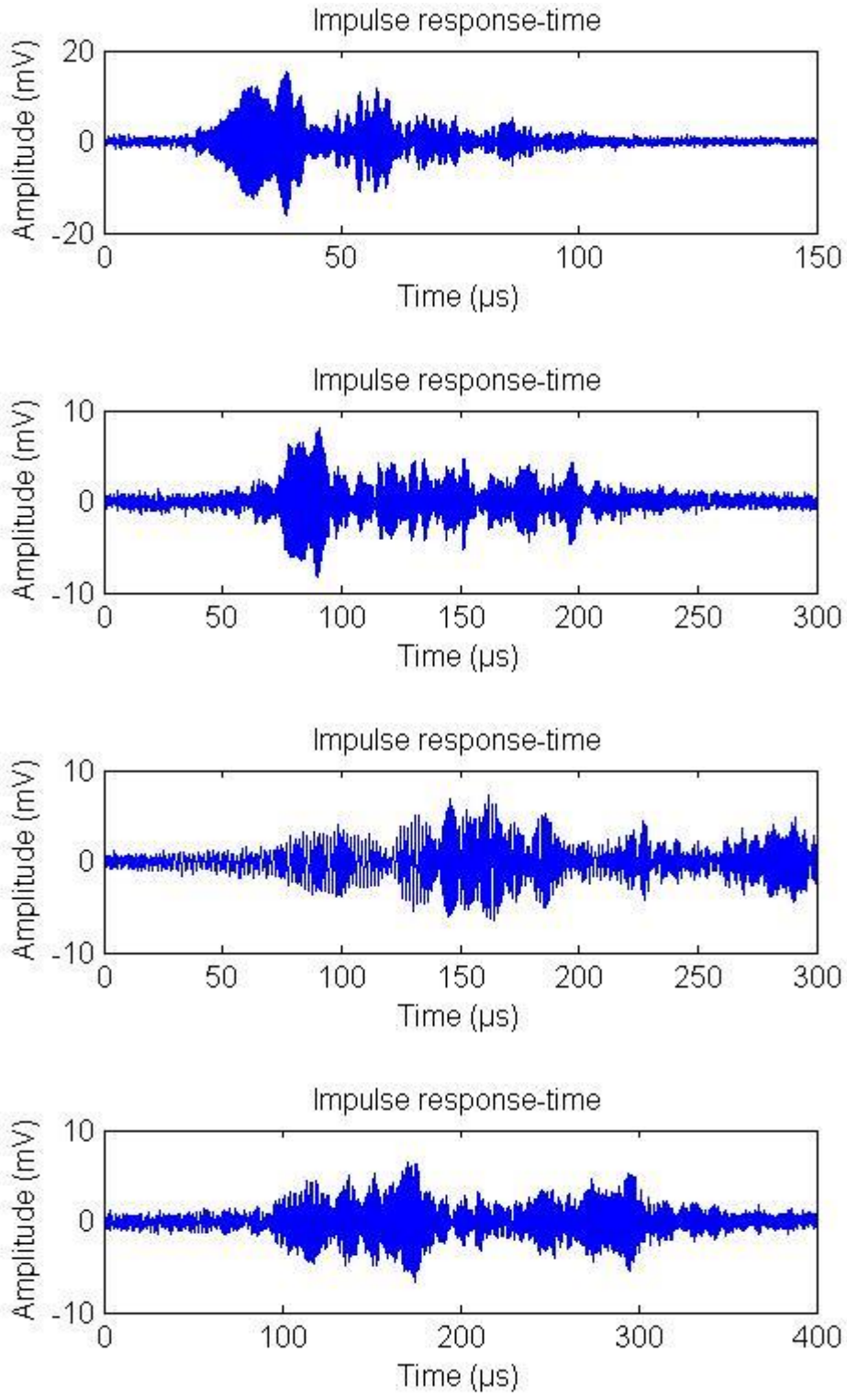

Figure 6.16: A comparison of received signal of four deferent length of concrete from the cut pillar (Figure 6.10) in pitch catch mode

6.5.3 Imaging of embedded rebars

Based on the preliminary test results on concrete pillars (Type A) described in the previous section, five concrete mixes were chosen for the testing of samples containing rebars, as shown in Figure 6.17. Samples were kept in a water tank for 28 days to allow curing process.

Figure 6.17: After 28 days of curing in water tank, the finished product of concrete slabs with rebar inside ready for testing

Experiments were performed using a pitch-catch arrangement. The two transducers were coupled side by side in the transducer holder as shown in the photograph of Figure 6.18 (a). A regular grid was marked on the top surface, as in Figure 6.18(b), to facilitate the scanning process for imaging purposes. In order to avoid scattering of the sidewall, only the yellow marked area was scanned with an area of 40 mm x 40 mm. Piezocomposite transducers with centre frequency of 270 kHz were used for this scanning process.

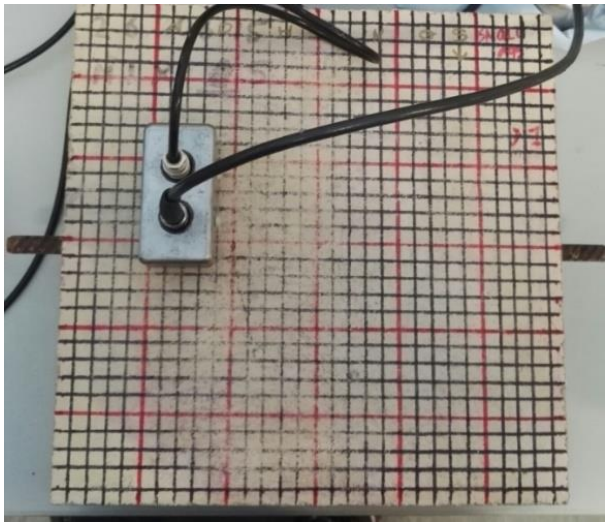

(a)

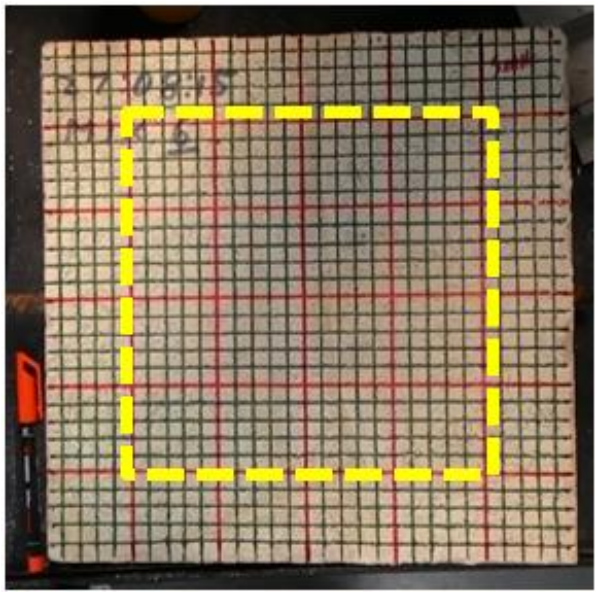

(b)

Figure 6.18: (a) Photograph of the two piezocomposite transducers in pitch-catch mode on the surface of a concrete sample; (b) Scanning area (marked in yellow) with the gridded marking ready for the scanning process

The following results were from a sample with the geometry shown in Figure 6.19, and using Mix 6 of Table 6.1. Typical outputs from the pulse compression processing are shown in Figure 6.20 for when the transducer pair were (a) well away from the rebar, and (b) directly over it. It can be seen that the back-wall echo is present in both cases (red arroes), but that when the rebar is present, a significant reflection was detected (blue arrow) as in the Figure 6.20(b).

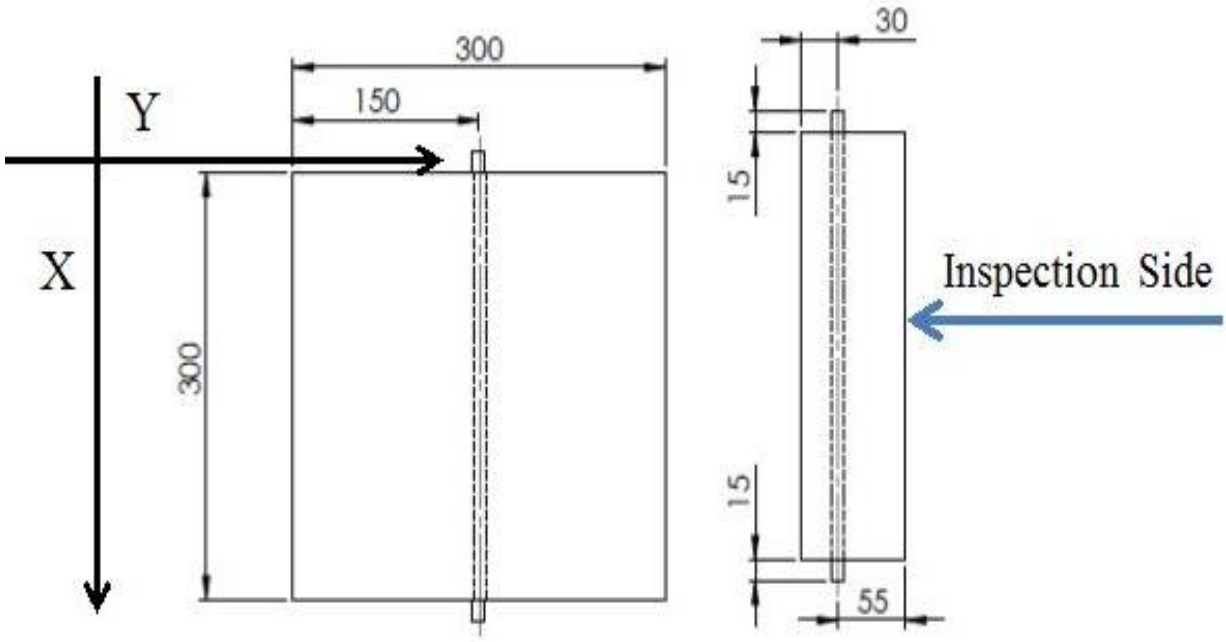

Figure 6.19: Top and side view of the concrete slab plan and the marking of the inspection direction

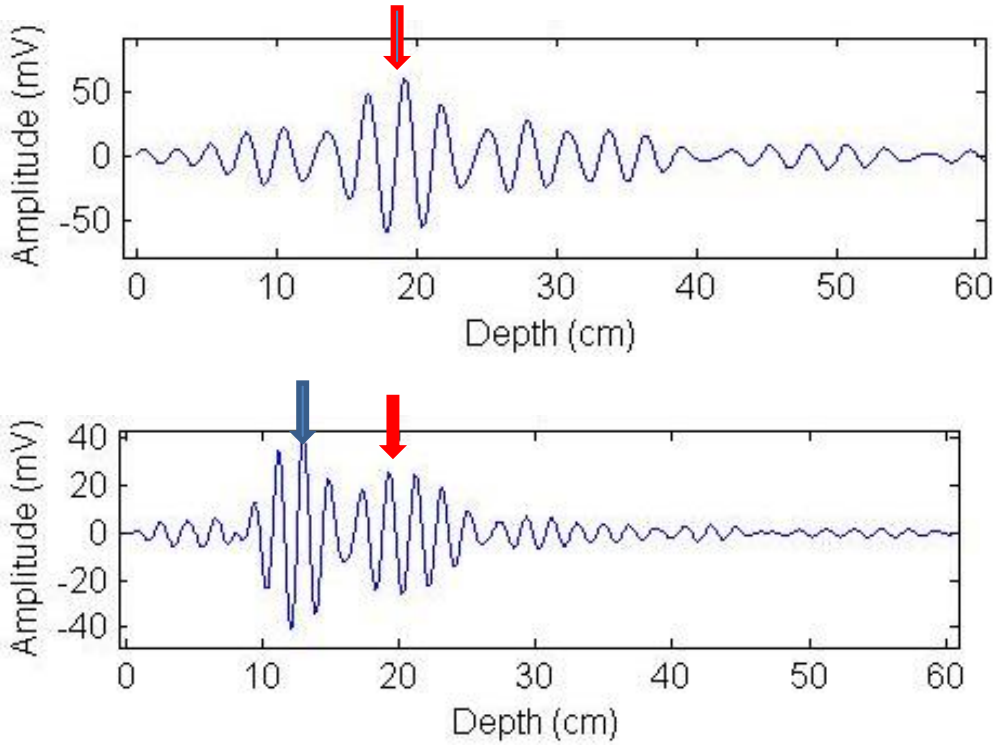

Figure 6.20: Pulse compression waveforms when the transducer pair were (a) well away from the rebar, and (b) over the rebar. The output is in the form of an unrectified and unsmoothed signal. The arrows show the position of the back-wall and rebar echoes.

Data was now collected as the transducer pair was scanned over the grid pattern on the sample surface. A C-scan image was then produced using a time window which covered the expected arrival time of the echo from the rebar. The result, shown in Figure 6.21, shows four C-scan images from the scan with a good indication that the rebar was present, but the quality of the image was highly dependent on the size distribution of the aggregate within the sample. The reinforcement bar was harder to detect in the presence of bigger aggregates. This was because bigger aggregates caused more scattering when compared to smaller ones.

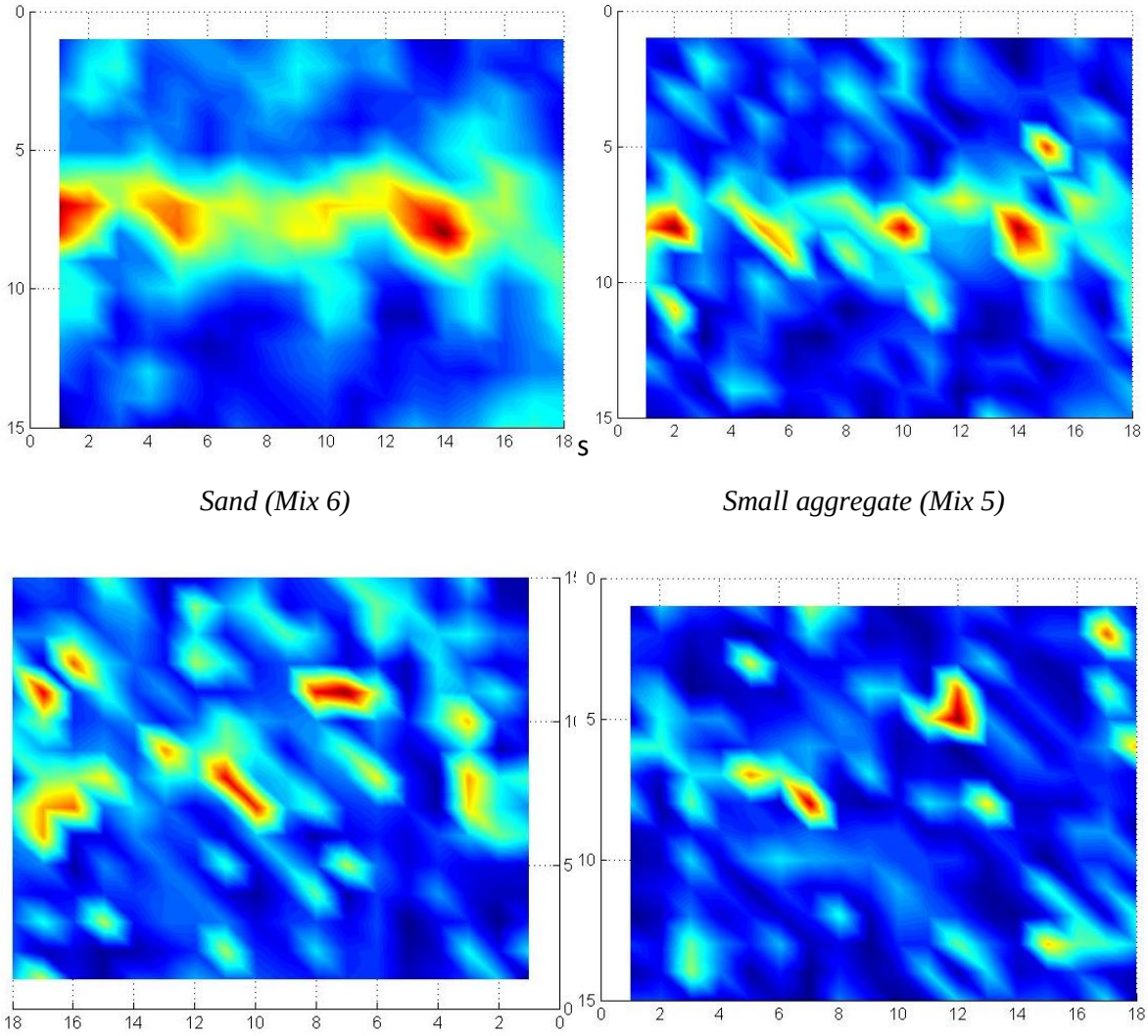

Sand (Mix 6) *Small aggregate (Mix 5)*

Normal aggregate (Mix 1) *Big aggregate (Mix 4)*

Figure 6.21: C-scan visualization of the scanning data after normalized with the back wall.

6.5.3 Ultrasonic testing of a larger concrete block

The pulse compression system was also tested on an additional concrete sample containing a rebar. This sample was far bigger and thicker than what was discussed earlier. It was meant to test whether there was any limitation to the ultrasonic system. The sample was a mixture produced from 'Mix 3' (previous test) in the size of a 40 cm cube. The location of the rebar of 10 mm diameter is at 10 cm depth from the top and 30 cm from the bottom. Figure 6.22 shows a photograph of this concrete sample. The ultrasonic signals were the same as that used in other tests within this Chapter.

Figure 6.22: A larger concrete sample containing a rebar.

Figure 6.23 below presents the experimental results of the above sample. Here, it can be seen that the ultrasonic signal was able to penetrate a 40cm-thickness of concrete. As can be seen in Figure 6.22, the result from the through transmission measurement indicates the thickness of the concrete sample. Figure 6.22(b) is the results of measurement carried out over the rebar location from the top side. It produced defect echo which shows the depth

where the rebar was positioned. However, the test performed over the rebar location from the bottom end was unable to produce any defect echo.

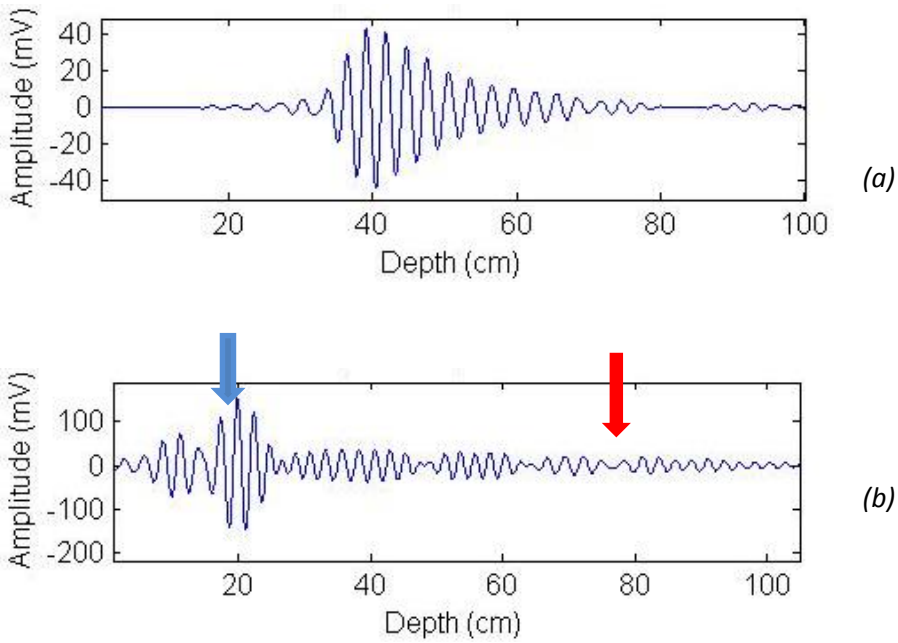

Figure 6.23: (a) through transmission measurement of the sample given the thickness of the sample; (b) Pulse echo result over the top of the rebar showing an earlier arrival time (blue arrow) indicated the rebar and red arrow marked the location of expected back wall echo.

6.6 Inspection of refractory anchor bricks

Figure 6.24 shows the refractory anchor bricks which are commonly used in a high-temperature furnace in the metal fabrication industry. As discussed earlier; at the beginning of this chapter, anchor bricks have a tendency to break after being used for a period of time. It is difficult to detect a broken anchor brick using standard ultrasonic NDT, even if the fracture extends all the way across the brick. This is because the material is highly scattering and attenuation, due to the materials within it, and the fact that it is pillar shaped with non-flat walls, which encourages scattering from the walls as well. In addition, they are embedded deep within the concrete or furnace wall. Accessibility to perform this test also worsens the situation because the only option is to perform an ultrasonic test from the external surface. The long physical structure of anchor pillar (30 cm – 50 cm) with small

surface area (10 cm square) and uneven side surfaces (claws) causes too much noise and wall reflection for a conventional NDT test. Pulse compression was thus tried.

Figure 6.24: Refractory anchor bricks

6.6.1 Preliminary experiments

For the pulse compression studies, a low frequency chirp signal was used to obtain good penetration in the samples, and at a frequency range of 120-220 kHz, with a center frequency of 170 kHz and signal duration of 10 ms. A pair of piezo-composite transducers with a 55 mm diameter were used in a pitch-catch mode, as shown in Figure 6.25. The center frequency of the transducers was 170 kHz. Every measurement was recorded and repeated three times. The findings were plotted as a graph of normalized amplitude vs depth in the sample.

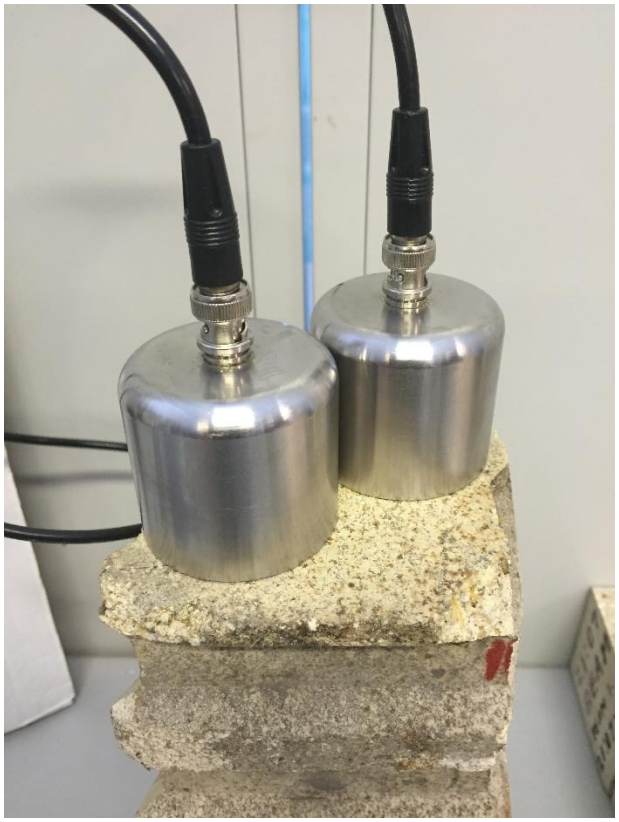

Figure 6.25: Photograph of a pair of piezocomposite transducers at the surface of a brick sample for pulse compression testing.

Figure 6.26 shows pulse compression outputs from single measurements for various brick lengths, obtained by cutting the samples to different lengths for the experiment. This shows that, at certain length, a back-wall echo could be obtained from the pulse compression system, provided the transducers were located in certain positions on the surface. A crack would effectively relocate the back wall reflection, and hence this measurement could potentially be used. However, in practice, the results were highly variable from one transducer location to the next – small shifts in position caused a different pulse compression output, as can be seen in Figure 6.27, where the three signals are very different from each other. It can also be observed that the signal obtained is very random with no recognisable pattern relatable to the physical form of the sample. This situation was probably due to the

small outer surface testing area (100 mm x 100 mm) compared with the sample length (354 mm). Furthermore, the unevenness of the sample wall (claws) complicates matters.

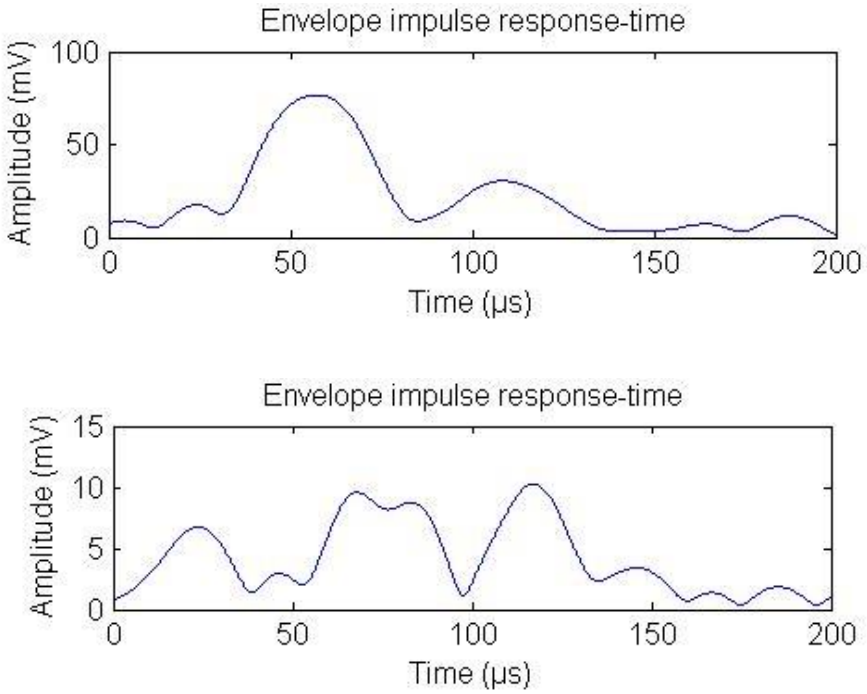

Figure 6.26: Pulse echo measurements for two different lengths of pillar, (a) signal of 10 cm brick where the back-wall echo at 50 μs; (b) signal of 20 cm brick show that the back-wall echo is not obvious.

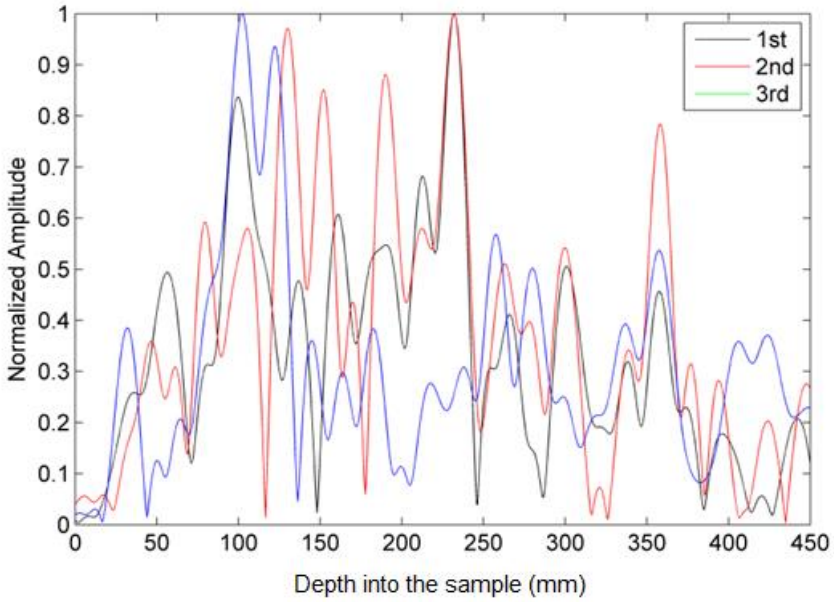

Figure 6.27: Three acquisition of the repeated measurement on the same sample (of thickness 35 cm) with random movement of transducers on the top surface, but at the same distance apart (0.5 cm).

6.6.2 A statistical method for estimating crack depths

If the presence of a major crack was to be detected, the data had to be further processed. Therefore, a new technique was introduced based on a statistical analysis which could highlight the differences between the undamaged and damaged bricks. This statistical analysis was again developed by Dr Marco Ricci and Mr Stefano Laureti at the University of Perugia, Italy. The main idea was to analyze the spatial and temporal distribution of the reflected energy in order to understand if there are noticeable variations between broken and unbroken bricks. In this study, two different excitation bandwidths were investigated experimentally by the author for this set of measurements: Narrow-band (80-120 kHz) and Broad-band (100-200 kHz).

In this method, the total integrated energy was obtained by summing the contributions scattered back to the top surface from each incremental depth into the material. A plot was then produced as the value of this total reflected/backscattered energy increased with time (and hence distance into the sample). Eventually, this reached a maximum saturation level. A threshold level for the cumulative reflected energy was then chosen – in this case at 90% of the maximum level. The depth within the sample at which this energy was reached was obtained from each individual measurement. This was repeated by moving the transducer pair randomly to different positions on the top surface so that ten different values of the threshold distance could be recorded. The data was then plotted as a histogram of the number of measurements that reached the 90% level at a particular depth into the sample (plotted from 0 - 450 mm). In this way, it was easier to determine the location of the main reflection of energy back to the surface.

Figure 6.28 (a) shows the cumulative reflected energy for both broad bandwidth (red) and narrow bandwidth (green) chirps in which the total energy received as a function of time was re-plotted as a function of distance, using the value of acoustic velocity quoted above. Ten measurements were taken for each bandwidth. From every measurement, an interval was set at the waveforms regarding the arrival time of back wall echo. Then, the cumulative energies were plotted using the acquired data with the interval that has been set. From the results, it clearly shows that the amplitude of cumulative energy produced by broad bandwidth was higher than the narrow bandwidth, as expected. However, this result does not show significant signs that can be related to sample's condition. The cumulative energy trend between measurements was also significantly different and was not consistent. This condition was caused by many factors which could affect the measurement. These include coupling variations, pressure on the transducer during the measurement and transducer position. However, the situation was much different when the maximum amplitude in the cross-correlation was normalized to the same value for all traces as shown in Figure 6.28(b). Because broadband data gave better results compared to narrowband excitation, a broad bandwidth was used in all subsequent experiments.

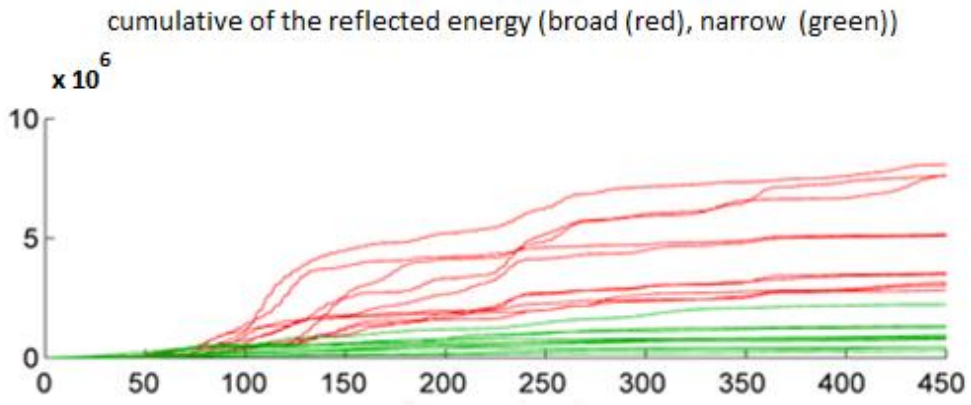

(a)

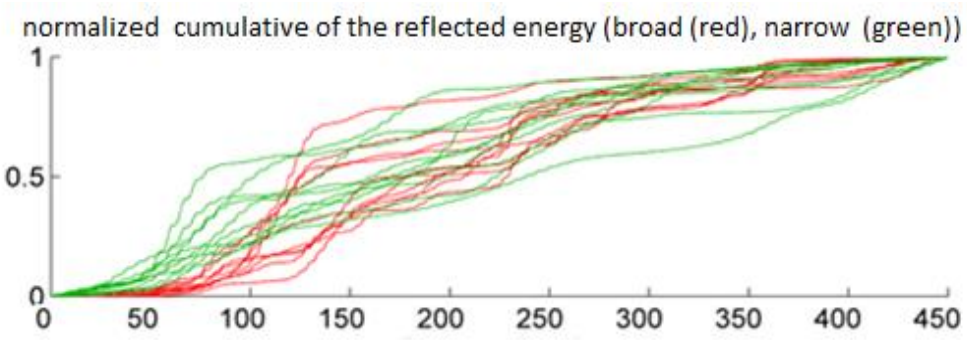

(b

Figure 6.28: Cumulative energy received at the top surface for 10 different transducer locations. Data is shown for both narrow bandwidth (green) and broad bandwidth (red) excitation, for (a) data as recorded, and (b) normalized data. The horizontal axis is the distance in mm from the top surface of the sample.

Figure 6.29 shows the average velocity of each sample 1 to 6, together with the average velocity for this set of samples, which was estimated at 3,208 ms^{-1} (the red line). The data for each transducer was then analyzed by finding the distance into the sample at which the total accumulated energy reaches 90% of the total value recorded at the receiver by the end of the waveform. The distance from each location was then plotted in a histogram. Figure 6.28 shows the results for 6 refractory bricks that were tested with the same method. All samples have the same nominal length of 354 mm, but the histogram data (Figure 6.30) shows a variation in the estimated position of the back wall. This was almost certainly due to the variations in the acoustic velocity in each sample because the velocity test gave a different reading for every sample.

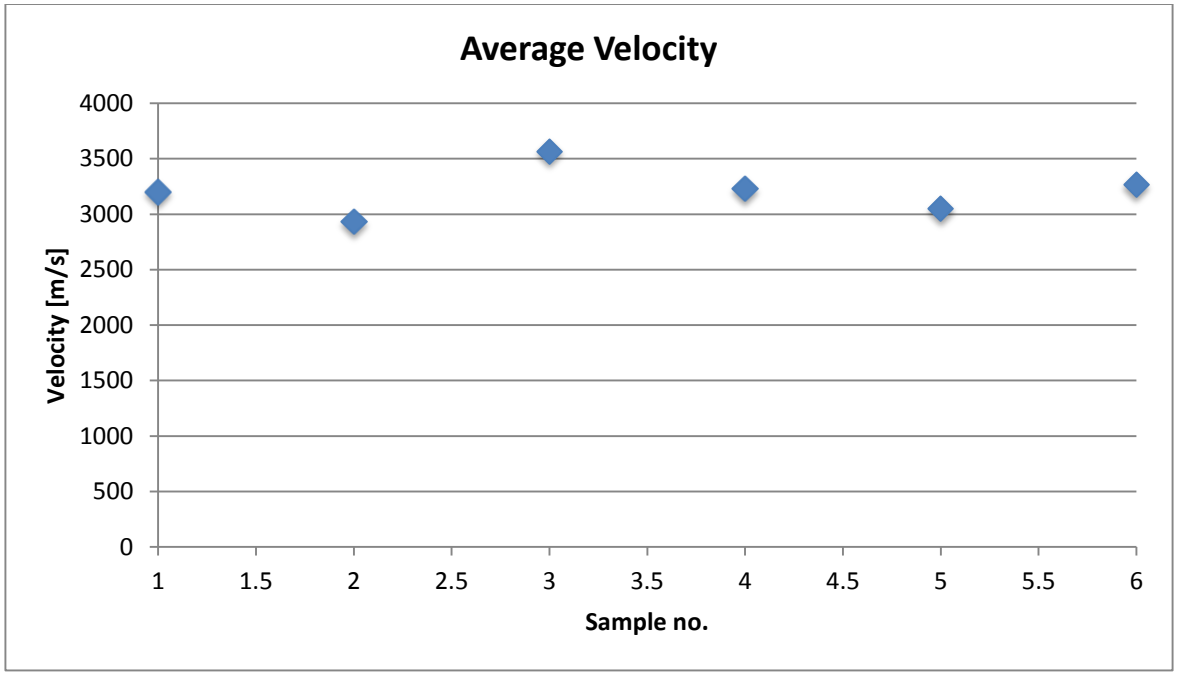

Figure 6.29: Average velocity of 6 samples

BRICK 1

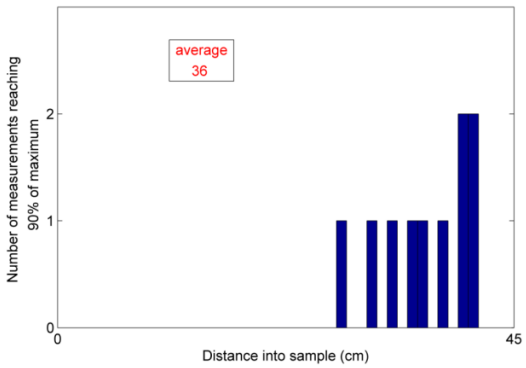

BRICK 2

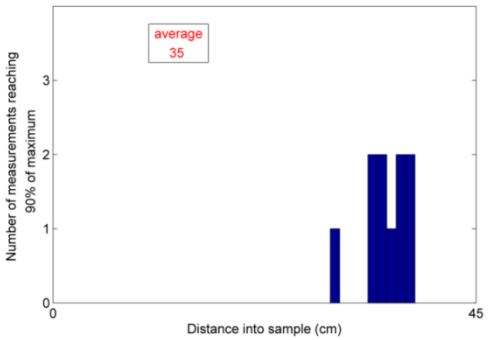

BRICK 3

BRICK 4

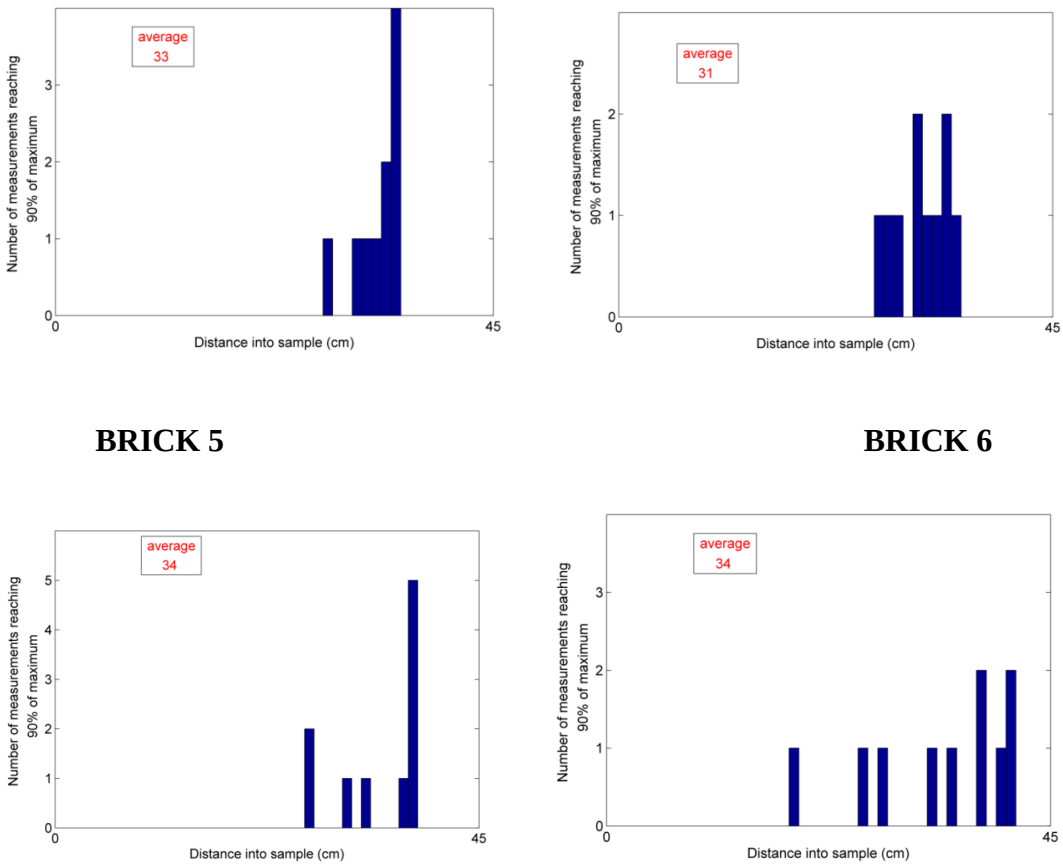

Figure 6.30: Histograms for an additional 6 unbroken bricks, using a 90% threshold level on normalized data.

An illustration of the difference in the energy accumulation curves at a single location for an unbroken and a thin section is shown in Figure 6.31. It can be seen that the thinner section would give a smaller value for distance into the sample at the 89% (0.9) threshold value. A clear difference in the behavior of the cumulatively reflected energy can be appreciated.

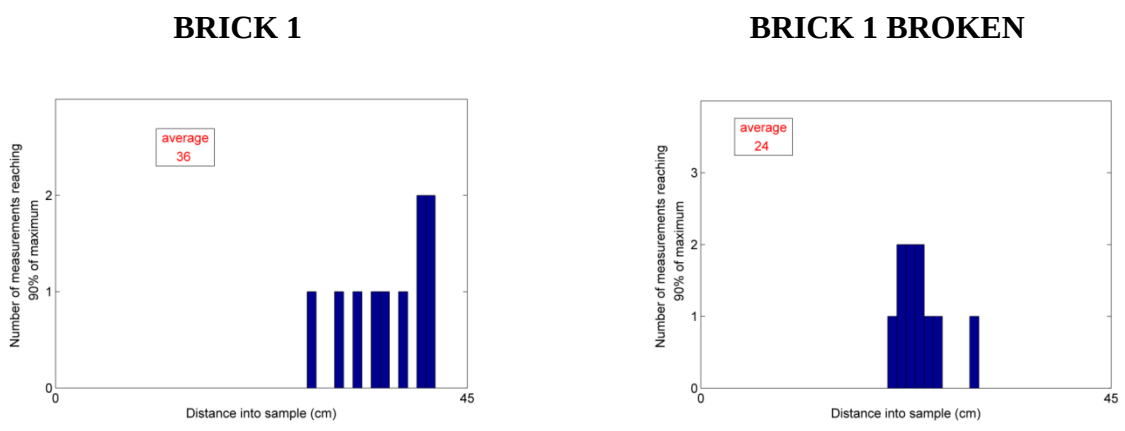

Figure 6.31: Comparison of the results for sample no. 1 when at full length (left) and broken (right).

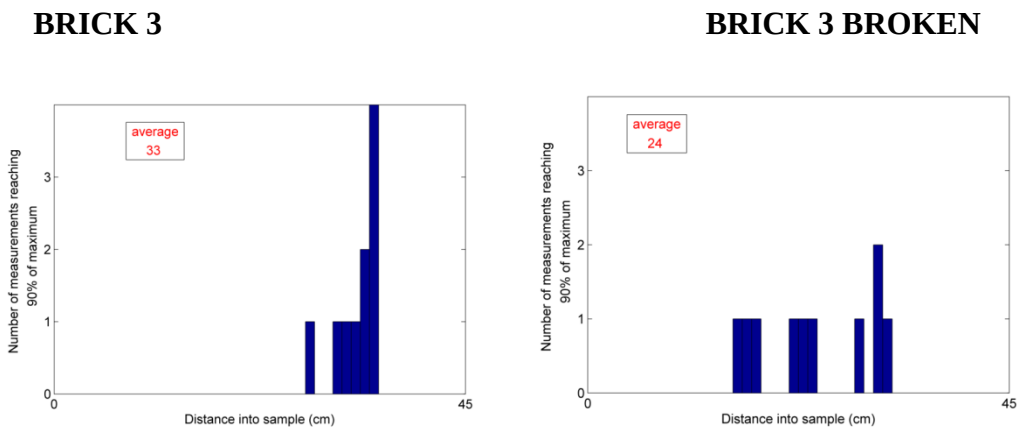

Figure 6.32: Comparison of the results for sample no. 3 when at full length (left) and broken (right).

Another strategy was explored to overcome this uncertainty in order to differentiate between complete and broken samples. Figure 6.33 shows the trend of the cumulative reflected acoustic energy (normalized) as a function of the distance into the sample. This is shown for sample no. 1 in both its original and broken state. It can be seen in Figure 6.33 that the amount of energy returning to the top surface in pitch-catch mode increases more quickly to the 90% threshold level for the broken sample (black line) than for the full-length one (red line). The idea is that the slope of this line, obtained by differentiating this curve, can be used as a parameter to distinguish a full-length sample from a broken one. The new method seems to give a good indication of the likely position within a sample of a major change, such as the brick breaking completely. The variations in the results might be due to changes in velocity within different parts of the same brick, and between individual bricks.

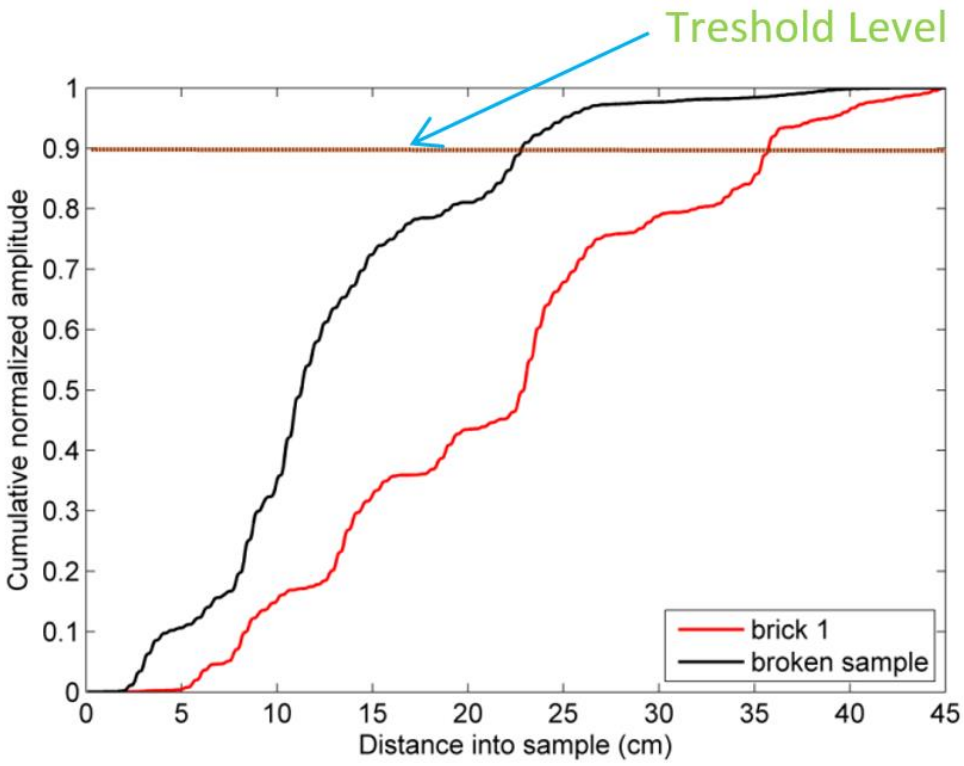

Figure 6.33: Cumulative reflected acoustic energy (normalized) as a function of the distance into the sample

6.7 Conclusions

From the tests that have been carried out, it was clearly shown that the composition of the conventional concrete materials greatly affects the propagation of the ultrasonic signal. It was shown in Test 1 that not only the size of aggregate but also the ratio of other materials such as sand and cement influences the test result. The results of this test have been used as a guide in preparing some further samples which were concrete slabs containing rebar (Test 2). From the results, it shows that the developed ultrasonic system was successfully able to detect and locate the location of the rebar that was embedded within the concrete. In addition, the test results have proved that this system managed to test the concrete thickness of 40 cm and surprisingly able to locate rebar at a depth of 10 cm using a pitch-catch mode.

The tests on the refractory brick were more challenging, due to both the highly scattering medium and shape of the samples. With the use of pulse compression and further statistical processing, it was shown that the developed ultrasonic system was able to detect and distinguish if there are any defect or crack in the refractory anchor brick using pulse echo method. This is the most important achievement of this study because it has a direct contribution to the industry. The test method that was used in this regard also considered the nature and accessibility that exists in the real situation of furnace linings used in the steel industry.

References

[1] B. C. Kim and J. Y. Kim, "Characterization of ultrasonic properties of concrete," *Mech. Res. Commun.*, vol. 36, no. 2, pp. 207–214, 2009.

[2] M. Schickert, M. Krause, and W. Müller, "Ultrasonic Imaging of Concrete Elements Using Reconstruction by Synthetic Aperture Focusing Technique," *Journal of Materials in Civil Engineering*, vol. 15. pp. 235–246, 2003.

[3] S. K. Verma, S. S. Bhadauria, and S. Akhtar, "Review of Nondestructive Testing Methods for Condition Monitoring of Concrete Structures," vol. 2013, no. 2008, 2013.

[4] A. Demolenko, H. A. Visser, and R. Akkerman, "Ultrasonic measurements of undamaged concrete layer thickness in a deteriorated concrete structure," *NDT &E Int.*, vol. 77, pp. 63–72, 2016.

[5] G. A. Khoury, "Concrete Spalling Review," *Design*, no. June, p. 60, 2000.

[6] A. Neville, "Chloride attack of reinforced concrete: an overview," *Mater. Struct.*, vol. 28, no. 2, pp. 63–70, 1995.

[7] S. Bae and O. Bayrak, "Early Cover Spalling in High-Strength Concrete Columns.," *J. Struct. Eng.*, vol. 129, no. 3, p. 314, 2003.

[8] M. Z. Jumaat, M. H. Kabir, and M. Obaydullah, “A review of the repair of reinforced concrete beams,” *J. Appl. Sci. Res.*, vol. 2, no. 6, pp. 317–326, 2006.

[9] A. S. Al-Harthy, M. G. Stewart, and J. A. Mullard, “Concrete cover cracking caused by steel reinforcement corrosion,” *Mag. Concr. Res.*, vol. 63, no. 9, pp. 655–667, 2011.

[10] X. Dérobert, J. Iaquinta, G. Klysz, and J. P. Balayssac, “Use of capacitive and GPR techniques for the non-destructive evaluation of cover concrete,” *NDT E Int.*, vol. 41, no. 1, pp. 44–52, 2008.

[11] “Concrete cover meter.” [Online]. Available: http://www.proceq.com/nondestructivetestequipment/concrete-testing/cover-meter-rebar-detector/profometer-pm-600.html?pqr=3.

[12] “Bosch rebar locater.” [Online]. Available: http://www.hirehere.ie/rebar-detector-locator.

[13] A. Guerriero, C. Guaragnella, C. Pasquale, and F. Quaranta, “Differentiation between recycling refractory bricks by texture analysis,” in *Conference Record - IEEE Instrumentation and Measurement Technology Conference*, 2008, pp. 2055–2058.

[14] T. Shimizu, K. Matsuura, H. Furue, and K. Matsuzak, “Thermal conductivity of high porosity alumina refractory bricks made by a slurry gelation and foaming method,” *J. Eur. Ceram. Soc.*, vol. 33, no. 15–16, pp. 3429–3435, 2013.

[15] C. Sadik, I.-E. El Amrani, and A. Albizane, “Recent advances in silica-alumina refractory: A review,” *J. Asian Ceram. Soc.*, vol. 2, no. 2, pp. 83–96, 2014.

[16] “field furncae refractory.” [Online]. Available: http://www.fieldfurnace.com.au/anchors-ezp-6.html.

[17] “refractory anchor brick.” [Online]. Available: http://keramserviss.lv/public/index.php?lang=en&section=439.

[18] H. Hayashi, T. Saitou, N. Maruyama, H. Inaba, K. Kawamura, and M. Mori, “Thermal expansion coefficient of yttria stabilized zirconia for various yttria contents,” *Solid State Ionics*, vol. 176, no. 5–6, pp. 613–619, 2005.

Chapter 7

Ultrasonic System Technique for Composites and Multi-Layered Structures

7.1 Introduction

Composites are materials that are widely used in various fields. However, composites come in a wide range of materials and multi-layered structures, which can lead to difficulties in NDE for integrity assessment [1-4]. This Chapter describes measurements performed on several such materials and structures. These are pipe insulation material and composites used in the aerospace industry.

7.2 Pipe insulation material

7.2.1 The problem

Pipelines are important industrial structures, especially in the oil and gas industry. They are used to transport materials including oil, liquefied gas or other substances [5]. In pipelines used for long-distance transportation, it is very critical to maintain the temperature inside the pipelines at a higher than the ambient temperature because of certain reasons such as to avoid the formation of gas hydrates, enhancing the product flow properties and to avoid the formation of wax in the pipes [6]. However, in the case of liquefied gas transport pipelines, the opposite situation occurs, where temperatures in the pipes should be maintained at a low enough level to preserve it in the form of liquid [7-9]. In both conditions mentioned above, insulators are needed to insulate the pipes so that the temperature inside the pipes can be maintained. Among the materials that often used as the insulation for carrier pipes are polypropylene, polyurethane and polyethylene [10-11]. The most important

property of these materials is thermal conductivity [12]. Table 7.1 shows the thermal conductivity of some materials that have been used in this application. These materials have different thermal conductivity values and are used depending on the particular application. Basically, there are two types of insulation, namely wet insulation and dry insulation. Dry insulation requires an outer barrier to prevent water ingress. This type structure is known as a pipe-in-pipe (PIP) insulation system, and most deep-water pipelines included in this category [13-14]. Normally, the outer pipe and carrier pipe are placed concentrically. In between the outer and the carrier pipes there is a layer of material (can be up to a few layers) called the annulus, which is very important for maintaining the temperature within the carrier pipe. Among the materials often used as insulators in dry insulation are closed-cell polyurethane foam (CCPF), open-cell polyurethane foam (OCPF), extruded polystyrene, and fiberglass [13, 15-16]. Figure 7.1 shows some example of insulators that have been used in this study and Table 7.2 shows some of their properties.

Insulation Type	*U*-Value	
	(Btu/h ft^2 °F)	W/m^2 K
Solid polypropylene	0.50	2.84
Polypropylene foam	0.28	1.59
Syntactic polyurethane	0.32	1.81
Syntactic PUF	0.30	1.70
PIP syntactic PUF	0.17	0.96
Composite	0.12	0.68
PIP high efficiency	0.05	0.28
Glass syntactic polyurethane	0.03	0.17

Table 7.1: Thermal conductivity of some materials that have been used as insulators [9]

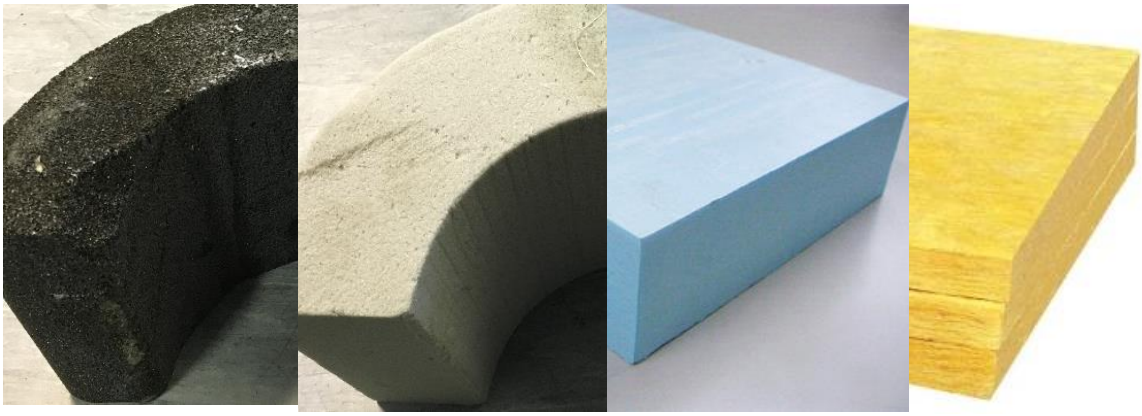

Glass foam ("Foamglas") | *Polyurethane foam* | *Expanded polystyrene* | *Fiberglass wool ("Rockwool")*

Figure 7.2: Insulating materials that have been used in this study

Insulation Material	*k*-Factor at 75°F (Btu/h ft^2 °F)	Density (lb/ft^3)	Compressive Strength (psi)	Service Temperature (°F)
CCPUF		3–6	10–65	
OCPUF		2–4		
PIF	0.190	1.8–2	19–24	−297–300
Polystyrene	0.259	6	20	−297–165
Fiberglass	0.24	3.5–5.5		0–850
Mineral wool	0.25	8.7		1292
VIP	0.036–0.055	3.7–9.0		320

Table 7.2: Basic properties of insulators [9]

Problems can be encountered with the pipelines insulation system when it has been used for a certain period of time, where it tends to leak due to the extreme environment especially at bends and joints [17]. Leakage through the outer protection layers and/or insulation can cause water ingress, which could then lead to corrosion of the carrier pipe. This could be dangerous and harmful, and lead to leakage of the contents of the pipe or even catastrophic failure. This problem is called corrosion under insulation (CUI), and is a major

problem in the oil and gas industry [18]. Due to the specific properties of the layers of insulator, it is hard for the conventional ultrasonic system and other NDT techniques to penetrate the material. The insulators can be considered as substances with high ultrasonic attenuation and the situation is multi-layered. Therefore, in this study, low-frequency ultrasonic signals (sub-MHz ultrasound) were examined to see whether the technique could be used to penetrate through these materials. If so, there would be a possibility of both detecting water ingress, and also trying to estimate pitting of the carrier pipe at its outer surface.

7.2.2 Initial ultrasonic study on different types of insulator materials

The purpose of this experiment was to examine whether the developed ultrasonic system (sub-MHz ultrasound) could be applied to the materials that are often used as an insulator. The three most common insulation materials of Figure 7.1 (glass foam ("Foamglass"), polyurethane foam and fiberglass wool ("Rockwool") were tested, as shown in Figure 7.2. These materials are known as not being ultrasonic-friendly because of their shape and condition (e.g. Rockwool has many air gaps with a multi-layered structure). They have been tested to see if the ultrasonic signal from our developed system can penetrate such materials by working on certain parameters, such as ultrasonic velocity that in turn can be associated water ingress. In addition, corrosion and severe pitting of the pipe could possibly be detected by a change in path length for reflection from the outer surface of the carrier pipe. An experiment was thus conducted using a pair of piezo-composite transducers with a central frequency of 170 kHz and a chirp with a 200 kHz bandwidth. Figure 7.2 shows these three materials under test (using through transmission mode), together with the corresponding pulse compression output. From the results, it was possible to estimate the ultrasonic velocity of each material. The velocities within polyurethane foam, fiberglass foam and fiberglass wool was found to be 508 m/s, 2,327 m/s and 340 m/s respectively. It

also can be seen that the amplitudes for every measurement vary, with the fiberglass foam gave the highest amplitude and followed by the polyurethane foam (about 25% of the amplitude of the fiberglass foam) and fiberglass wool gave the lowest amplitude among them (1% of the amplitude of fiberglass foam materials).

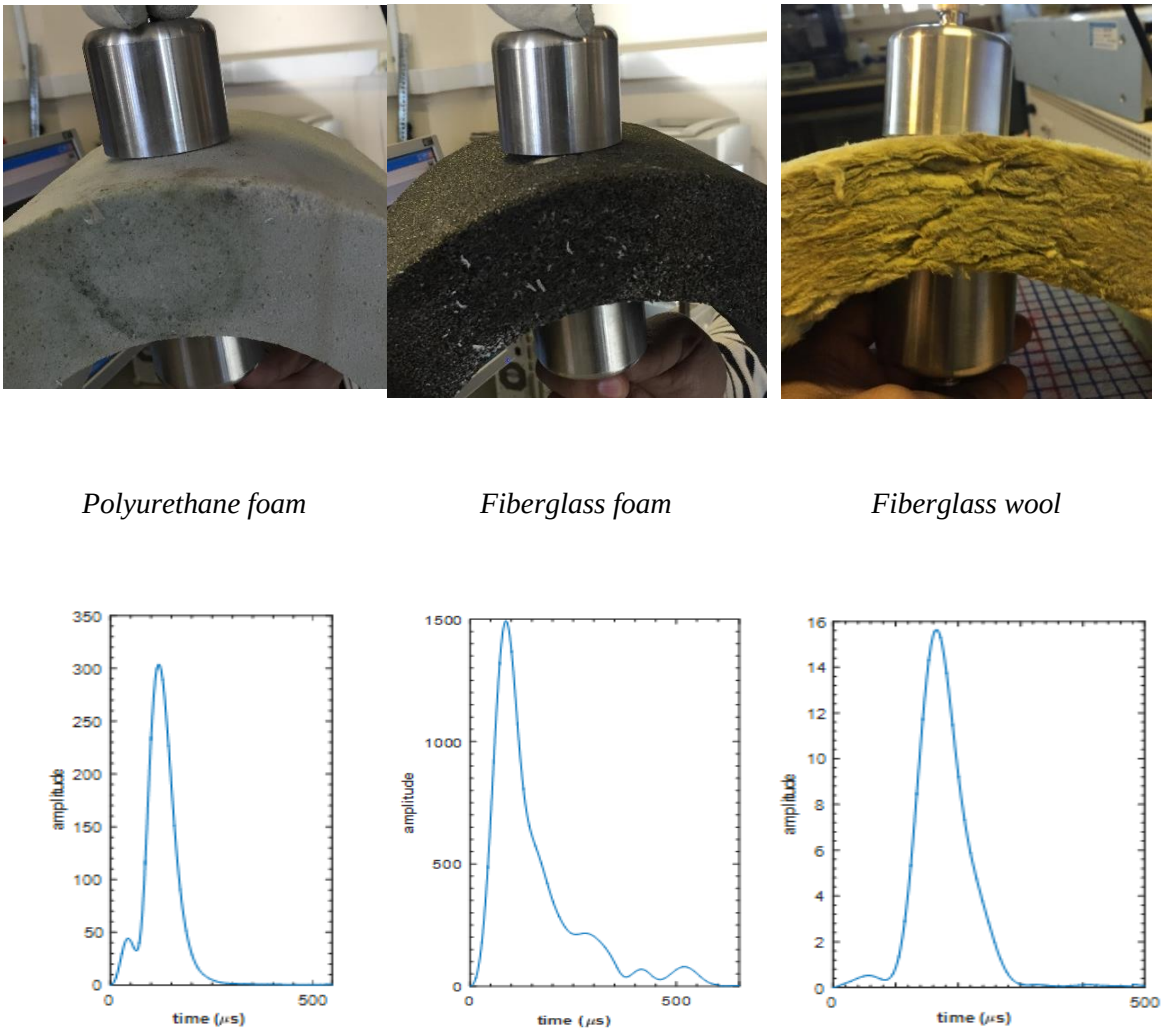

Figure 7.2 Top: the insulator samples and how the through transmission tests have been conducted; bottom: the signal acquired from the through- transmission test

It can be seen from Figure 7.2 that signals with a good SNR could be obtained in all three materials. In addition, expanded polystyrene was also tested, and shown to have even better transmission (being less porous and scattering than the three other materials.

7.2.3 The effect of water ingress

One of the common problems in insulated pipework is the corrosion of the carrier pipe due to water ingress. This can occur not only around the area that has a leakage in the outer pipe, but also at other locations such as low points or bends in pipework, where water can tend to accumulate. Under these conditions, significant corrosion can occur, and it is important not only to detect the presence of water, but also to try and measure whether significant wall thinning of the carrier pipe has occurred. Therefore, a study was conducted to examine whether the ultrasonic signal could be used to detect any difference if moisture was present within the insulator material. For this purpose, a portion of fiberglass wool with a thickness about 22 mm was submerging in water until it became saturated. Then, ultrasonic testing was conducted on the insulator as it dried out. The measurement was carried out as shown in Figure 7.3 and the pulse compression output recorded at intervals of 20 minutes as the material gradually dried out.

Figure 7.3: A 22 mm fiberglass wool sample under test as it dried, after being submerged in water.

The results of this experiment are displayed in Figure 7.4, where a graph of velocity vs time has been plotted. From the graph, it can be clearly seen that the velocity decreased linearly with time as the insulation material become dryer. From the results above, it is known that the sound velocity of the material is 340 m/s (slightly higher than the velocity of sound in air (330 m/s)) and when it fully wet the velocity has increased to over 900 m/s (as the velocity in water is 1,480 m/s). This is because water has replaced air within the highly porous structure. This condition can be utilized in the future to determine the moisture content in the insulator, which could indicate water leakage into the piping system.

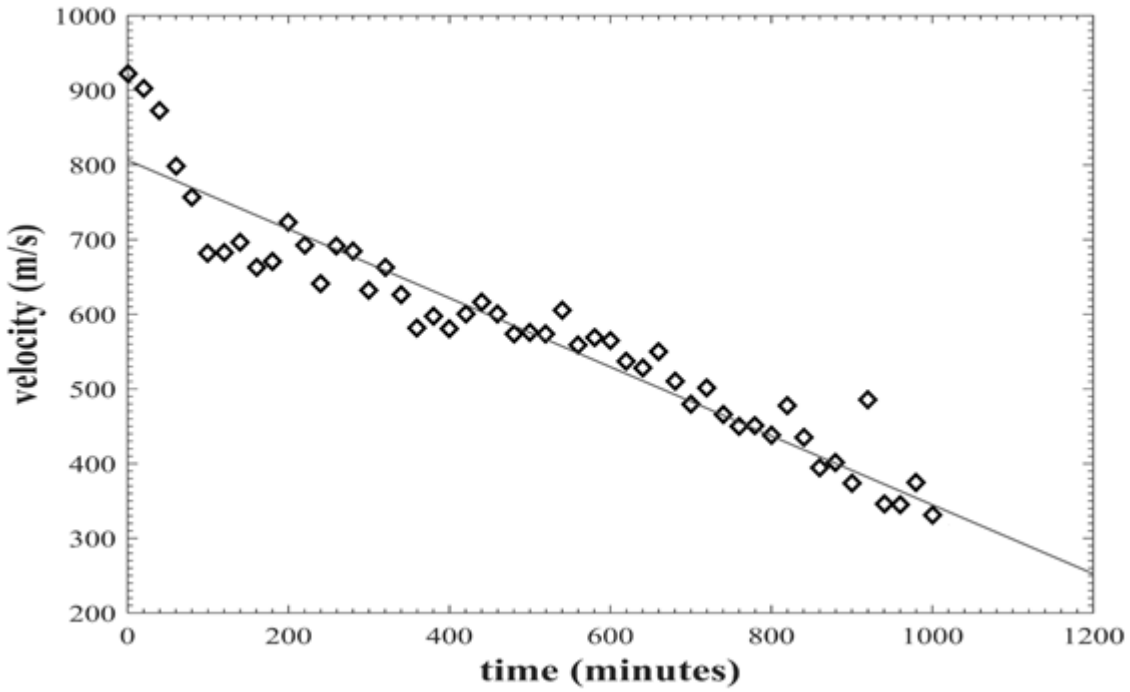

Figure 7.4: Graph velocity vs time for 1,000 minutes of measurement after the fibreglass wool sample submerged in the water

It is also possible to detect when the external shape of the carrier pipe has changed, as for example when severe corrosion has caused pitting of the surface. To simulate this, an experiment was performed on a flat metal plate, covered in insulating material, which contained few steps of flat-bottomed hole of 5 mm intervals as in the technical drawing in Figure 7.5 (a). and the real plate is shows in the Figure 7.5 (b). The groove was fully filled with water before the insulator material, which is an extended polystyrene (Figure 7.5 (c)) was placed on top of the metal plate. A transducer pair was used in pitch-catch mode (as in the previous experiments on the concrete samples), and scanned over the top surface of the insulator at 5 different locations as marked in the Figure 7.5 (c). Noting that all 5 scan locations are with different depths.

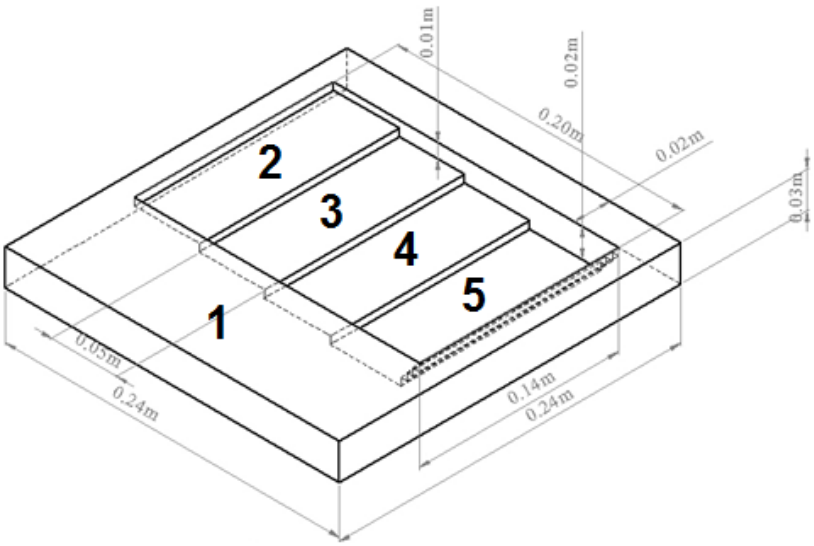

(a)

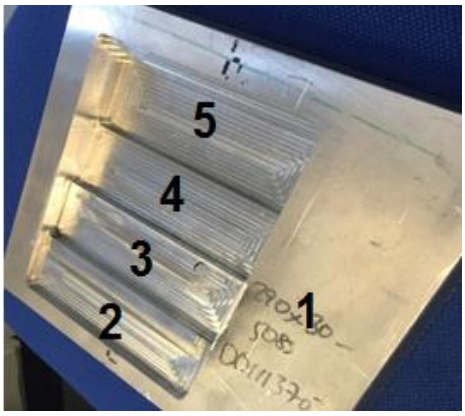

(b)

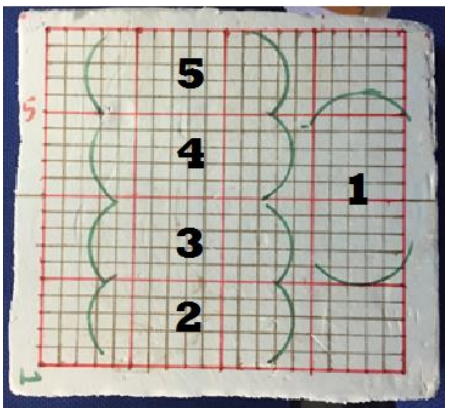

(c)

(d)

Figure 7.5: (a) technical drawing of the metal block with the details measurement ;(b) photograph of the Aluminum block; (c) the insulator sample with 5 scanning locations; (d) experimental set-up

Figure 7.6 shows the waveforms of three different locations starting with Figure 7.6 (a) is the waveform over a normal surface, (b) and (c) when the transducer pair was positioned over the location 2 and 3 respectively. It can be seen from the pulse compression output that there was a change in arrival time due to the increased path length. The 1st peaks of all the waveforms are static at the same arrival time indicated that they are represent the 1st interface between the layer or the back wall echo of the insulator. The 2nd peaks of all three waveforms show that they were moved toward the right indicated that the 2nd interface were changed as the depth of the steps are deepened. Note that the signal must have travelled through the water into the hole, and back again, noting that the insulation materials are often of low density with a sound velocity in the case of extended polystyrene was close to that of water.

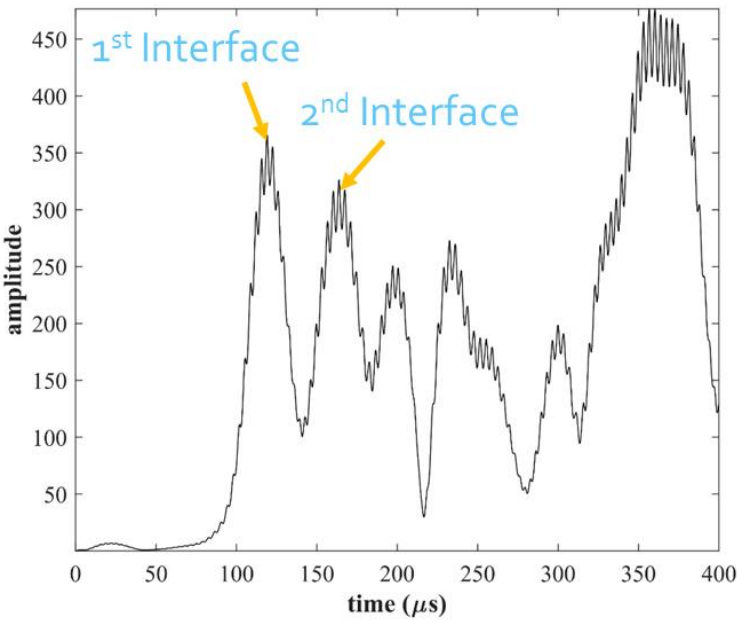

(a)

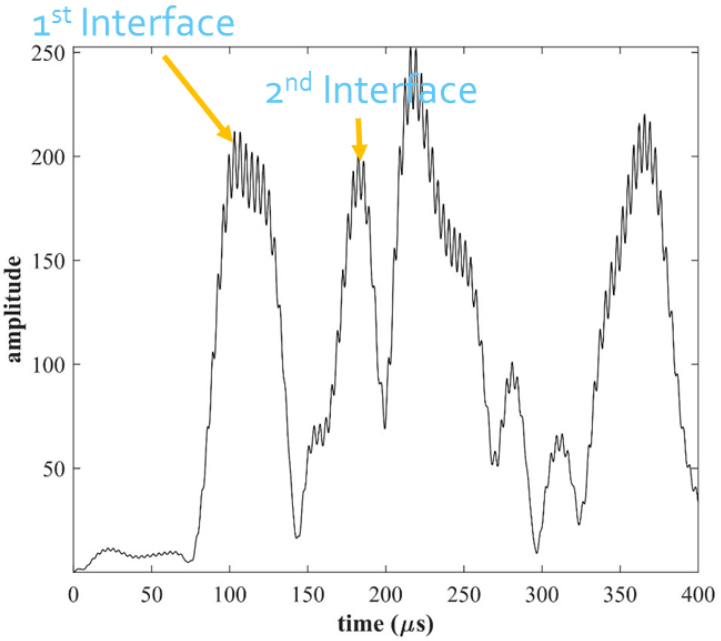

(b)

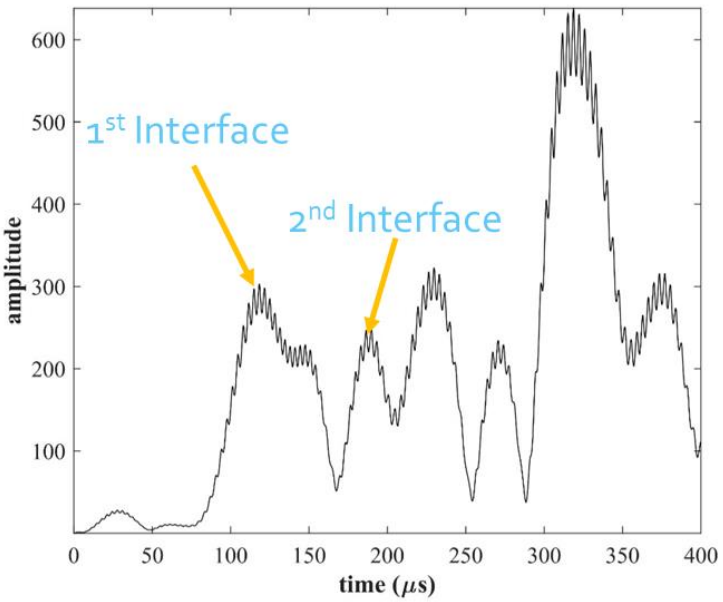

(c)

Figure 7.6: waveforms of three different locations (a) normal surface at location 1; (b) location 2 (c) location 3. All the waveforms are showing the changes of peak 2 with the movement of the scanning location

Figure 7.7 shows the plotted graph of all 5 scanning points. It shows that all 5 scans indicated that time of flight changed with the changes of the depths. It proved that the

developed system is capable of detecting the changes under the insulating material that is very important in performing detecting any anomalies (especially corrosions) under insulation in piping system. Figure 7.7 also shows the result of experiment with air as the gap between the insulator and the metal plate. It can be seen that the same trend (with the time of flight shifted) as the experiment of water was recorded. It strengthened the trust the system will be beneficial in performing testing on insulated pipe that it is also capable of detecting the changes in medium under insulator that can be related to the appearance of moisture under the material.

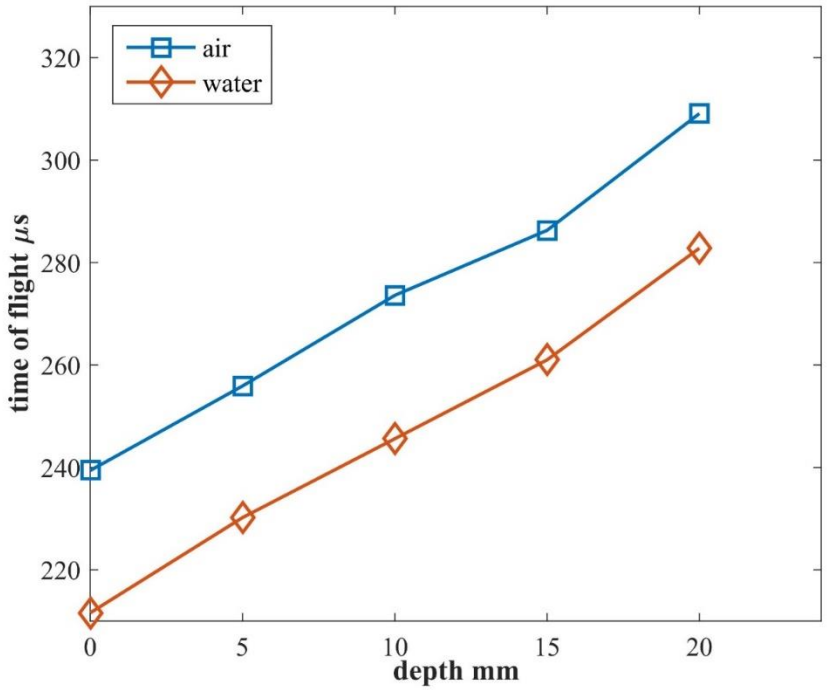

Figure 7.7: graph of time of flight over depth (location) at five location points for water and air as the medium in the metal groove

7.3 Multi-layered composites

7.3.1 Background

Composite materials are widely used in the manufacture of marine and aerospace structures. In some cases, composites are formed in combination with other materials and also layered in thick sections (multi-layered structure) that can improve their properties even more. Multi-layered composites are widely used in the aerospace industry because these types of structures typically have strong physical properties but light in weight that make it very suitable for this application. Although the combination of several layers of material bonded together can enhance the strength of the resulting structure, there are also disadvantages because the integrity of the structure is very difficult to determine. In this situation, conventional NDT methods such as radiography and thermography have been used to verify the internal structure but these techniques have some limitations [19-21]. Ultrasonic testing can be difficult to apply on these materials because of the high attenuation and scattering that can occur in thick, multi-layered industrial samples. However, ultrasonic testing can offer an option for the NDT practitioners as it is a non-ionizing technique.

This section will demonstrate that low-frequency ultrasound in the region of 100-400 kHz has been utilized over a wide bandwidth for testing reasonably thick, multi-layered structures. It is shown that by reducing the frequency of ultrasonic testing, improving bandwidth and using advanced signal processing techniques, a good trade-off can be obtained to overcome the signal attenuation while maintaining a reasonable resolution. The combination of sub-MHz ultrasonic frequencies with pulse compression signal processing technique and the use of coded signals in performing the inspection on this multi-layered structure will be explained below.

The structure to be tested was part of a cowling used to surround the engines of a large passenger aircraft. It has a multi-layer structure which contained glass fibre, carbon fibre and metal honeycomb layers. A photograph of such a structure is shown in Figure 7.8. The inner layer is a conformal layer which sits next to the fan blade tip to form a seal. This is then surrounded by other layers, which aim to be strong and lightweight, but also able to contain the blade in case of failure. Tests were performed in both pitch-catch and through-transmission modes, initially on individual layers of the composite, and then on the full structure. The aim was the detection of artificial defects.

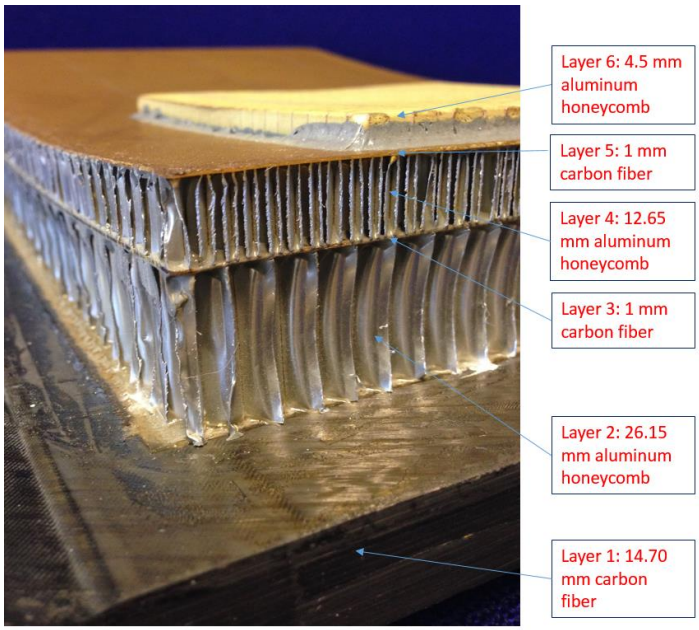

Figure 7.8: Photograph of a section of composite engine cowling, with the inner surface at the top. Each layer is identified as shown.

7.3.2 Testing of sub-structures within the multilayered composite structure

The multilayered structure that was tested is a part of the structure that comprised of a layer of fiberglass, aluminum honeycomb layer (few layers with different thickness) and other materials that were stacked together to form a very strong and lightweight structure.

Before conducting the experiment on multilayered structure, a series of tests was carried out on an individual layer structure to find out whether the ultrasonic signal from the system that has been developed can penetrate these materials. The ultrasonic velocity for these materials was obtained as it is an important guide when interpreting the results for the multilayered structure.

Figure 7.9 shows a sample (Sample 1) with 2 layers: 1.5 mm of carbon fibre composite attached to 30 mm of aluminum honeycomb that has been used in the multilayered structure shown in Figure 7.8. This sample has been tested using the ultrasonic system with piezo-composite transducers at a 250 kHz center frequency in both through-transmission and pitch-catch orientations.

Figure 7.9: Sample 1: 30 mm thick structure (28.5 mm honeycomb aluminum; 1.5 mm carbon fiber)

Figure 7.10(a) below shows the through transmission results in which the signal is cleaner and less noise as compared with the result of the pitch-catch measurement (Figure 7.10(b)) which shows that more scattering has occurred.

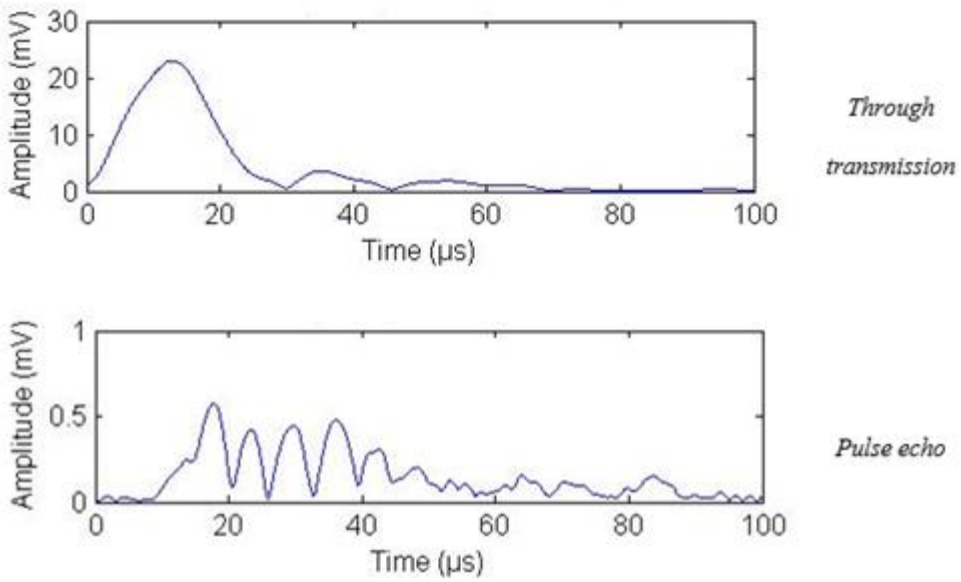

Figure 7.10: Through-transmission and pitch-catch pulse compression results for Sample 1

Figure 7.11 shows another sample (Sample 2) with 3 layers - 1.5 mm carbon fiber; 35 mm honeycomb aluminum; 3.5 mm aluminum plate) and in this sample, there is a 15 mm diameter hole (Figure 7.11-back side)

Side view *Front side* *Back side*

Figure 7.11: Structure of Sample 2 with three layers of different types of material stuck together; 40mm thick structure (1.5 mm carbon fiber; 35 mm honeycomb aluminum; 3.5 mm Aluminum plate

Figure 7.12 shows that the result from the through transmission is almost similar to the result of Sample 1. However, in Figure 7.12 (Pulse echo-defect), there are some changes noted on the signal that is believed to be corresponded to the defect but not clearly seen. Further analysis has to be carried out in order to identify the position of the defect and lamination.

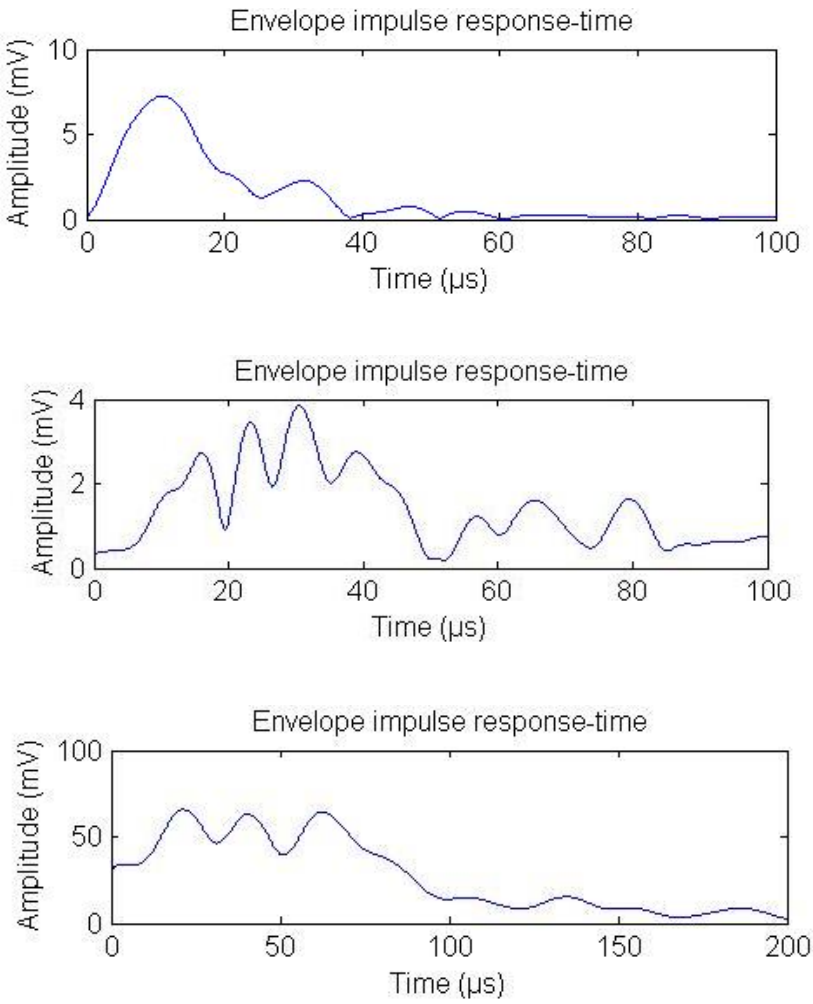

Through-transmission

Pitch-catch

Pitch-catch over the defect

Figure 7.12: The through transmission and pulse echo of pulse compression results for Sample 2.

Finally, an experiment was carried out on a thick carbon fiber plate that has been used as the outer layer of the multi-layered structure shown earlier in Figure 7.5. This is to obtain a signal that travels in this material alone and can be used to estimate the sound

velocity in this material. It can be a guide in the interpretation when examining the whole multilayered structure later. Figure 7.12 shows the through transmission test and pulse echo mode conducted on the carbon fiber layer.

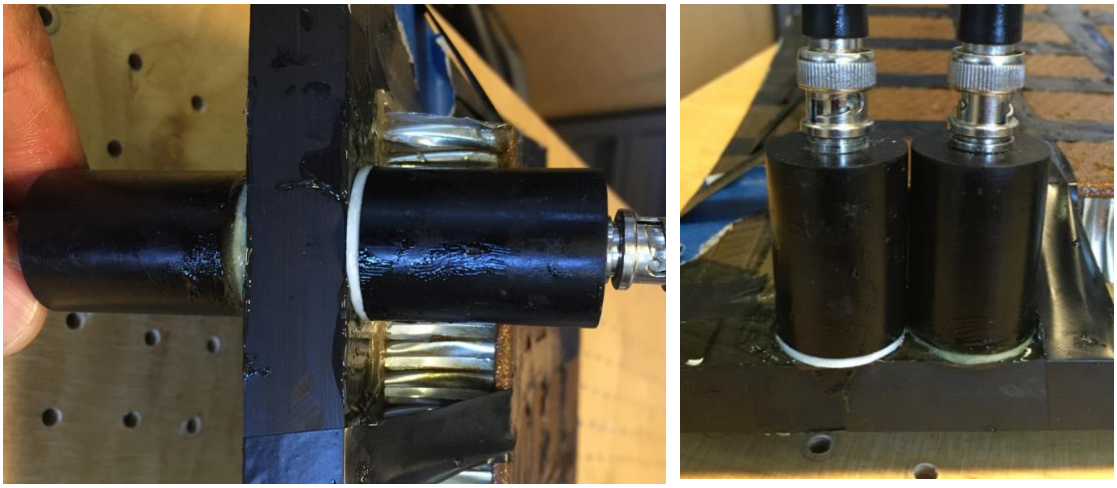

Figure 7.13: Through transmission (left) and pitch-catch (right) tests conducted on the carbon fiber layer

The results in Figure 7.14 shows that signal travel from the through-transmission mode is approximately 2.2 μs for carbon fiber layer with 14.70 mm thickness. Therefore, the estimated velocity is around 6,681m/s. The results of these tests can be compared with later measurement of the multilayered structure as a guidance in the interpretation of the results.

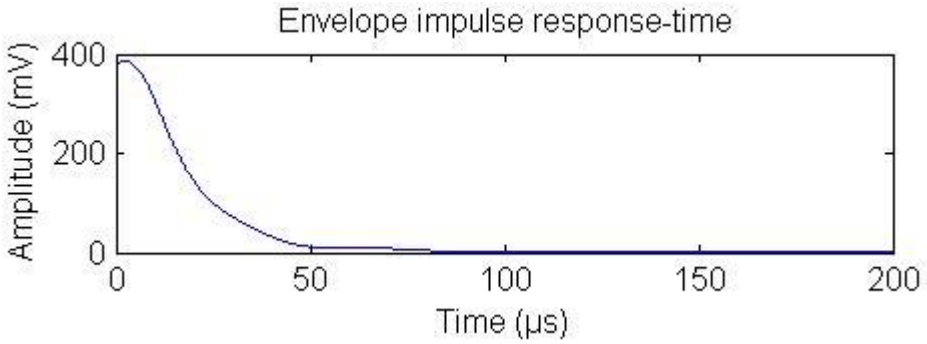

(a)

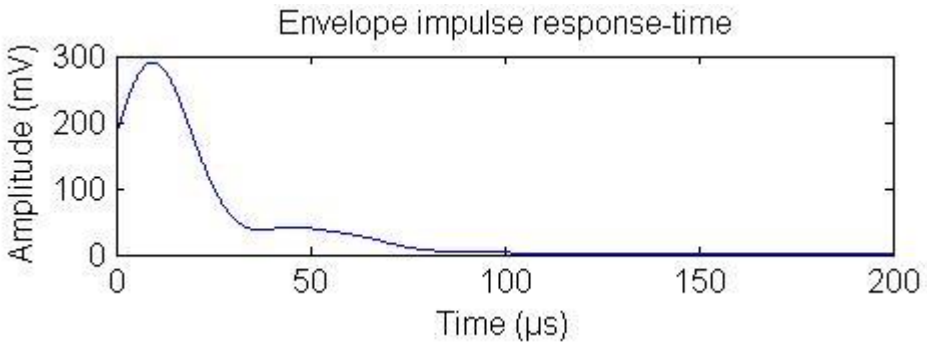

(b)

Figure 7.14: Results of through-transmission (top) and pitch-catch tests in the thick carbon fibre sample.

7.3.3 Tests on the full structure

In the experiment on the full multilayered structure (Figure 7.5), the input drive signal was a 5 ms standard linear chirp from 100 to 400 kHz. The sample surface was marked with locations divided into 3 columns (A, B, and C) and 5 rows (1, 2, 3, 4, and 5). Both the inner and outer surface of the sample were identified as shown in the Figure 7.15. The transducers were placed in through-transmission mode by placing the receiver transducer on the inner surface and the transmitter on the corresponding area on the outer one. Measurements were taken at each of the 15 individual areas (Figure 7.15). Next, a pitch-catch configuration with another 15 measurements was conducted again in the same area as above on the inner side of the sample. Because of the asymmetry of the structure, the pitch-catch measurement was also repeated in the outer surface. In total, 45 recorded measurements were taken. As can be seen in Figure 7.15 (inner side), there is an additional composite layer in a small portion (4.5 mm thickness) located at B4 and B5 in the grid.

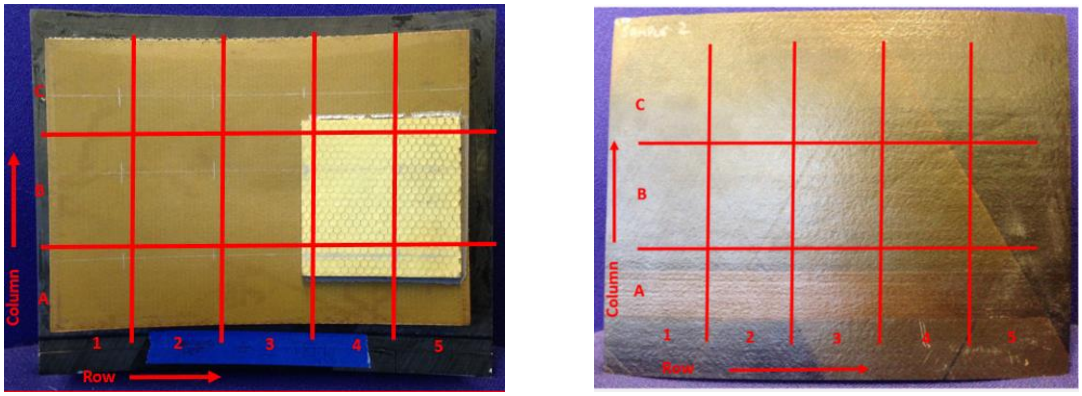

Inner side *Outer side*

Figure 7.15: photograph image of the sample for the (a) inner surface, (b) outer surface with boths images showing the scanning location of 15 points.

A. Through-transmission tests

A typical pulse compression output result for through-transmission is shown in Figure 7.16. The first large peak at around 11μs corresponds to the direct path through the sample. The whole thickness of the structure is 60 mm, which means the average velocity for the whole lump of the multi-layered structure is approximately 5,455 m/s. The smaller peak that appears around 31 μs corresponds to the secondary back wall echo and so another peak raised at around 45 μs can be correlated as the 3rd reflection echo though it's a bit slower than what it should be. However, the focus is on intermediate peaks (first and second peak), which should correspond to reflections occurring at the interface between different layers and the probability to detect if there are any delamination between the layers.

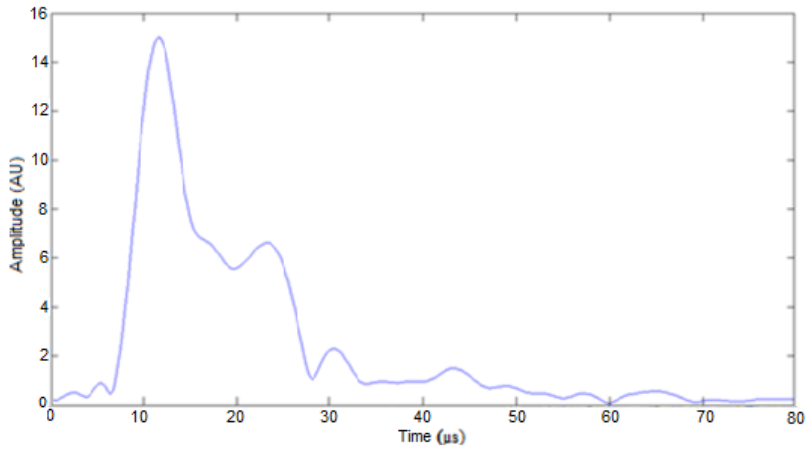

Figure 7.16: Typical through-transmission pulse compression output.

The pulse compression normalized outputs for all 15 positions are superimposed and shows in Figure 7.17. It can be noted that the first peak of every measurement was consistent at around 11 µs. The amplitudes of the peaks (first peaks) show some variations that can correspond to the inconsistency of the coupling during the measurement by which the surface structure is not so smooth and quite rough. Positions for B4, B5, C2, and C5 show that there is an additional clear peak at around 17.75 µs. Most of the positions show a peak around 21 µs, except B1, B3, C1, and C2 where there is no recognizable peak, though that is probably due to it being relatively small and simply being buried in the slope of the neighbouring peaks. There are also significant variations in the frequency spectrum for the different measurement points, but interpreting the spectrum is even more complicated than with the time domain information.

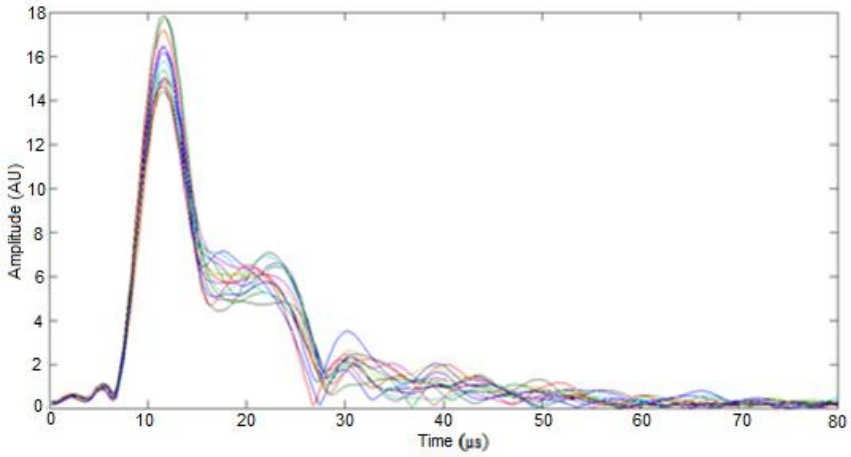

Figure 7.17: All through- transmission plots superimposed

Figure 7.18 illustrates the differences in amplitudes of the first three peaks for all 15 measurements corresponding to their locations. From Figure 7.18(a), it can be concluded that the value of the amplitude of the row A and row C is quite consistent with almost the same amplitude value were recorded. But there are variations in row B that can be attributed to a small 4.5 thickness honeycomb layer at position B4 and B5.

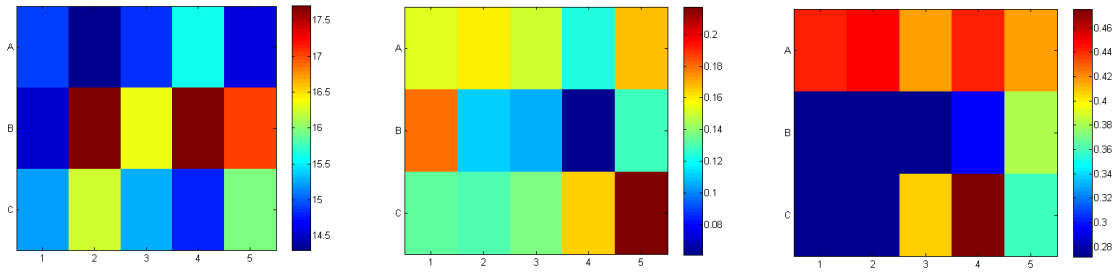

(a) *(b)* *(c)*

Figure 7.18: Normalized amplitude of initial peak (11 µs) and relative amplitudes of peaks near 21 µs and 30 µs

B. Pitch-catch measurements

The signals are now more complicated as compared to the through transmission mode, due to multiple reflections from the different interfaces before the reflection from the back surface. Measurements were carried out on both sides of the surface (inner and outer surface) and the result for both are displayed in Figure 7.19(a) and Figure 7.19(b). Comparison of the initial measurements that were carried out on the inner surface has produced a result with higher noise than the measurement of the outer surface. From the through transmission result, the time of flight (TOF) is around 11 μs, so the TOF from the pulse echo measurement is supposed to be at least 22 μs or slower because of the multi-layered materials with different acoustic impedances that can slower down the TOF. From Figure 7.19(a), it can be noted that there are several peaks detected before 22 μs, which likely corresponds from the reflection of the different interfaces in the structure. But the interpretation of the result is not easy because there are too many parameters and factors to be considered. The result in Figure 7.19(b), it somewhat less complicated as compared to the one measured from the inner side.

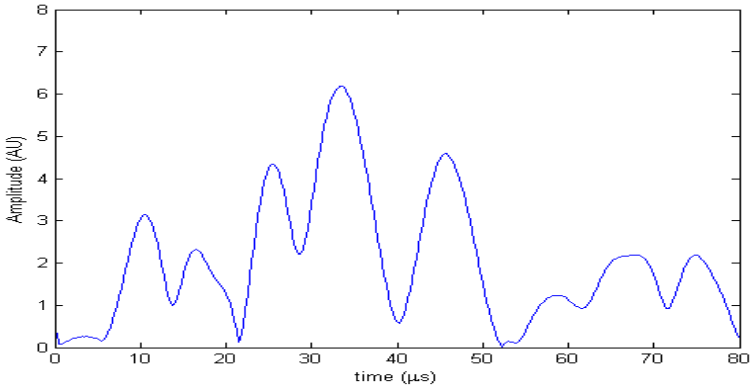

(a)

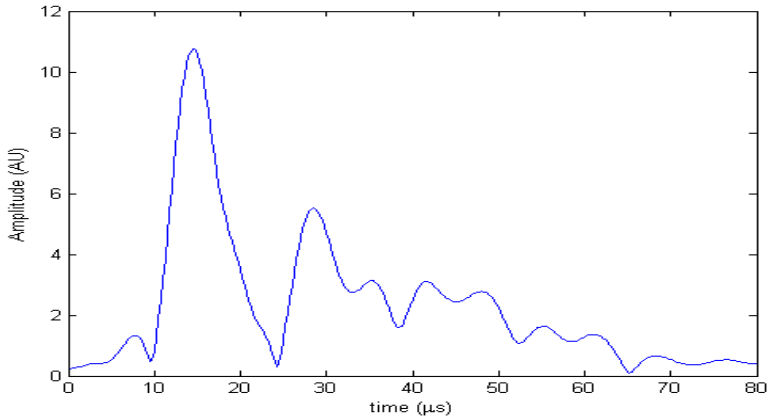

(b)

Figure 7.19: Typical pulse echo pulse compression signals from inner surface

Figure 7.20 shows the superimposed result of normalized pulse compression outputs for all 15 positions. When measuring from the outer surface (Figure 7.20(b)), the signal appears to be dominated by the reflection from the first layer which is the carbon fiber - honeycomb interface, and this could well mask reflections later because the amplitude is very high as compared to other peaks. If compared the measurements carried out on the inner and outer side, the outer side shows better consistency. Nevertheless, the measurement of the outer side less effective because most of the energy reflected within the carbon fibre layer since the difference in impedance between the layers of multi-layered structure. It is difficult to carry out direct interpretation because it is too complicated as the process involves many layers with different impedance values.

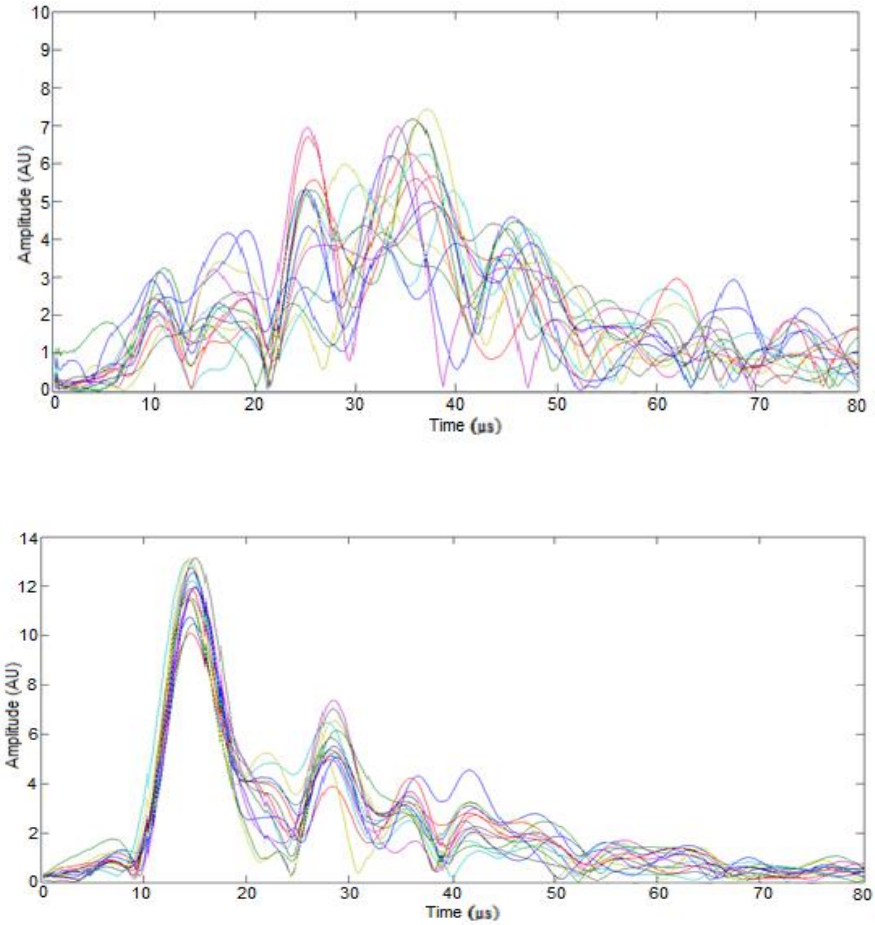

Figure 7.20: Superimposed results of normalized pulse compression output for all sample positions; (a) inner surface; (b) outer surface

The results of the above measurements have also been displayed in another format to facilitate the interpretation process. Figure 7.21(a) shows a portion of the sample was scanned (row B) via through-transmission mode and the result (in the form of cross-correlation envelope) are displayed in the form of a cascade plot represents all five rows in the column as in Figure 7.21(b). It can be seen that at the location B4 and B5 the peaks have raised at a later timescale which represents the differences in the thickness as compared to the other location on the grid.

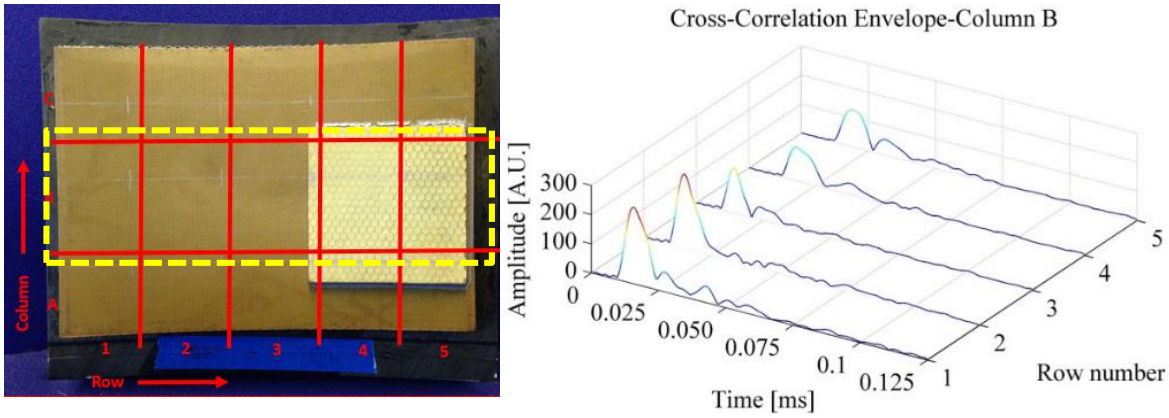

(a) *(b)*

Figure 7.21: Yellow box in dash shows the corresponding column B; on the right is the result (cascade plot) for column B

Figure 7.22 shows a complete comparison of through-transmission measurement of three columns (A, B, C) for all 15 measurements (corresponded to Figure 7.21(a)). To the left in each case are the time waveforms, and to the right are the corresponding frequency spectrum. Results show that most of the measurements give almost similar TOF value for all measurements, with an exception for B4 and B5 where the TOF arrived at the later time which corresponded to the extra layer presence at this location. It can be concluded that the ultrasonic signal that has been generated has a high probability of penetrating the material in this test but the scattering is very high due to the different of the impedance of different layers of materials.

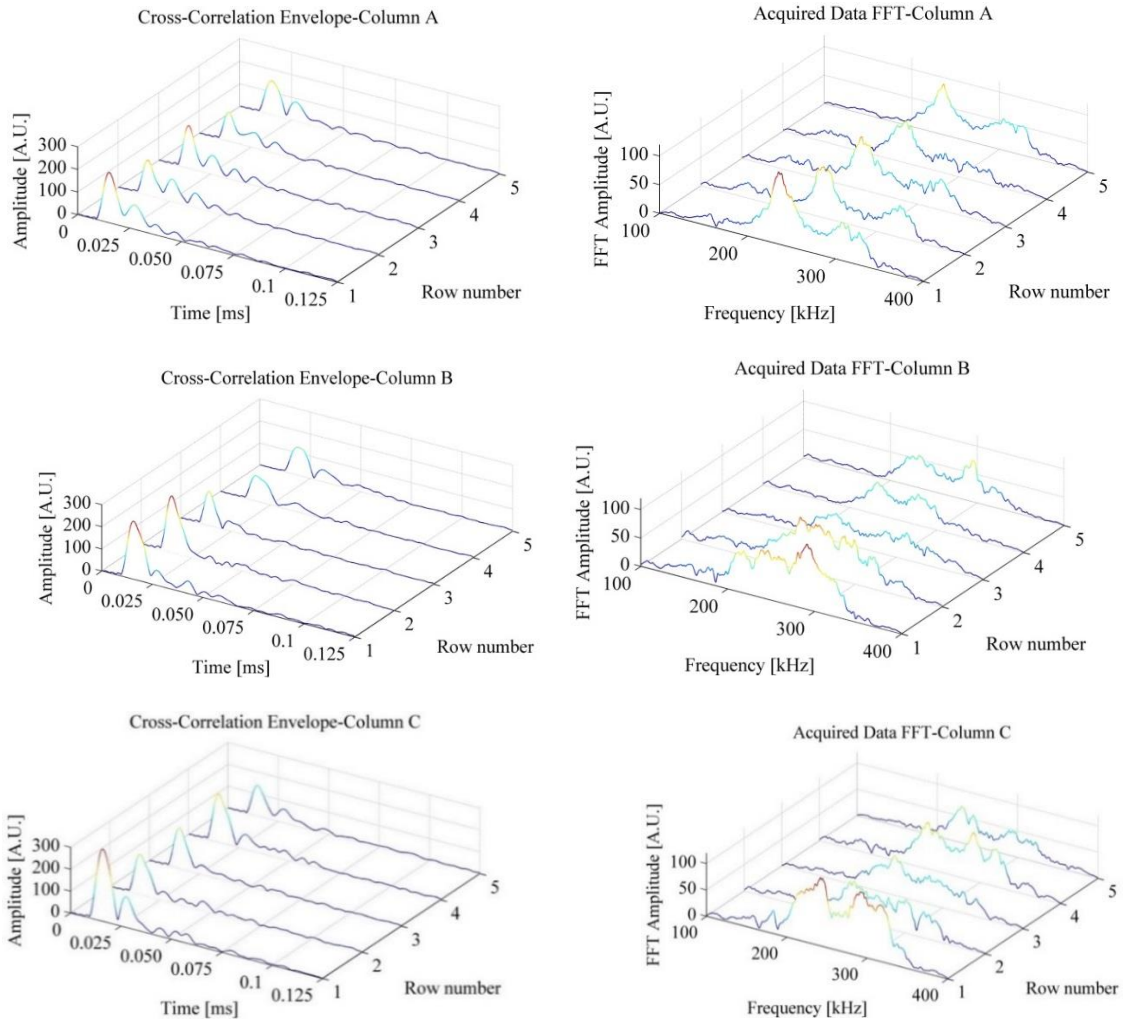

Figure 7.22: Through-transmission data for sample 1, showing time waveforms (left) and frequency spectra (right for each location with the pulse-echo transducer on the outer surface of the sample

Figure 7.23 shows a complete comparison of the three column (A, B, C) for the row that has been tested correspond to Figure 17.11(inner side) for pulse echo mode (pitch-catch). The result shows that the measurement in column A, the result obtained is somewhat random when compared to the five rows, even if the amplitude of row 2 and row 3 is higher than the rest. But in terms of frequency response measurement of the five have given the frequency range that is almost evenly at around 200 kHz to 300 kHz, although there are some variations in amplitudes. For Column B, it can be concluded that they reflect the

presence of a thin layer of honeycomb sat on the top (inner side) where the timescale on the location, especially on a short B5 shows TOF compared with the rest.

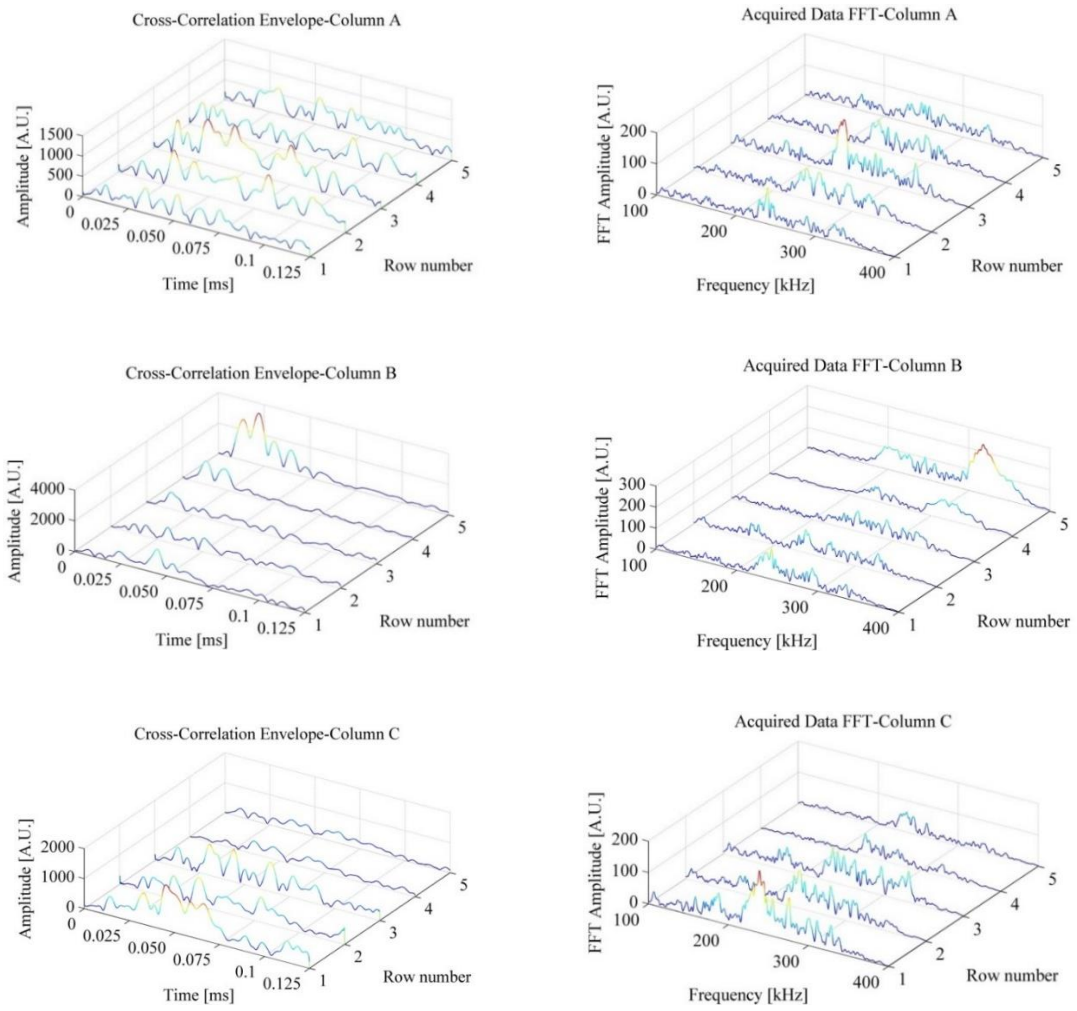

Figure 7.23: Pitch-catch data for sample 1, showing time waveforms (left) and frequency spectra (right for each location with the pulse-echo transducer on the inner surface of the sample

Figure 7.24 shows a complete comparison of the three column (A, B, C) for the row that has been tested correspond to Figure 7.15(outer side) for pulse echo mode (pitch-catch). The displayed results are in agreement with what has been discussed at the result in Figure 7.19 (b) and Figure 7.20 (b) where the signal appears to be dominated by the reflection from the first layer (carbon fibre) which could well mask the other reflections later because the amplitude is very high as compared to others.

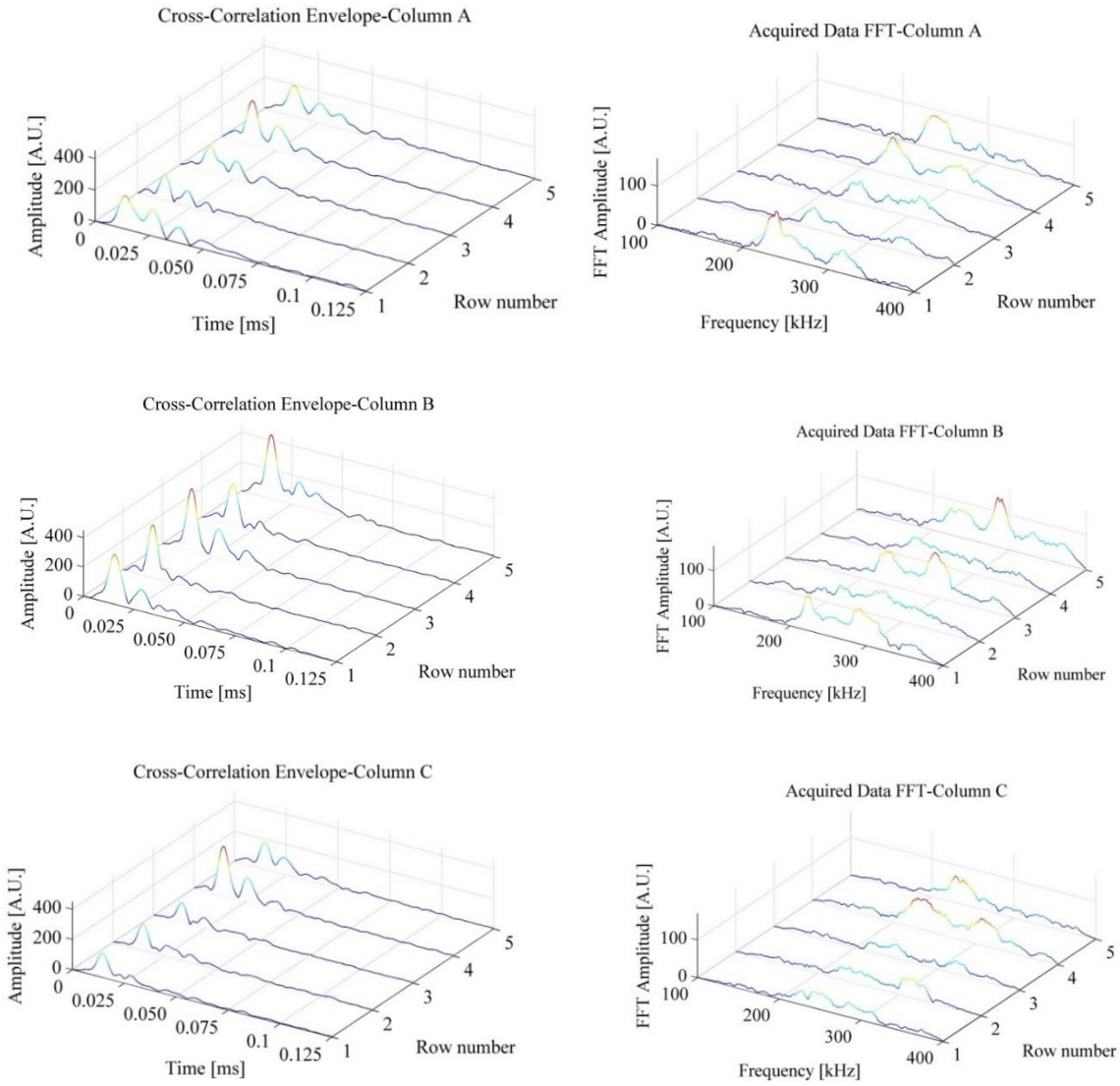

Figure 7.24: Pitch-catch data for Sample 1, showing time waveforms (left) and frequency spectra (right for each location with the pulse-echo transducer on the outer surface of the sample

7.4 Conclusions

The above results indicate that the pulse-compression system with piezo-composite transducers has successfully transmitted signals through both individual layers and the full thickness structure. The response in through-transmission was simpler than that from pitch-catch from one surface, but the response from the inner and outer surfaces was very different. This is because of the location of each layer that makes up the full structure.

Multiple peaks in the time and frequency plots indicated a complicated set of reflections within the structure. From these, it should be possible to identify defects at the interfaces between the separate layers. This was not taken further in this research. It is suggested that a computer model be performed, so that the origin of each peak in the response can be identified. Then, changes in this can be monitored.

References

[1] R. Sicard, J. Goyette, and D. Zellouf, "A SAFT algorithm for lamb wave imaging of isotropic plate-like structures," *Ultrasonics*, vol. 39, pp. 487–494, 2002.

[2] D. P. Gianettino, "Inspecting Pipe Radiographically Through Asbestos Insulation," *NASA Tech Briefs*, no. February, p. 50, 1994.

[3] M. V. Lurie, *Modeling of Oil Product and Gas Pipeline Transportation*. 2009.

[4] T. Pootakham and A. Kumar, "A comparison of pipeline versus truck transport of bio-oil," *Bioresour. Technol.*, vol. 101, no. 1, pp. 414–421, 2010.

[5] O. Refineries, "Oil And Gas Infrastructure," *Qatar Oil Gas Rep.*, vol. Q2 2010, no. November 2009, pp. 53–56, 2010.

[6] E. G. Hammerschmidt, "Formation of gas hydrates in natural gas transmission lines," *Ind. Eng. Chem.*, vol. 26, no. 8, pp. 851–855, 1934.

[7] M. Economides, K. Sun, and G. Subero, "Compressed Natural Gas (CNG): An Alternative to Liquefied Natural Gas (LNG)," *SPE Prod. Oper.*, vol. 21, no. 2, pp. 318–324, 2006.

[8] H. Wang and I. J. Duncan, "Understanding the nature of risks associated with onshore natural gas gathering pipelines," *J. Loss Prev. Process Ind.*, vol. 29, no. 1, pp. 49–55, 2014.

[9] B. Guo, S. Song, A. Ghalambor, and T. R. Lin, "Chapter 9 - Pipeline Insulation," in *Offshore Pipelines (Second Edition)*, 2014, pp. 113–124.

[10] R. Strapasson, S. C. Amico, M. F. R. Pereira, and T. H. D. Sydenstricker, "Tensile

and impact behavior of polypropylene/low density polyethylene blends," *Polym. Test.*, vol. 24, no. 4, pp. 468–473, 2005.

[11] E. Ranzi, M. Dente, T. Faravelli, G. Bozzano, S. Fabini, R. Nava, V. Cozzani, and L. Tognotti, "Kinetic modeling of polyethylene and polypropylene thermal degradation," *J. Anal. Appl. Pyrolysis*, vol. 40–41, pp. 305–319, 1997.

[12] N. Sarier and E. Onder, "Thermal characteristics of polyurethane foams incorporated with phase change materials," *Thermochim. Acta*, vol. 454, no. 2, pp. 90–98, 2007.

[13] M. Hausner and M. Dixon, "Optimized Design of Pipe-in-Pipe Systems," *SPE Prod. Facil.*, vol. 19, no. 1, pp. 1–13, 2004.

[14] P. A. Fokaides and A. M. Papadopoulos, "Cost-optimal insulation thickness in dry and mesothermal climates: Existing models and their improvement," *Energy Build.*, vol. 68, no. PARTA, pp. 203–212, 2014.

[15] O. Kaynakli, "Economic thermal insulation thickness for pipes and ducts: A review study," *Renewable and Sustainable Energy Reviews*, vol. 30. pp. 184–194, 2014.

[16] A. Keçebaş, "Determination of insulation thickness by means of exergy analysis in pipe insulation," *Energy Convers. Manag.*, vol. 58, pp. 76–83, 2012.

[17] M. N. Ilman, "Analysis of internal corrosion in subsea oil pipeline," *Case Stud. Eng. Fail. Anal.*, vol. 2, no. 1, pp. 1–8, 2014.

[18] S. Nicola, V. Carreto, R. A. Mentzer, and M. S. Mannan, "Corrosion Under Insulation Detection Technique," in *NACE*, 2013, no. 2570, p. 2570.

[19] R. J. Dewhurst, "Review of Progress in Quantitative Nondestructive Evaluation," *Opt. Acta Int. J. Opt.*, vol. 32, no. 7, pp. 747–747, 1985.

[20] I. G. Scott and C. M. Scala, "A review of non-destructive testing of composite materials," *NDT Int.*, vol. 15, no. April, pp. 75–86, 1982.

[21] S. K. Verma, S. S. Bhadauria, and S. Akhtar, "Review of Nondestructive Testing Methods for Condition Monitoring of Concrete Structures," vol. 2013, no. 2008, 2013.

Chapter 8

Conclusions and Future Works

8.1 General Conclusions

This thesis was originally focused on solving problems in carrying out ultrasonic testing of samples or materials with high degree of attenuation. Materials such as multilayered composites, polymers, concrete and large and thick structures are often problematic when to be tested for NDT, especially by using ultrasonic testing. An ultrasonic system that is capable of examining those materials with high degree of attenuation has been developed during this study. The system is utilizing Sub-MHz frequency ultrasound that could reduce the attenuation and scattering effect especially when performing experiments on high attenuation materials. The system that equipped with piezo-composite transducers that are capable of producing broader bandwidth at lower frequency. The coded waveforms that were used in conjunction with pulse compression technique, gave the advantage to the system over other conventional techniques.

Chapter 1 started by describing some basic background of ultrasonic wave propagation and discussion on the basic properties of sound, such as transmission mechanisms through a medium, absorption, attenuation, propagation across the interface, beam spread and mode conversion. There are also some explanations on ultrasonic transducer design and piezoelectric materials.

Chapter 2 discussed in details the overview of ultrasonic testing of highly attenuation materials. It started with a brief discussion on propagation of ultrasonic signals in high attenuation materials and followed by review of attenuation and scattering mechanism that are very important elements in this study. Chapter 2 also covered some typical materials of

interest that have been used throughout this study such as polymer based materials, concrete materials as well as multi-layered composite structure. Materials such as composites, polymers, concrete and large components present challenges when tested using ultrasonic techniques. The study was focused on the production of an ultrasonic system for use on materials that have a high attenuation such as polymer, concrete, composite multi-layered and bulky material. It has emphasised on the use of ultrasonic low frequency ultrasound below the MHz range. The work was devoted to the use of piezo composite transducers and was combined with coded waveforms such as chirps and bipolar Golay that provided advantages when used in conjunction with cross correlation techniques of signal procession. In addition, other signal processing and image reconstruction technique was also exploited. All data and results obtained from this experiment were analysed and displayed accordingly.

Chapter 3 described the design of the experimental system that has been the backbone of this research. Among the content were the discussion about ultrasonic coded signal such as frequency modulated chirps and the binary sequences that include Golay complementary sequences. There was also some overview on signal clipping and how vital this effect on the experimental results. Signal processing techniques such as Pulse Compression (PuC) and the synthetic aperture focusing technique (SAFT) were also discussed in this chapter. In addition, the relationship between the signal, its frequency spectrum, the effect of signal clipping on the results and the use of windowing was described. The Chapter that follows explained how these concepts were applied in actual NDE experiments.

Chapter 4 contained a description of the developed system that was specifically established to deal with attenuating materials. It covered both the hardware and the software that have been used within the system as well as the way they have been integrated together. It has been discussed how the coded signal in conjunction with pulse compression technique

can improve signal to noise ratio of the testing result. There was some discussion about the calibration of the system and the signal processing that had took part in the latter stage of the chapter.

This system, which used sub-MHz ultrasonic frequencies, was designed to improve penetration ability, which is a major problem when conducting ultrasonic testing of high attenuation samples such as concrete, multi-layered composites and thick sections of polymers. This chapter described in detail the hardware that was used within the system such as the National Instruments PXI instrumentation system and the piezocomposite transducers. This combination was an important aspect of this work – it needed the combination of bandwidth and processing to achieve the results shown in later Chapters. In addition, this chapter also discussed the software that has been developed with a research group from the University of Perugia, which is part of our research collaboration. Finally, this chapter was closed with a discussion on calibration that was used throughout this study as well as image processing techniques are also an important element contributing to the success of this system.

Chapter 5 is the first chapter that contains experimental work involving one of the industrial samples that has been used in this study, namely polyurethane polymer structure. This is an important type of material that has been used in the oil and gas industry particularly as bend stiffeners in seabed oil logging. It was demonstrated how the developed system that utilised sub-MHz frequency ultrasound can be used to detect some anomalies within the polyurethane structure. The results showed that the developed system can be used to investigate materials with high attenuation of ultrasonic signals. The experiments looked at 15 cm thick polyurethane, where the use of conventional NDT at frequencies >1 MHz would not be possible. Chirp signal and bipolar Golay have proven suitable to be used in conjunction with the PuC technique at low frequencies, where the attenuation is more

manageable. It was shown that a broad bandwidth transducer has the advantage compared to the narrow bandwidth transducer as suitable for use with Chirp and bipolar Golay codes, as bandwidth is important in PuC techniques both for assuring high SNR gain and inspection resolution.

From the experiment results, the scan images showed that this technique can be used to detect and reveal defects or flaws that are present in thick and highly-attenuating materials. It is simply a matter of how to increase the capacity in terms of signal processing and image reconstruction in order to get a more precise result, particularly in terms of sizing and locating of the defect. However, several methods of signal processing such as generation of 3-D hypercube C-Scan imaging and 3-D SAFT imaging in which SAFT has shown that it can improve the spatial resolution of the measurement.

Chapter 6 is the second chapter concerning experimental work, this time on concrete samples. The chapter began with a review on structural problems in reinforced concrete that comprises deterioration of rebars and concrete cover spalling. There was also some brief discussion on refractory brick anchors, which was an important additional material that required study. Concrete sample preparation was described, and various mixes with different aggregates prepared.

From the tests that have been carried out, it was clearly shown that the composition of the conventional concrete materials greatly affects the propagation of the ultrasonic signal. It was shown in Test 1 that not only the size of aggregate but also the ratio of other materials such as sand and cement influences the test result. The results of this test have been used as a guide in preparing some further samples which were concrete slabs containing rebar (Test 2). From the results, it shows that the developed ultrasonic system was successfully able to detect and locate the location of the rebar that was embedded within the concrete. In addition, the test results have proved that this system managed to test the

concrete thickness of 40 cm and surprisingly able to locate rebar at a depth of 10 cm using a pitch-catch mode.

The tests on the refractory brick were more challenging, due to both the highly scattering medium and shape of the samples. With the use of pulse compression and further statistical processing, provided via the collaboration with Perugia, it was shown that the developed ultrasonic system was able to detect and distinguish if there are any defect or cracks in the refractory anchor brick using a pitch-catch mode system from the top surface only. This allows the technique to be implemented by the metal forming industry, who only have access to the external wall of the furnace.

Chapter 7 involved a study of highly attenuating insulation materials and multi-layered composite structures. The experiments discussed in this chapter include some type of composites from two different industries, namely insulating materials from oil and gas industry and the multi-layered composites are widely used as an aircraft structure. It has been shown how the developed ultrasonic technique can detect some changes (presences different types of material and the difference in thickness) under the insulators that can be the answer to the detection of the corrosion under insulation (CUI) problem. Besides, it has also shown that procedures have been used to test the multi-layered honeycomb structure and the result that was obtained. Although it did not manage to provide absolute solution to the problem raised, but the initial tests were quite promising that can be a good starting point in tackling the problem that has been occur for so long.

Finally, the conclusions from the work presented in this thesis are presented in Chapter 8, together with suggestions for further works.

There are some publications that were published throughout the study. For example, the finding from Chapter 5 that involved polyurethane sample from oil and gas industry was submitted to the Non-destructive Teasing and Evaluation journal as a journal paper and the

work has also been presented in the European NDT Conference (ECNDT) in Czech Republic. The results from Chapter 6 that concerning concrete samples and refractory brick was presented in the IEEE Ultrasonic Symposium (IUS) Conference in Taiwan. A paper also will be submitted to a journal that consist of experiential result of the concrete samples as well the refractory bricks. Lastly, the results that was gained from the composites materials was presented in the World NDT Conference (WCNDT) in Munich.

8.2 Future work

The work presented in this thesis makes several noteworthy contributions that the use of ultrasound at Sub MHz frequencies is a better way to inspect materials with high degree of attenuation. It is hoped that this research will contribute in solving problem in NDT world especially in inspecting such materials.

The findings in this thesis provide the following insights for future research:

i. Construction of a portable system that is more suitable to be used at the field work which requires a smaller equipment and handy. One element that can be improved is to replace the PXI box with small and compact ultrasonic generator and data acquisition card as well as the use of smart devices (mobile gadgets) for the hardware and software integration as well as data processing.

ii. Explore further studies related to signal processing because it is an important tool in the study of high attenuation materials as often signal obtained is very weak and buried in a lot of noises. This can be done with the utilization of other types of filters for example.

iii. Extend the research on concrete samples, especially those with the rebars because it is always being a huge problem in the world of construction. This can be done by producing more concrete samples with rebars within larger concrete specimens, and also some with multiple layers of rebar. From the research

conducted, it was found that the aggregate size greatly affects the test results, noting that the rebars used in this study were in approximately the same size range as that of the nominal aggregates (and even in certain cases smaller)

iv. Using the shear wave technique might have advantages when used with a collimation technique because polarity element in shear wave can be utilized when dealing with high attenuation materials. Although this method requires the preparation of ultrasonic piezocomposite shear wave transducers, this may be possible in several ways (e.g. wedges and rotation of the piezocomposite).